ÇUKUROVA UNIVERSITY
INSTITUTE OF NATURAL AND APPLIED SCIENCES

MSc THESIS

Aykut ÇETİN

FLOW CONTROL IN THE WAKE OF A CIRCULAR CYLINDER BY MEANS OF PERFORATED SEMI CIRCULAR CYLINDER AND SPLITTER PLATE

DEPARTMENT OF MECHANICAL ENGINEERING

ADANA-2019

ÇUKUROVA UNIVERSITY
INSTITUTE OF NATURAL AND APPLIED SCIENCE

FLOW CONTROL IN THE WAKE OF A CIRCULAR CYLINDER BY MEANS OF PERFORATED SEMI CIRCULAR CYLINDER AND SPLITTER PLATE

Aykut ÇETİN

MSc THESIS

DEPARTMENT OF MECHANICAL ENGINEERING

We certify that the thesis titled above was reviewed and approved for the award of degree of the Master of Science by the board of jury on 26/07/2019.

………………………	……..……………	………………………………..
Prof.Dr.Hüseyin AKILLI	Prof.Dr.Beşir ŞAHİN	Asst.Prof.Dr.Tahir DURHASAN
SUPERVISOR	MEMBER	MEMBER

This MSc Thesis is written at the Department of Mechanical Engineering, Institute of Natural and Applied Sciences of Çukurova University.
Registration Number:

Prof. Dr. Mustafa GÖK
Director
Institute of Natural and Applied Sciences

This MSc Thesis was supported financially by the Scientific and Technological Researched Council of Turkey under contract no: 114R087

ABSTRACT

MSc THESIS

FLOW CONTROL IN THE WAKE OF A CIRCULAR CYLINDER BY MEANS OF PERFORATED SEMI CIRCULAR CYLINDER AND SPLITTER PLATE

Aykut ÇETİN

ÇUKUROVA UNIVERSITY
INSTITUTE OF NATURAL AND APPLIED SCIENCES
DEPARTMENT OF MECAHNICAL ENGINEERING

Supervisor : Prof. Dr. Hüseyin AKILLI
Year: 2019, Pages: 125
Jury : Prof. Dr. Hüseyin AKILLI
: Prof. Dr. Beşir ŞAHİN
: Assist. Prof. Dr. Tahir DURHASAN

The main purpose of the present experimental study was to control unsteady flow behaviors in the wake region of a circular cylinder (inner cylinder) by means of permeable semi circular cylinder (outer cylinder) and splitter plate. Inner and outer cylinder diameters and Reynolds number with respect to inner cylinder diameter were kept constant as 50 mm, 125 mm and Re=5000 respectively throughout the experiments. Two different porosity ratios were designated as cylinder porosity ratio (β_C) and plate porosity ratio (β_P). Three different cylinder porosity ratio and four different plate porosity ratio were determined as β_C=0.3, 0.5, 0.7 and β_P=0, 0.3, 0.5, 0.7 respectively. Also, plate angle (α) relative to the flow direction was defined to investigate the effect of splitter plate location to the flow behavior. And these plate angles were chosen as α=90°, 120°, 150°, 180°. For all configurations, dye visualization method was utilized initially, and then to have quantitative results PIV technique was applied. Results indicated that as the plate porosity ascends the TKE_{max} values has diminishing trend. Also cylinder porosity has remarkable influence on TKE_{max} values, TKE_{max} reduction was obtained for lower porous cylinders. And plate angles of 150° and 180° were found to be the most effective angles regardless of the plate porosity ratio. The highest TKE_{max} decrease was attained as 34% for the β_C=0.3, β_P=0.5 at 180°. On the other hand, β_C=0.7 has insignificant control over flow by reason of its high permeability. Consequently, β_C=0.3 and 0.5, β_P=0.5 and 0.7, and plate angles of 150° and 180° were found as the most effective parameters in order to control the flow.

Key Words: Cylinder, Passive control, PIV, Splitter plate, Turbulent Kinetic Energy

ÖZ

YÜKSEK LİSANS TEZİ

DAİRESEL SİLİNDİRİN ARDINDAKİ AKIŞIN DELİKLİ YARIM DAİRESEL SİLİNDİR VE AYIRICI PLAKA VASITASIYLA KONTROLÜ

Aykut ÇETİN

ÇUKUROVA ÜNİVERSİTESİ
FEN BİLİMLERİ ENSTİTÜSÜ
MAKİNE MÜHENDİSLİĞİ ANABİLİM DALI

Danışman : Prof. Dr. Hüseyin AKILLI
Yıl: 2019, Sayfa: 125
Jüri : Prof. Dr. Hüseyin AKILLI
: Prof. Dr. Beşir ŞAHİN
: Dr. Öğr. Üyesi Tahir DURHASAN

Bu deneysel çalışmanın temel amacı, geçirgen yarı dairesel silindir (dış silindir) ve ayırıcı plaka yardımıyla dairesel bir silindirin (iç silindir) ardındaki kararsız akış davranışlarını kontrol etmektir. Deneylerde iç ve dış silindir çapları ve iç silindir çapına göre Reynolds sayısı sırasıyla 50 mm, 125 mm ve Re= 5000 olarak sabit tutulmuştur. Silindir geçirgenlik oranı (β_S) ve plaka geçirgenlik oranı (β_P) olarak iki adet farklı geçirgenlik oranı belirlenmiştir. Üç farklı silindir geçirgenlik oranı ve dört farklı plaka geçirgenlik oranı sırasıyla β_S=0.3, 0.5, 0.7 ve β_P=0, 0.3, 0.5, 0.7 olarak belirlenmiştir. Ayrıca, ayırıcı plaka konumunun akış davranışına etkisini araştırmak için akış yönüne göre ayırıcı plaka açısı (α) tanımlanmıştır. Ve bu plaka açıları α=90°, 120°, 150°, 180° olarak seçilmiştir. Tüm konfigürasyonlar için, başlangıçta boya görselleştirme yöntemi kullanılmış ve daha sonra nicel sonuçlar elde etmek için PIV tekniği uygulanmıştır. Sonuçlar, plaka gözenekliliği arttıkça TKE_{max} değerlerinin azalma eğiliminde olduğunu göstermiştir. Ayrıca silindir gözenekliliğinin TKE_{max} değerleri üzerinde belirgin bir etkisi vardır, düşük gözenekli silindirler için TKE_{max} azalımı elde edilmiştir. Ayrıca, plaka gözeneklilik oranına bakılmaksızın, 150° ve 180°'lik plaka açılarının en etkili açılar olduğu belirlenmiştir. En yüksek TKE_{max} düşüşü 180°'de β_S=0.3ve β_P=0.5 için %34 olarak bulunmuştur. Öte yandan, β_S=0.7, yüksek geçirgenlik nedeniyle akış üzerinde kayda değer bir kontrol etkisi gösterememiştir. Sonuç olarak, β_S=0,3 ve 0,5, β_P= 0,5 ve 0,7, ve 150° ve 180°'lik plaka açıları, akışı kontrol etmede en etkili parametreler olarak saptanmıştır.

Anahtar Kelimeler: Silindir, Pasif Kontrol, PIV, Ayırıcı plaka, Türbülans Kinetik Enerji

EXPANDED ABSTRACT

Since the circular cylinder applications widely appear in engineering applications such as offshore structures, underwater pipelines and cables, wind turbines etc., flow behaviors around this significant, prevalent but simple geometry needs to be scrutinized. Because all applications that utilize cylindrical shape need to be durable and can withstand the adverse effects of the flow around them. When fluid flow runs over a bluff body such as circular cylinder, flow separation occurs at the shear layers. This flow separation phenomenon is the main reason of vortex formation downstream of the cylinder and vortex shedding which give rise to vortex induced vibration (VIV). Besides, this vortex formation in near wake region can give rise to vortex pair interaction which is another adverse effect for the cylinder. Accordingly, these adverse effects such as VIV need to be attenuated or controlled. Researchers have been studying flow structure around bluff bodies for many years and they have found lots of control techniques which are subdivided into two main categories as passive and active control techniques. Both flow control techniques have some advantages over each other, yet passive control techniques are more preferable by reason of its easy implementation and inessentiality of the external energy input. Since two passive control techniques (splitter plate and perforated semi circular cylinder with different porosities) utilized together in the present study, passive control methods were investigated more elaborately.

For the experiments, large scale water channel was utilized in the Fluid Mechanics Laboratory at the Cukurova University. To have a preliminary idea about the general flow behavior of the flow around the cylinder, dye visualization technique was applied initially. The main principle of the dye visualization is that the dye injected to the flow is illuminated by a continuous laser and the flow is recorded by high definition camera. Thereby, qualitative results can be obtained by dye visualization method. Subsequent to dye visualization technique, Particle

Image Velocimetry (PIV) method, which is a non-intrusive flow measurement technique, was utilized to have quantitative results about the flow structure. The principle of the PIV based upon the measuring the displacement of the particles, which are illuminated by pulsed laser source, at a definite time interval. In these experiments, flow around an inner cylinder with diameter of 50 mm was investigated. Porous semi circular cylinder, which has constant diameter of 125 mm, was situated downstream of the inner cylinder concentrically. And the splitter plate that has various porosity ratios was located between inner and outer cylinder (annular region). Reynolds number was calculated according to the inner cylinder diameter as 5000 and it was remained constant throughout the experiments. To determine the most effective flow control parameters, various porosity ratios were arranged. Porosity ratio of the cylinder and splitter plate can simply be defined as the gap area to the total surface area. β_C and β_P stand for the porosity ratios of outer cylinder and splitter plate respectively. Three different outer cylinder porosity ratios were determined as β_C= 0.3, 0.5 and 0,7. And for splitter plate porosity ratios, β_P= 0, 0.3, 0.5 and 0.7 values were designated. Also plate angle (α) was designated to investigate the most appropriate location of splitter plate for controlling the flow. Plate angle can simply defined as the perpendicular location of the splitter plate relative to flow direction and as the plate angles decrease it becomes more perpendicular to the flow direction. Four different plate angles were determined as 90°, 120°, 150° and 180°. As mentioned above there are three determinant and variable parameters to specify the most effective control parameters.

As mentioned earlier, in the first step dye visualization experiments were carried out to analyze the general flow behavior. More extensive field of view was examined throughout dye visualization experiments and focused on the wake region rather than the annular region. And the flow structure was tried to be interpreted according to Karman Vortex Street or vortex formation. In general cylinder porosity ratio of β_C= 0.5 was determined as the most successful one for almost all configurations. It provides a perfect flow control in the wake region especially for β_P= 0.5, 0.7 ratios. β_C= 0.3 can also be regarded as effective porosity ratio for the outer cylinder, except that causing jet like flow this porosity ratio provided remarkable flow control for most of the configurations. However, flow control could not be achieved for nearly all configurations with β_C= 0.7 ratio due to its high porosity ratio and excessive flow that passes through the outer cylinder.

More far-reaching investigation was carried out by PIV experiments and quantitative results were obtained. PIV experiments revealed more detail about the flow characteristics and flow behaviors were interpreted according to the time averaged streamlines $\langle\psi\rangle$, time averaged vorticity contours $\langle\omega\rangle$ and TKE distributions. These results indicated that plate porosity ratio has significant effect on the flow characteristics. As the plate porosity ratio increase the TKE_{max} value indicates certain diminishment. β_P= 0.5 and 0.7 found to be the most effective plate porosity ratios regardless of the plate angle with respect to TKE_{max} distributions. However, for lower porous splitter plates (β_P= 0 and 0.3) the plate angle comes into prominence. When the plate angles located more perpendicular way to the flow direction (90° and 120°) the flow is directed to the upper shear layer by reason of high blockage effect of low porous plates, causing higher momentum flow by upper shear layer. On the other hand, plate porosity ratios of β_P= 0 and 0.3 exhibited remarkably high flow control at 150° and 180°. β_C= 0.5 ratio for β_P= 0.5 and 0.7 can be regarded as the most efficient configuration for all plate angles according to time averaged streamlines $\langle\psi\rangle$, time averaged vorticity contours $\langle\omega\rangle$ by reason of no vortex pair interaction and vortex formation take place in the wake region. And TKE_{max} reduction of 20-22% was obtained in this configuration for $120° \leq \alpha \leq 180°$. β_C= 0.3 was another effective control parameter except that jet like flow takes place at the outer cylinder due to lower permeability. Although β_C= 0.5 was defined as the most effective cylinder porosity in general, the maximum TKE_{max} reduction was obtained with β_C= 0.3 as 34% for β_P= 0.5 at 180° plate angle. However, with β_C= 0.5 cylinder porosity ratio, even β_P= 0.3 exhibit more controlled flow for 120°≤α≤180° while β_P= 0.3 provides control only at 180° for β_C= 0.3 ratio. When β_P= 0.5 and 0.7 ratios utilized with β_C=0.3 this configuration can be presumed effective control parameters since the TKE_{max} values were diminished at all plate angles. Lastly, for the β_C=0.7 case, it cannot be said that there is a significant flow control. Cylinder porosity ratio β_C=0.7 could not achieve flow control except for few configurations due to its high porosity ratio and excessive flow that pass through easily.

In conclusion, in the present study, remarkable flow control was achieved for majority of the configurations in both annular and wake region. Vortex formation and Karman Vortex Street were attenuated and even annihilated for most of the configurations. Cylinder porosity ratios of β_C=0.3 and 0.5, plate porosity ratios of β_P= 0.5 and 0.7, plate angles of α=150° and 180° can be considered as the most effective and consistent parameters of the present experimental study.

GENİŞLETİLMİŞ ÖZET

Dairesel silindir uygulamaları, açık deniz yapıları, su altı boru hatları ve kabloları, rüzgar türbinleri vb. mühendislik uygulamalarında yaygın olarak görüldüğünden dolayı, bu önemli, yaygın ancak basit geometrinin etrafındaki akış davranışlarının incelenmesi gerekir. Çünkü silindirik şekli kullanan bu uygulamaların tüm sistemler gibi dayanıklı olması ve etraflarındaki akışın olumsuz etkilerine dayanabilmesi gerekir. Bir akışkan, dairesel silindir gibi bir küt bir gövdeyle karşılaştığında, alt ve üst kayma tabakalarında akış ayrılması gerçekleşir. Bu akış ayrılması durumu, silindirin art izinde girdap oluşumunun ve girdap kaynaklı titreşime (VIV) yol açan girdap dökülmesinin temel sebebidir. Ayrıca, silindire yakın bölgedeki bu girdap oluşumu, girdap çifti etkileşimine yol açabilir ve bu durumda silindir için ayrı bir olumsuzluktur. Bu nedenle, bu olumsuz etkilerin hafifletilmesi ve kontrol edilmesi gerekir. Araştırmacılar, yıllardır küt gövdelerinin etrafındaki akış yapısını incelemektedir ve pasif ve aktif kontrol teknikleri olarak iki ana kategoriye ayrılan çok sayıda akış kontrol tekniği bulmuşlardır. Her iki akış kontrol tekniğinin de bazı avantajları vardır, ancak pasif kontrol teknikleri, kolay uygulanması ve harici enerji girişinin gerekmemesi nedeniyle daha çok tercih edilmektedir. Bu çalışmada iki pasif kontrol tekniği (farklı gözeneklere sahip ayırıcı plaka ve delikli yarı silindir) birlikte kullanıldığından, pasif kontrol yöntemleri daha ayrıntılı olarak incelenmiştir.

Deneyler için, Çukurova Üniversitesi'ndeki Akışkanlar Mekaniği Laboratuvarı'nda bulunan büyük ölçekli su kanalı kullanılmıştır. Silindir etrafındaki akışın genel akış davranışı hakkında ön bir fikre sahip olmak için, başlangıçta boya görselleştirme tekniği uygulanmıştır. Boya görselleştirmesinin temel prensibi, akışa enjekte edilen boyanın sürekli bir lazer ışığı ile aydınlatılması ve akışın yüksek çözünürlüklü kamera ile kaydedilmesidir. Böylece, boya görselleştirme yöntemi ile nitel sonuçlar elde edilebilir. Boya görselleştirme tekniğinin ardından, akış yapısı hakkında nicel sonuçlar elde etmek için, akışı kesintiye uğratmayan bir akış ölçüm tekniği olan Parçacık Görüntülemeli Hız Ölçme Yöntemi (PIV) kullanılmıştır. PIV ilkesi, kesintili aydınlatma yapan bir lazer kaynağı ile aydınlatılan parçacıkların yer değiştirmesinin belirli bir zaman aralığında ölçülmesine dayanır. Yapılan deneylerde, 50 mm çapında bir iç silindir etrafındaki akış incelenmiştir. Sabit çapı 125 mm olan gözenekli yarı dairesel silindir, iç silindirin akış aşağısına eş merkezli olarak yerleştirilmiştir. Ve çeşitli geçirgenlik oranlarına sahip olan ayırıcı plaka iç ve dış silindir (halka şeklindeki bölge) arasına yerleştirilmiştir. Reynolds sayısı iç silindir çapına göre 5000 olarak hesaplanmış ve deneyler boyunca sabit tutulmuştur. En etkili akış kontrol parametrelerini bulabilmek için çeşitli geçirgenlik oranları belirlenmiştir. Silindirin ve ayırıcı plakanın geçirgenlik oranı, basit olarak, boşluk alanının toplam yüzey alanına oranı olarak tanımlanabilir. β_S ve β_P sırasıyla dış silindir ve ayırıcı plakanın geçirgenlik oranlarını ifade eder. Üç farklı dış silindir geçirgenlik oranı, β_S=0.3, 0.5 ve 0,7 olarak belirlenmiştir. Ayırıcı plaka geçirgenlik oranları için ise β_P=0, 0.3, 0.5 ve 0.7 değerleri belirlenmiştir. Ayrıca, akışı kontrol etmek için en uygun ayırıcı plaka yerini araştırmak üzere plaka açısı (α) tanımlanmıştır. Plaka açısı basitçe, ayırma levhasının akış yönüne göre dikey konumu olarak tanımlanabilir ve plaka açısı azaldıkça akış yönüne daha dik hale gelmektedir. Dört farklı plaka açısı 90°, 120°, 150° ve 180° olarak belirlenmiştir. Yukarıda da belirtildiği gibi, en etkili kontrol parametrelerini belirlemek için üç belirleyici ve değişken parametre incelenmiştir.

Daha önce belirtildiği gibi, genel akış davranışını analiz etmek için ilk olarak boya görselleştirme deneyleri yapılmıştır. Boya görselleştirme deneyleri boyunca daha geniş bir görüş alanı incelenmiş ve iç-dış silindir ara bölgesi yerine silindir ardındaki bölgeye daha fazla odaklanılmıştır. Akış yapısı Karman girdap caddesi ve girdap oluşumuna göre yorumlanmaya çalışılmıştır. Genel olarak β_S=0.5 silindir geçirgenliği, neredeyse tüm konfigürasyonlar için en başarılı geçirgenlik oranı olarak belirlenmiştir. Bu geçirgenlik oranı silindir art izinde, özellikle β_P=0.5, 0.7 oranları için mükemmel bir akış kontrolü sağlamıştır. β_S=0.3, dış silindir için bir diğer etkili geçirgenlik oranı olarak kabul edilebilir, jet benzeri akışa neden olması dışında, bu geçirgenlik oranının çoğu konfigürasyon için kayda değer akış kontrolü sağladığı tespit edilmiştir. Bununla birlikte, yüksek geçirgenlik oranı ve dış silindirden geçen aşırı akış nedeniyle β_S=0.7 geçirgenlik oranı için neredeyse tüm konfigürasyonlarda akış kontrolü sağlanamamıştır.

PIV deneyleri ile daha geniş kapsamlı araştırmalar yapılmış ve nicel sonuçlar elde edilmiştir. PIV deneyleri akış özellikleri hakkında daha fazla detay ortaya koymuş ve akış davranışları, zaman ortalamalı akım çizgileri $\langle\psi\rangle$, zaman ortalamalı girdap kontürleri $\langle\omega\rangle$ ve TKE (Türbülans Kinetik Enerji) dağılımlarına göre yorumlanmıştır. PIV deneyleri, levha geçirgenlik oranının akış özellikleri üzerinde önemli bir etkiye sahip olduğunu göstermiştir. Plaka geçirgenlik oranı arttıkça, TKE_{max} değeri belirli bir azalma göstermiştir. β_P=0.5 ve 0.7, TKE_{max} dağılımlarına göre plaka açısına bakılmaksızın en etkili plaka geçirgenlik oranları olarak belirlenmiştir. Bununla birlikte, daha düşük gözenekli ayırma plakaları (β_P=0 ve 0.3) için plaka açısı daha da önem kazanmaktadır. Plaka açıları, akış yönüne daha dik bir şekilde (90° ve 120°) yerleştirildiğinde, akış, düşük gözenekli plakaların yüksek blokaj etkisi nedeniyle üst kayma tabakasına yönlendirilir, bu da üst kayma tabakasında daha yüksek momentumla akışa sebep olur. Diğer yandan, β_P=0 ve 0.3 levha geçirgenlik oranları, 150° ve 180°'de oldukça iyi akış kontrolü sağlamıştır. β_P=0.5 ve 0.7 için β_S= 0.5 oranı, zaman ortalamalı akım çizgileri $\langle\psi\rangle$ ve zaman ortalamalı girdap kontürlerine $\langle\omega\rangle$ göre girdap oluşumu ve etkileşimi gözlemlenmediğinden dolayı tüm plaka açıları için en etkili konfigürasyon olarak kabul edilebilir. Bu konfigürasyonda 120°≤ α ≤180° için ortalama olarak %20-22 arasında TKE_{max} düşüşü elde edilmiştir. β_S=0.3, düşük geçirgenliği nedeniyle dış silindirde jet benzeri akışa sebep olması dışında bir diğer etkili kontrol parametresi olarak düşünülebilir. Her ne kadar β_S=0.5 genel olarak en etkili silindir geçirgenliği olarak tanımlansa da, maksimum TKE_{max} azalması 180° plaka açısında β_P=0.5 için β_S=0.3 ile % 34 olarak elde edilmiştir. Bununla birlikte β_S=0.5 silindir geçirgenliği, β_P=0.3 için bile 120°≤ α ≤180° açılarında kontrollü akış sağlarken, β_P=0.3, β_S=0.3

oranı için sadece 180°'de kontrol sağlamıştır. β_P= 0.5 ve 0.7 oranları β_S=0.3 ile kullanıldığında, bu konfigürasyon TKE_{max} değerlerinin tüm plaka açılarında azalmasına sebep olduğu için etkin kontrol parametreleri olarak kabul edilebilir. Son olarak, β_S=0.7 durumu için, önemli bir akış kontrolünün olduğu söylenememektedir. Silindir geçirgenlik oranı β_S=0.7, yüksek geçirgenlik oranı ve kolayca geçen aşırı akış nedeniyle birkaç konfigürasyon dışında akış kontrolü sağlayamamıştır.

Sonuç olarak, bu çalışmada, hem iç-dış silindir ara bölgesinde hem de silindir art izinde, konfigürasyonların çoğu için dikkate değer bir akış kontrolü sağlanmıştır. Girdap oluşumu ve Karman girdap caddesi, konfigürasyonların çoğu için bastırılmış hatta yok edilmiştir. β_S=0.3 ve 0.5 silindir geçirgenlik oranları, β_P=0.5 ve 0.7 plaka geçirgenliği oranları, α=150° ve 180°'lik plaka açıları bu deneysel çalışmanın en etkili ve tutarlı parametreleri olarak kabul edilebilir.

ACKNOWLEDGEMENTS

I am grateful to my supervisor Prof.Dr. Hüseyin AKILLI for his splendid guidance and endless time he spent with me to share his experience, this study could not be possible without his encouragement. Likewise, I want to thank to Prof. Dr. Beşir Şahin who encourage me with his incentive attitude and wisdom. Also I appreciate that he gave me the opportunity to work in his project and the privilege to work with him.

I am also thankful to Asst. Prof.Dr. Tahir DURHASAN, Asst. Prof.Dr. İlyas KARASU, Asst. Prof.Dr. Engin PINAR and Asst. Prof.Dr. Göktürk Memduh ÖZKAN for their help to teach me the utilization of the PIV system thoroughly.

I also sincerely thank to Res. Asst. Osman OHTAROĞLU and Res. Asst. Umutcan OLMUŞ for their contribution to this study. Besides, I am grateful to Project Asst. Mehmet Oğuz TAŞCI and Sefa MERAL for their assistance.

I am grateful to the Scientific and Technological Research Council of Turkey (TUBITAK) for funding this study under contract No: 114R087.

I would like to thank sincerely to my dear friends Fatma Nur KÖSE and Hüseyin ALTAN. They have always been with me and supported me.

I would like to thank specially to my dear friend Enver KULAK, his precious wife Aysel Can KULAK and their beloved handsome and cute son Alparslan KULAK for their friendship, support and motivation. They have always been with me and encouraged me to become a Research Assistant and a good person.

Lastly, I would like to thank my whole family from my heart one by one for their patience and supportive attitudes. But, I would like to thank especially to the latest member of our family, my newborn niece, beautiful and sweet Gökçe ÇETİN for bringing an extra motivation and cheer not only to the last period of my thesis work, but also to our life. She touched to our lives with her lovely smile.

CONTENTS **PAGE**

LIST OF FIGURES **PAGE**

LIST OF ABBREVIATONS

D_i	: Diameter of inner cylinder
D_o	: Diameter of perforated outer cylinder
β	: Porosity ratio
β_C	: Outer cylinder porosity ratio
β_P	: Splitter plate porosity ratio
α	: Splitter plate angle
h_L	: Laser sheet height
h_W	: Water level
H	: Depth of the water in the channel
$<\psi>$	: Time averaged streamlines
$<\omega>$	: Time averaged vorticity contours
U	: Free stream velocity
u	: Instantaneous velocity
TKE_{max}	: Maximum turbulent kinetic energy
Re	: Reynolds number
ν	: Kinematic viscosity

1. INTRODUCTION

Many engineering applications in nature, the designed structures are exposed to flow around them. That flow generates unsteady loads and unsteady vortices around the designed structures. The reason of unsteady loads and vortices is that at certain speeds, flow around bluff bodies like circular cylinder can no longer remain attached to the surface and flow separation occurs. In other words, flow take place around the circular cylinder creates vortex shedding due to the separation from the surface of the structure. This unsteady separations and vortex shedding generate vortex induced vibration (VIV). And this VIV shorten the life of the structure and it is the main reason of fatigue and even structural failure. In many engineering applications the basic geometrical shapes are utilized such as cylinder, spheres etc. Easy implementation and endurance to the environmental effects make the cylinders one of the most versatile structural design for many engineering applications and attract notice. Underwater pipelines (figure 1.1-a) and cables (figure 1.1-b), bridge piers (figure 1.1-c), wind turbine towers (figure 1.1-d), offshore structures (figure 1.1-e), chimneys (figure 1.1-f) and other cylindrical buildings can be counted as an example of this versatile geometrical shape.

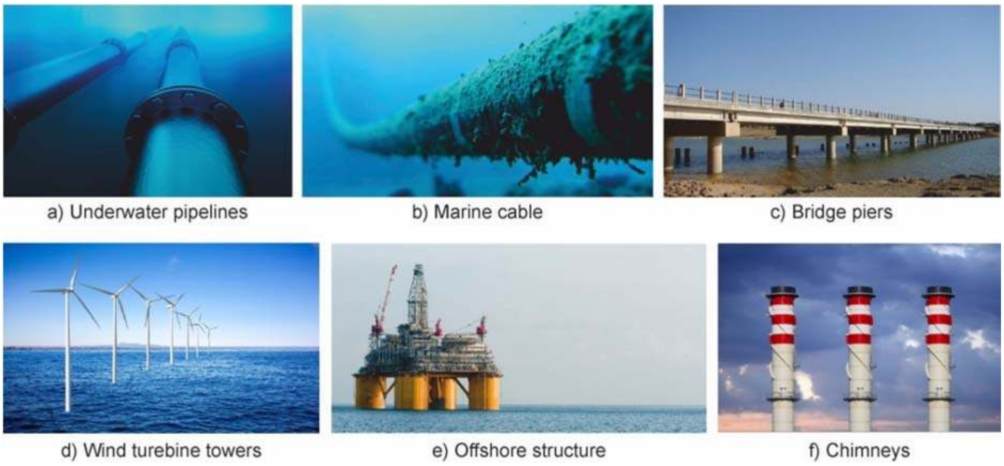

Figure 1.1. Circular cylinder applications in engineering

To understand the concept of flow around bluff bodies like circular cylinder, complex flow mechanisms (boundary layer separation, vortex shedding, shear layers and recirculating regions) must be understood well. Because boundary layer separation, vortex shedding and VIV are the main reasons for energy loss and failure of the system. To overcome these undesirable effects, researchers have come up with some control techniques. Abundance of cylinder-like structures in engineering applications have attracted many researcher from past to present, and the desire of controlling the flow around this basic circular cross section paved the way for understanding of complex flow mechanisms and some flow control techniques. In the present study, the main aim is to scrutinize the flow around circular cylinder and attenuate the undesirable vortex shedding and VIV and to have more stable and more controlled flow by means of passive control methods.

1.1. Flow around a Circular Cylinder

Flow around bluff bodies has drawn interest of researchers for many years due to its simple but explanatory nature for complex flow mechanisms such as flow separation, vortex shedding and shear layer instability. To understand these mechanisms, vortex shedding mechanism needs to be studied in a detailed way since it is the main reason for VIV and has a destructive nature. The common occurrence in nature and in engineering applications, this basic but versatile circular cylinder shape became one of the first studies to examine. Strouhal's study of vortex shedding around circular cylinder can be accepted as the milestone of the flow behavior around bluff bodies and this study inspired many others (Strouhal, 1878).

When a flow encounters with cylindrical shape, flow separation, vortex shedding and shear layer instability arise from for different Reynolds numbers and as a consequence of these undesirable lift and drag forces may be exerted on the cylinder. In the absence of external forces, the dynamics of flow around a cylinder depends only on the Reynolds number ($Re = U_\infty D / \nu$ where U_∞ is the free-stream velocity far from the cylinder, D is the cylinder diameter and ν is the kinematic viscosity). Characteristics of this flow are well-recognized for a wide range of flow regimes, from creeping flows (*Re* <<1) to fully turbulent flows (*Re*≈ 107). The flow regimes at low Reynolds numbers can be classified as follows:

The flow is steady and two-dimensional for *Re* < 6 with only one separation point. For the range 6 < *Re* < 47, flow separates from the trailing edge of the cylinder and stationary vortex pair (Figure 1.2-a) form in the wake whose recirculation length grows as the Reynolds number increases.

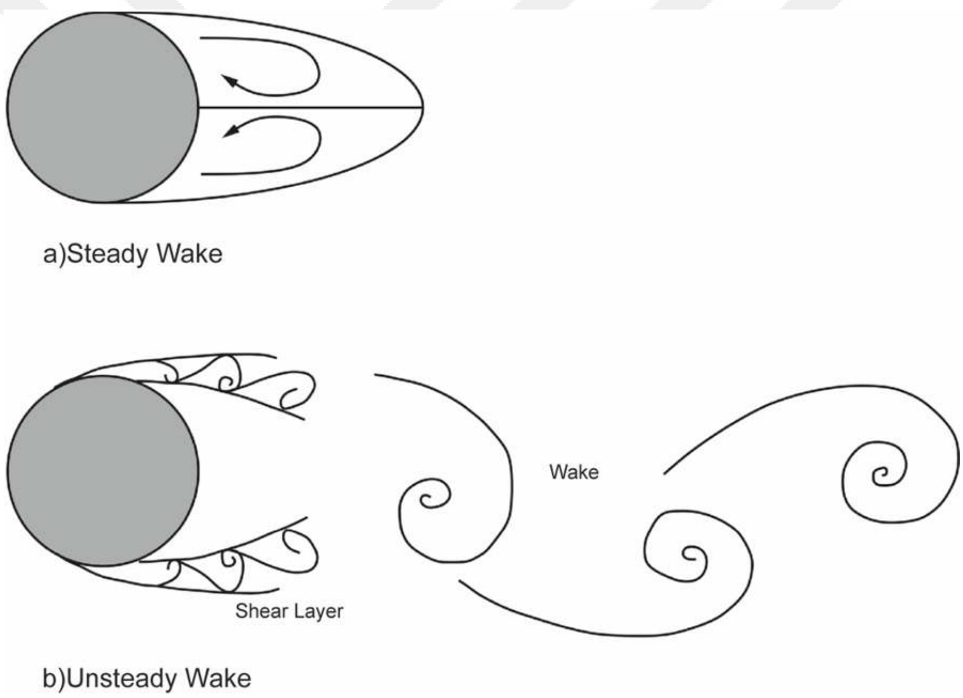

Figure 1.2. Cylinder wake at different Reynolds numbers. a) Steady wake structure for 6 < Re < 47, b) Unsteady wake structure for 47 <Re < 200

At the critical Reynolds number (*Re*≈ 47), even though all conditions are kept constant, instabilities increase all of a sudden and vortex shedding appears behind the circular cylinder, resulting in the well-known von Karman Vortex Street (Figure 1.2-b).

For $47 < Re < 200$, unsteady and periodically oscillating forces occur on trailing edge of the cylinder. Instabilities are developed by recirculation region whose amplification and strength grow with Reynolds number resulting in alternating high and low pressure regions on the leeward of the body and the cylinder experiences a periodic net force because of these regions. This oscillation may amplify the vortex shedding, because now the cylinder itself is moving in the flow, forcing the vortex street to occur with large amplitude. The frequency of the vortices is given by dimensionless Strouhal number St (Strouhal number, $St = f D/ U_\infty$, where f is the frequency, D is the cylinder diameter, U_∞ is the free-stream velocity, and the vortices produced in this manner are called Strouhal vortices. Consequently, for higher Reynolds numbers (Re>200), the flow becomes turbulent and three-dimensional.

For better understanding Gerard illustrated the vortex shedding mechanism as it can be seen from figure 1.3 (Gerard, 1964).

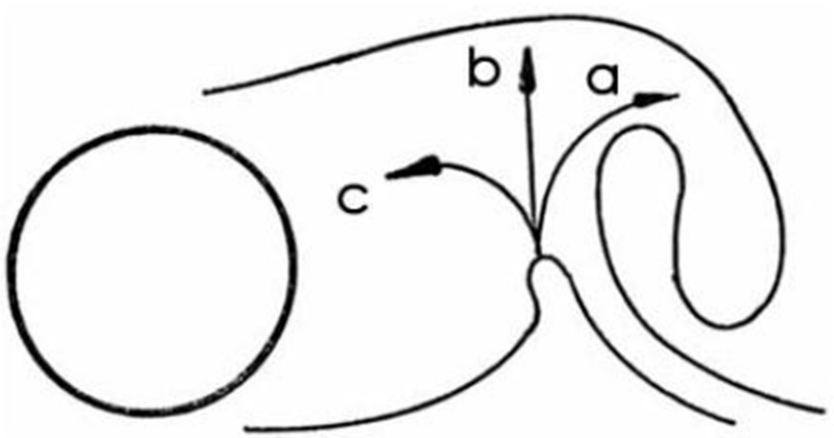

Figure 1.3. The Vortex Shedding mechanism proposed by Gerard (1964)

Figure 1.3 depictures the vortex shedding mechanism that Gerrard (1964) came up with. When the cylinder encounter with fluid flow the flow separation takes places on both upper and lower side of the cylinder. So the upper and lower shear layers bring about transition waves due to flow separation. At sufficiently high Reynold numbers these transition waves generate vortex formation (upper or lower) and one of them surpasses the other one. So there are two vortices that have opposite sign. When the dominant vortex (upper or lower) starts growing, it draws the corresponding shear layer on the opposite side across the wake. After that the weaker vortex is start growing and annihilates the supply of the dominant vortex and makes it shed. The process repeats itself alternately at the either side of the body and generates the vortex shedding mechanism, thus creating Vortex Street at the wake of the body.

1.2. Karman Vortices and Kelvin-Helmholtz Vortices

There are two types of streamwise vortices that have been introduced in the laminar and transitional wakes of the cylinders. When the Reynolds number is sufficiently high, transition waves appear in the shear layer, which is separated from the cylinder surface. These waves are perceptible in the wake region, which is extending from the separation point on the body surface to the first appearance of the large-scale Karman vortex. Consequently, the local pressure changes cause a vortex to shed from the cylinder surface every time. For this reason, the cylinder is exposed to a fluctuating drag and lift accompanied by the mean drag and lift forces. The drag, lift and vortex shedding frequencies are stated as dimensionless forms which are C_D, C_L and St and they stand for the drag coefficient, lift coefficient and Strouhal number respectively. These three dimensionless parameters depend on flow characteristic and structure of the cylinder. When the cylinder is located near a plane boundary, the bed proximity, the velocity gradients in the boundary layer and the turbulent characteristics of the boundary layer have some influence on these parameters.

At sufficiently high Reynolds number values, transition waves appear in the form of Kelvin-Helmholtz vortices which is shown in figure 1.4. These small-scale vortices are also referred as Bloor-Gerrard vortices. Inception of the transition waves is considered to be a strong function of the disturbance level of the free stream, by taking into consideration that they result from convective-type instability, as described by Ho and Huerre (1984). Initially, Bloor (1964) detected the small-scale vortices for Reynolds number Re>1300, but Unal and Rockwell (1988) first noted these vortices at Re_d=1900. Also Wu et al. (1994) discussed the possible effect of background disturbance levels and observed these waves over the range of Reynolds numbers 1000≤Re≤3000.

The Kelvin-Helmholtz vortices in the shear layer are corollary of the transition from laminar to turbulent state. Another result of this transition state is the Karman vortices, which can be seen at Re=5000 is basically turbulent. The Karman vortices in the wake of a cylinder can be seen in the figure 1.4.

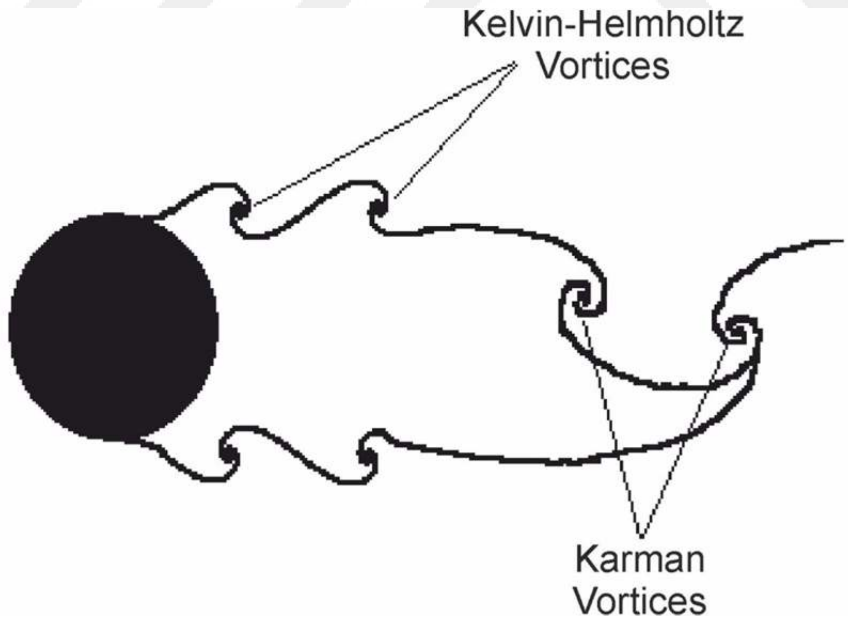

Figure 1.4. The Kelvin-Helmholtz vortices and the Karman vortices in the cylinder wake region

1.3. Flow Control

Vortex shedding downstream of bluff bodies have been one of the most salient subject for many researchers since Roshko first measured the period of Karman vortex shedding downstream of a bluff body in 1954 (Roshko, 1954). The reason vortex shedding and near wake flows are so salient is that the flow around bluff bodies can be encountered with in nature and in engineering application too often. So researchers have been scrutinized the flow separation and shear layers behind the bluff bodies due to their fundamental significance and practical importance in fluid dynamics. In these situations, bluff bodies are exposed to unsteady loads because of the flow separation and formation of vortex shedding. This vortex shedding brings about a significant pressure drop on the back surface of the body. Also VIV (vortex induced vibration) takes place due to the vortex shedding and this situation can cause failure of the system. For this reason design of such an application is very important for engineers to alter or reduce these undesired loads and vibration that is exerted on the body.

Therefore the efficient methods are needed to eliminate vortex shedding and VIV, and researchers have been developed some control methods to attenuate the vortex shedding for many years. Control of the wake region and flow separations could considerably diminish the unsteady loads on the body; resulting less structural vibration. Scientists offered many control methods for essentially attenuate the vortex formation and potential influences of this formation. These control methods can be categorized into two main groups as passive and active control methods. The passive control methods can simply expressed as modification of the body geometry to manipulate the pressure gradients or adding external geometries such as splitter plate or porous media to reduce drag. For passive control techniques external energy input is not required in contrast with active ones. On the other hand, active flow control methods need external energy input to manipulate the flow behavior around the bluff body.

1.3.1. Active Flow Control Techniques

Flow control techniques are widely used to manipulate the flow pattern and augment the efficiency of the designed structure. These techniques also provide environmental compliance and enhanced performance, accordingly help us to overcome the instabilities like flow separation and vortex shedding. Among other flow control techniques, active control techniques have come into prominence in recent years due to its advantageous nature. Researchers have been studying the active flow control techniques in recent years elaborately and lots of studies are available in literature at the moment. In contrast with passive flow control, active flow control needs an external energy or auxiliary power input to carry out the desired flow control. Although it is not as easy as to implement like passive flow control techniques, active flow control has two main advantages on the contrary to passive flow control. First one is that active flow control provides a natural stability to the flow and makes it possible to obtain very high effect by using very small localized energy input. In other words, more precise and effective flow control can be achieved by introducing the control input at any critical location or high receptivity region. The second advantage is that it can be used to control complex, dynamical processes like turbulence production in turbulent boundary layers to reduce skin friction and viscous drag. However it has some disadvantages like it may be difficult to implement active control methods to the real engineering applications because of the complexity of the actuators and the external energy that is needed.

1.3.1.1. Feedback Control

Feedback control method has been studied nearly twenty years by the researchers. This technique has been utilized for several applications in thermal and fluid engineering. This method includes the triad of flow phenomena, actuators/sensor and control situation. Actuators are very important for this control method because it is the determinant of the whole process. It is responsible to control the flow and alter the flow field. So, low energy consumption, low cost, easy implementation and fast response are the desired qualifications of the actuators. The early study of Berger (1967) promoted feedback control method to the suppression of the flow instabilities at low Reynolds number using an oscillating body. This method attracts notice of a lot of researchers recently. Potential effects of feedback control method on the cylinder was investigated experimentally Fujisawa et al. (2001).

A hot-film probe, a phase shifter, amplifiers and a dynamic shaker are utilized to apply feedback control. So as to obtain strong signal of vortex shedding, the hot-film probe is located in one of the shear layer of the wake. Also a sensor is located downstream of the actuator in the feedback control loop in order to measure the controlled flow parameters. The signal that obtained from the feedback probe are phase- shifted and amplified to drive the shaker which is connected to the cylinder to produce perturbations in the wake region. A monitor hot-film probe is also situated in the wake to appraise the control effect on vortex shedding. The obtained signals from both feedback and the monitor probes are turned into frequency spectra by the help of a computer.

1.3.1.2. Electro-magnetic Control

Electro-magnetic control, which is also known as Magnetohydrodynamics (MHD), is an active flow control technique. And it is accepted as a boundary layer control method. This method is very advantageous for conducting fluids because of the Lorentz force that acts as a volume force inside the fluid, and it can be regulated to behave only in a specific region of the flow. The principle of this technique is simply based on utilizing the magnetic field in a conductive fluid. If any movement takes place in the magnetic field, an electric current is generated. In the presence of the magnetic field and the current, the unit volume is exposed to a fluid force that is named as Lorentz force. The Lorentz force has an impact opposite direction to the flow and it bring down the flow velocity, provide a certain stability to the flow and affects the drag and lift forces significantly. Many techniques have been promoted since 1960s utilizing the electric and magnetic field to control the turbulent boundary layer and drag reduction.

The implementation of the method is that the body is coated with electrodes and permanent magnets adjacent to each other. To arrange the exact layout, positive electrode, N-pole magnet, negative electrode and S-pole magnet are located side by side respectively and the sequence is repeated. If a cylinder is to be coated, the sequence must repeat itself until the end. Also the direction of Lorentz force can be reversed by only changing the poles of the electrodes. Figure 1.5 illustrates the arrangement of the magnets and electrodes.

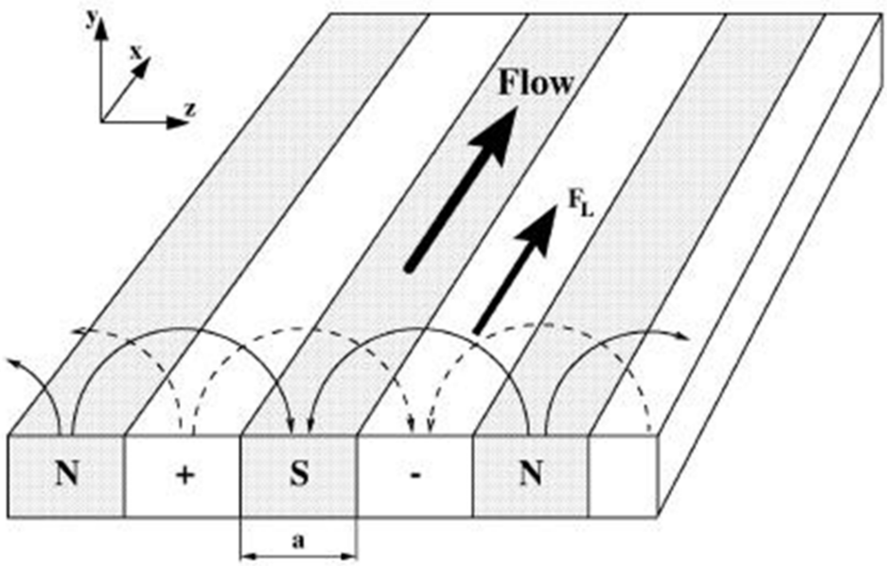

Figure 1.5. Lorentz force generated by magnetic fields

Also to understand electro-magnetic control method better Figure 1.8 illustrate how low and high magnetic field affects the vorticity contours. Also vorticity contours without magnetic field effect is shown.

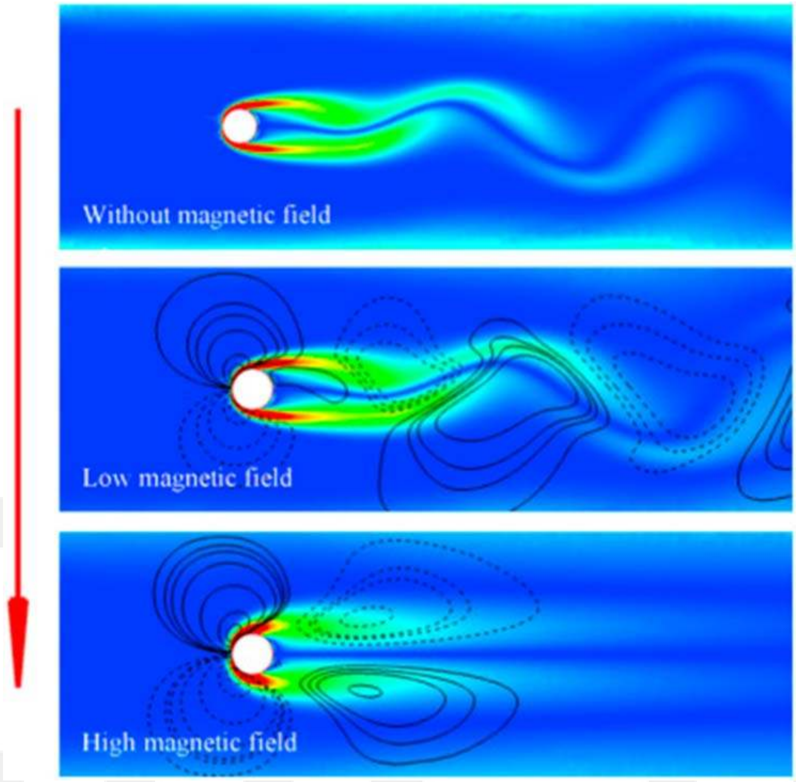

Figure 1.6. Vorticity contours at different magnetic field strength at Re=100 (Rashidi, Hayatdavoodi, and Esfahani, 2016)

1.3.1.3. Generating a Secondary Flow

Suction and blowing are the active flow control methods that rely on generating a secondary flow and just like the other active control methods it requires energy input. This method is utilized in some practical engineering applications such as aircrafts, turbine blades etc. Suction and blowing methods are useful to solve the problems in engineering applications that is related to fluid dynamics.

Although both suction and blowing have the same principle of generating a secondary flow, their influence to the flow is way too different. To begin with suction, it has two basic effects when it is applied to cylinder base. First one is that the suction method enhances the magnitude of negative velocities. The latter is that it reduces the length of the recirculation zones and thus reduces the streamwise extent.

In other respects, the effects of blowing are contrary to effects of suction. The linear temporal growth rates in the near wake are anticipated to decrease due to reduced back flow, and the extent of absolute instability is anticipated to enhance. So in both condition, we have to rest on phenomenological observations, and specify which method surpass the other one and provide us the desired effects.

1.3.1.4. Wake heating

Wake heating can be effective method for horizontally situated cylinder or other structures to attenuate the vortex shedding by utilizing the heat input. But since the fluid that flows around the bluff body change, this method may have different effects for air and water flow. The basic principle of the wake heating is that the desired region is heated to alter the flow pattern. Since the viscosity change of gases and liquids shows different reactions to heat, one should take into consideration that which fluid is flowing around the bluff body for wake heating method. For air flow case, increment of heat input to the cylinder can be helpful to attenuate the vortex shedding. However for water flow case, increment of heat input may be detrimental rather than advantageous. But for liquids, the range of heating conditions, which the buoyancy effects are negligible, is more limited.

The discrepancy of liquids and gases propound that this control is about both changes of dynamic viscosity and density with temperature and it is not only related with density variance as Yu and Monkewitz (1990) suggested. So this discrepant behavior of air gas and liquid propound that the change of viscosity is predominant for wake heating method. The explanation of this situation is that generally the viscosity of liquids decrease with increment of heat input while the viscosity of gases increase with increment of heat input without exceptions. So we can say heating the near wake lead to density and viscosity change and this situation affects the velocity profile, instability and the amplitude of the shedding vortices.

1.3.2. Passive Flow Control Techniques

The need for controlling the flow in a way that is more stable and controlled manner gave rise to researchers to find out new techniques. Among other flow control techniques the passive flow control techniques are the most preferred techniques due to its easier implementation, simplicity and lower cost. Also the unnecessity of external energy expenditure and complex actuators make the passive control methods practical and favorable. These methods can easily be applied to suppress vortex shedding and reduce drag force significantly. Passive control methods can also be implemented for underwater applications such as marine risers and underwater pipelines etc. to annihilate the vortex induced vibration and acoustic noise. The logic behind the passive methods is that changing or reshaping the geometrical shape of the body or adding external devices such as splitter plate. In other words, passive control methods are based on modifying the geometry to manipulate pressure and velocity gradients and to control the flow separation. Some applications of passive control methods are utilizing porous structure, adding perforated cylinders and splitter plate, designing the wavy or rough surface and applying base bleed. These methods mentioned above have proved themselves and used in the past to suppress vortex shedding, reduce the drag coefficient and instabilities.

Roshko (1954) and Zdravkovich (1981) are among the first investigators, Zdravkovich (1981) classified control techniques into three categories:

(i) The control of shear layer by the help of surface protrusion (tripping wire, fin, helical strakes and wires, studs, etc.), which acts upon flow separation lines (James and Truong, 1972); this can be further subclassified into omnidirectional and unidirectional. The omnidirectional methods are those not influenced by the direction of flow velocity; for instance, helical strakes, and helical wires. The unidirectional are those effective only for a certain direction of flow velocity; for instance, straight fins.

(ii) The full shrouds are omnidirectional, whereas incomplete shrouds become unidirectional.

(iii) The control of the entrainment layers by shrouds (perforated gauze, axial rods, etc.) that provide irrotational fluid to the entrainment layers (Knell, 1969)

(iv) The instability control of wakes by near-wake stabilizers (splitter plate, guiding plates, base-bleed, slits cut along the models, etc.) that reduce the interaction of two opposite shear layers (Roshko, 1954, Bearman, 1965, Apelt, West and Szewczyck, 1973).

1.3.2.1. Splitter Plate

Many flow control methods have been developed to suppress the vortex shedding and control the undesired effects of the flow around bluff bodies. Researchers is still studying and trying to find more effective and easier methods to control the flow. But they have already found consistent and effective control methods such as splitter plate. Splitter plate is one of the successful and preferred methods due to its consistency and easy implementation. Being a passive control method and requiring no energy input is a determinant for splitter plate to be preferred. It has been studied a lot and attracted notice of abundant number of researchers due to its success of suppressing vortex shedding. Generally a splitter plate is located to the rear surface of the cylinder and its direction coincides with the centerline of the cylinder. Attached splitter plate modifies the geometrical shape of the body and performs splendid changes on the vortex shedding frequency depending on the length of splitter plate. As well as length of the splitter plate, the Reynolds number is another important factor for the vortex shedding frequency. At sufficiently high Reynolds number, the vortex shedding frequency does not diminish gradually as the splitter plate length increases. The vortex shedding frequency diminishes for $L<D$ and increases for $D<L<2D$, and finally it diminishes as the length of the splitter plate increases (L is the splitter plate length and D is the diameter of the cylinder).

When the splitter plate length is bigger than the critical length, the vortex shedding around the cylinder vanishes totally, and this critical length is proportional with the Reynolds number. At a certain Reynolds number, the drag force exerted on the body is substantially reduced by the splitter plate and for the minimum drag force there is an optimal length of the splitter plate.

So the splitter plate length, Reynolds number and drag force are related to each other. And studies and previous experiments showed that up to 40% of drag force reduction is applicable when the splitter plate is located to the right place. Also the distance between the cylinder and splitter plate is another determinant and it should not be larger than the critical distance to achieve the drag reduction.

In this study, splitter plate is utilized with another passive control method together and it is located at different angle to the flow direction and the possible effects of the splitter plate are scrutinized.

1.3.2.2. Porous structure and Perforated Cylinder

Porous structure or perforated cylinder is a passive flow control technique that does not require any energy input as well as splitter plates. This method allows manipulating the flow in a desired fashion without changing the geometrical shape of the bluff body. Just like splitter plates, porous structures have been studied and attracted notice in recent years. Easy implementation, low cost, consistency and keeping the geometry unchanged make this method preferable and useful for suppressing the vortex shedding and reducing the drag. This method is a beneficial alternative to the active flow control methods due to the unnecessity for energy input and complex actuators/sensors.

Lots of useful experimental and numerical results have been reported by the researchers and this method took place in literature. The methodology utilized in this passive control method comes into existence by separating the bluff body surface from the direct flow by a porous interface. Here the logic is to create an intermediate flow that decreases the boundary layer effect and especially reducing the flow velocity. When a permeable cylinder is located concentric to the inner cylinder, the flow encounters with permeable surface and velocity gradients is reduced between the outer permeable cylinder and inner cylinder. This allows having more stable shear layer that the effect of transition waves and flow separation are less dominant, resulting less drag force.

In this study perforated cylinder is implemented as well as splitter plate. And a combined or hybrid passive control method, which consists of splitter plate and perforated semi circular cylinder, is studied experimentally.

1.3.2.3. Surface Roughness

In underwater engineering applications, attenuation of vortex shedding is quite a bit important due to the destructive effects of VIV for marine risers, underwater pipelines etc. the importance of controlling the vortex shedding and VIV gave rise to some flow control techniques and surface roughness is one of them. Surface roughness is an effective way to suppress the vortex shedding and it has also a great impact on the drag coefficient around a circular cylinder at a certain Reynolds number range. Because the drag coefficient is related to the separation point and since the surface roughness alters the separation point it is also has an effect on drag coefficient. When a flow takes place around a circular cylinder, the surface roughness leads to a shift in the separation point along the body and this rough surface accelerate the transition into a turbulent flow range. So it changes the wake flow structure by changing the flow separation point. O-ring and trip wire are just some of the surface protrusion methods and they are utilized widely in literature.

1.3.2.4. Base Bleed

Base bleed is another passive flow control method that is useful for suppressing the vortex shedding around bluff bodies. It also has been studied widely as well as other passive control methods. Consistency, easy implementation and low cost make it an advantageous control method for flow control. This method is applied to bluff bodies by making a slit or some other gap on the blunt base to make the flow pass that gap as well as around the body and generate a secondary flow. Base bleed is also an effective and well-known method for vortex shedding suppression at some supercritical Reynolds numbers as well as other passive control methods.

2. PREVIOUS STUDIES

To investigate the flow structure around a bluff body experimentally, a researcher needs to create an archetype of the real engineering or environmental application. Since the real applications exposed to fluid flow around the bluff body, air and water tunnel is widely utilized to examine the flow around a bluff body. In the present study, even though water channel was utilized, the compilation of previous study involves air tunnel, water channel and even some numerical studies. Flow around bluff bodies and control of this flow and vortex shedding downstream of a circular cylinder have been topic of too many studies and lots of investigation have been carried out. Among the other cylindrical shape squared and circular cylinders are the most popular ones due to their significance and prevalence in the real engineering applications. In literature, even though the spherical, cone and square bodies were investigated, circular cylinder is still the most prevalent one to examine. And because of significance and prevalence in real life applications and being the keystone of the present study, the circular cylinder will be the main issue of this previous studies title.

Another concern of the flow around bluff bodies is the control methods that are used for attenuation of vortex shedding, suppression of VIV and reduction of drag/lift coefficient. Flow control methods are categorized in two groups as active and passive according to their energy requirements. Active flow control techniques need an external energy input, while passive control is based upon the modifying the geometry or adding external geometries to the flow. Although many investigations have been carried out about active and passive control methods, the passive flow control was analyzed in a more detailed way, since the present study involves two passive control methods (splitter plate and perforated cylinder).

2.1. Passive Flow Control Techniques

Passive control methods have remarkable advantages over active control methods to control the flow and vortex shedding downstream of a circular cylinder. Because passive control methods do not require an external energy input and complex actuators, and implementation of passive methods are easier than active ones. The previous techniques utilized as passive control involves basically splitter plates, surface protrusion, base bleed, adding porous elements etc. and the basic passive control methods will be investigated and introduced.

2.1.1. Passive Control by Splitter Plate

Using splitter plate as a passive control method is one of the most effective and prevalent technique to control the flow and suppress the vortex shedding. Easy utilization, low cost, consistency and convenience to observe experimentally; making splitter plate a salient method. This method has the ability to manipulate the whole flow characteristic and wake structure, and the first study of splitter plate date back 1950s.

Roshko (1954) carried out some experiments about vortex shedding downstream of a circular cylinder and found successful results of splitter plate for suppression of vortex shedding. He conducted the experiments at Re=14500 by using a plate that the length of 5D (D is the diameter of cylinder) located at the cylinder base and he was able to attenuate the vortex shedding completely. Moreover, the splitter plate gave rise to an increment in the base pressure and a reduction of net drag force. Another observation that he made was that when the plate was situated downstream of the cylinder at the distances of lesser than 4D, the plate was able to work efficiently in the wake, it diminished the Strouhal number and enhanced the base pressure.

Another experimental study was carried out in 1965 by Bearman (1965) about wake flow behind a two dimensional bluff body that a splitter plate attached to it. He determined that the space between fully formed vortex and model base was adversely proportional to the base pressure coefficient. In addition to this, he classified the flow into five category, as for that the distinctive wake behaviors along with the increment in the length of the splitter plate.

Gerrard (1966) investigated the vortex generation mechanism and tried to explain that mechanism in detail. He also examined the frequency, size, formation and influence of vortex behind a circular cylinder at $Re_D=2x10^4$. He accounted for the influence of the splitter plate on the vortex shedding frequency in the sense of the frequency determining mechanisms in the vortex formation region and the shear layer diffusion length. One can make inferences from his study that the Strouhal number diminishes when the splitter plate length is less than D (cylinder diameter), but it increases for D<L<2D. Over and above these, he proposed that the vortex formation zone under a strong elongation when the splitter plate is used and two modes of vortex formation could arise as for that the length of the splitter plate and the space between splitter plate and the experimental model.

Apelt et al. (1973) and Apelt and West (1975) carried out a consecutive experimental studies to scrutinize the effect of the splitter plate on the flow characteristics by means of pressure distribution, flow visualization techniques and frequency of vortex shedding. The consequence of this experimental study gave lots of useful and effective details about flow mechanism by the use of splitter plate. The splitter plate led to drag force reduction, increment of base pressure, narrowing of the wake width and alteration of the Strouhal number. Another contribution of their study was the change of wake flow structure and other flow mechanisms according to the length of the splitter plates. The short plates were utilized to stabilize the separation points increasingly and diminish the wake width with increasing plate length. In addition to that, the trailing edge of the short plates facilitates a fixed vortex formation point. On the other hand, the long plates prevent the interaction of the discrete shear layers and diminished roll-over effect of the vortices. And finally, enhancing the plate length (long plates) enabled to annihilate the vortices from crossing the base line.

Unal and Rockwell (1988) split the wake region into two discrete regions and defined them as the pre-vortex formation region and post-vortex formation region. They discovered that the interaction between the wake and splitter plate was able to control the instability of the near wake on a large scale.

Nakamura (1996) conducted a series of experiments to examine the vortex shedding mechanisms of different cross-sectional shapes by making use of an extended splitter plate. One observation that he made is that the dynamics of the wake is determined by the impression of shear layer instability. He discovered that the Strouhal number ascends gradually in accordance with increasing the length of the splitter plate. Additionally, the experimental study of Nakamura (1996) comprehended single-layer instability and the formation of vortex shedding when an extended plate is attached to the bluff bodies (circular and semi circular cross section) with or without a rectangle shape block. Basically, four different bodies that they used had the splitter plate attached to them. The dimensional parameters that were designated for the circular cylinder can be collocated as in this way; the diameter of the circular cylinder (D) which was 20 mm and the 2 mm thick plate and when it comes to calculate the length of the cylinder, dimensions were taken from the center of the cylinder. This study revealed that utilization of splitter plates with the bluff bodies which have divergent structural shape is mostly depends on Strouhal number (St). The significance of the Reynolds number (Re) and cross-section geometry were reported to be less dependent.

Another study of vortex shedding mechanism downstream of a circular cylinder and interaction of splitter plate with the vortex shedding were carried out by Kwon and Choi (1996) at the 80-160 Reynolds number range. Their study revealed that the vortex shedding frequency change in a similar fashion as the earlier studies for the $Re_D \geq 120$, however the frequency of vortex shedding diminishes gradually as the plate length enhances for the $Re_D \leq 100$. They predicate the ascended shedding frequency to a formation of the secondary vortex at the edge of the splitter plate for L>D and the ReD≥120. And that secondary vortex formation near the trailing edge of the splitter plate may accounts for the origin of the vortex induced noise.

An important and illuminative study was carried out by Anderson and Szewczyk (1997) and it revealed that utilization of splitter plate stabilize the transverse flapping of the discrete shear layers, so that reduction of the three-dimensionality level in the vortex formation region can be accomplished. In addition to this, splitter plate reduced the momentum thickness of the shear layer more or less 45% in opposition to the plain cylinder case.

Ozono (1999) indicated that in the presence of splitter plate, different distances between the cylinder base and the tip of the splitter plate have an effect upon the Strouhal number and make it go beyond the natural vortex shedding frequency of the plain cylinder case. The reason of this situation is explained as that when the flow is compelled to the gap between the splitter plate and the cylinder, shear layer separated from the gap side and results in enhanced interactions in the near wake.

Zhou et al. (2005) carried out a numerical investigation to suppress the fluid forces on a squared cylinder in cross-flow by the help of flat plate. They concluded that the presence of control plate alters the flow characteristic completely in the front region of the squared cylinder. The net drag force exerted on the cylinder and the total drag force on the bodies (squared cylinder and the attached flat plate) was reduced significantly by the flat plate. For a specific flat plate height, the optimal reduction of the drag force that is exerted on the squared cylinder and the ideal location of the plate are determined in this study. Moreover, they discovered that when the flat control plate is utilized, amplitude of the fluctuating lift on the cylinder can be attenuated. They reported that, when the control plate is located to a proper position and height of the flat plate is regulated to a certain value, the fluctuating lift can be suppressed completely.

An extensive experimental research was carried out by Akilli et al. (2005). They analyzed the effects of discrete splitter plates which were located at different distance from cylinder base on the vortex shedding suppression in shallow water by means of PIV (Particle Image Velocimetry). To explain the flow characteristic in detail, velocity vector field and associated vorticity contours, streamline topology and Reynolds stress concentrations were utilized. The splitter plates utilized in the experiments had variable thickness and constant length of 50 mm, which was also the diameter length of the cylinder. Another variable in the experiment was the distance, which it was ranged from 0 to 2D, between the cylinder base and the leading edge of the plates. For better comprehension of the flow characteristic of different arrangements on suppression of the vortex shedding the gap ratio (G/D) and the plate thickness ratio (T/D) were defined. Despite the fact that, suppression of vortex shedding was achieved considerably for the gap ratio between 0 and 1.75D, almost no effect was determined when the gap ratio was 2D (Figure 2.1). The effects of plate thickness were also investigated according to thickness ratio which has values of 0.016, 0.04 and 0.08 and the results showed similarity to the effects of gap ratio. After passing the splitter plates, the oscillation takes place with smaller frequency than the natural frequency of the bare cylinder.

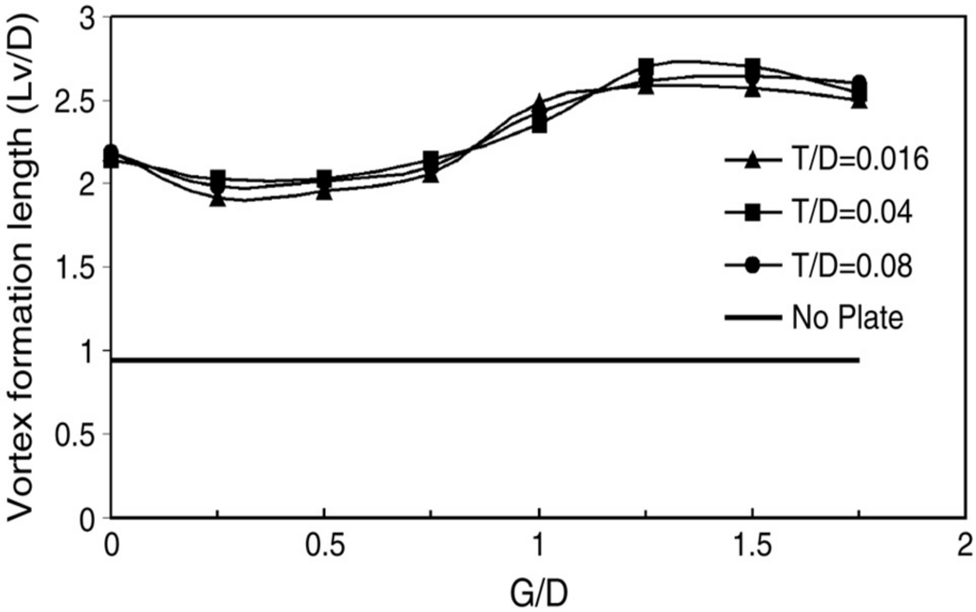

Figure 2.1. The change of vortex formation length according to gap ratio for three different splitter plate thicknesses. (Akilli et al., 2005)

Turki (2008) numerically scrutinized the flow control by attaching a splitter plate behind a squared cylinder in a horizontal channel. The study was carried out for fixed position cylinder at Reynolds number varies between 110 and 200 and blockage ratio ($\beta = h/H = 1/4$) was kept constant. He also investigated the possible influences of the splitter plate length and its position in the wake region on the drag and lift coefficients and the Strouhal number. He made a deduction that, for a given Reynolds number the Strouhal number indicates two distinct behaviors as the splitter plate length changes. Another observation that he made that, the change of Strouhal number (St) and drag coefficient (C_D) depends on the splitter plate location (G). When the Reynolds number range between 150 and 200, sudden increment in St and C_D takes place at the optimal location of splitter plate (G= 3.27).

Akilli et al. (2008) scrutinized the effect of splitter plate to the vortex shedding downstream of a circular cylinder experimentally. But this time they conducted the experiments to determine the effects of splitter plate length and they located the plates adjacent to the cylinder in shallow water. The Reynolds number was kept constant at the value of 6300 throughout the experiment. To analyze the flow characteristic according to the length of the splitter plate, L/D was designated in this study and this value ranged from L/D=0.2 to L/D=2.4. Velocity distributions and streamline topologies evidently proposed that the varying length of the splitter plate has a significant influence on the flow characteristic. The crucial conclusion that this study indicated, the flow characteristic in the wake region change abruptly up to L/D=1.0, however over this value, slight changes takes place in the flow characteristic.

Assi, Bearman and Kitney (2009) utilized a two dimensional control plates and obtained successful results. They accomplished the suppression of vortex shedding and VIV of a circular cylinder and by using the control plate they were able to reduce the drag coefficient inferior to that the drag coefficient of the fixed plain cylinder. They also pointed out how the vortex induced vibration can be annihilated in a practical way by the help of control plates that are capable of rotating without constraint. The attenuation of the drag coefficient reached up to 60% of those fixed plain cylinders. The maximum Reynolds number value that was utilized 30000 in this experiment.

Shukla et al. (2009) studied flow around a circular cylinder and preferred hinged-rigid splitter plate rather than fixed ones. The hinged-rigid plates utilized in the experiment made out of two plastic sheets having the thickness of 100 μm and very flexible plastic sheet of 30 μm thickness which was located between them. PIV technique was utilized to carry out the experiments and to analyze the flow characteristics. In this study the two primary parameters were designated as Reynolds number (Re) and the ratio of splitter plate length to the cylinder diameter (L/D). In other respects, the relative mass of the plate, the stiffness and the internal damping effect of the hinge were not taken into consideration in this study, in other words they are neglected and assumed that they had no effect on flow characteristic. The oscillation of the splitter plate leads to instantaneous changes in the magnitude and character of it and this situation may cause vortex induced vibration. This study emphasized the significance of the L/D ratio for specifying the magnitude and the characteristic of the oscillations in the hinged splitter plate case. From the experimental results they concluded that as the Reynolds number increase, the oscillation of the splitter plate increase and after a significant value of Reynolds number the oscillations of the splitter plate remain unchanged. The most important discovery of the experiment is that there are three distinct facts for three different splitter plate lengths. Firstly, for the small lengths ($L/D \leq 3.0$) periodic oscillations were observed. Secondly, when the splitter plate length is ascended beyond $L/D \geq 4.0$, the oscillations behaves in aperiodic manner with smaller amplitudes. And finally for the case of $L/D \geq 5.0$ the hinged splitter plate loose its character and behave like fixed splitter plate.

Gim et al. (2011) scrutinized the flow characteristic of the case in which control rods of different sizes were utilized behind a circular cylinder by means of particle image velocimetry technique in water channel. The experimental study was conducted for different control rod sizes and cylinder diameter of 50 mm. Another variable parameter was the Reynolds number and it ranges from 5000 to 20000. Time averaged velocity field, turbulence intensity and Reynold stresses were acquired in this experiment. And when they deduced from the parameters above that the cylinder wake was notably affected by the presence of the control rods due to the interactions of the vortex pairs formed in the upper and lower shear layers. So we cannot mention about an optimum rod size for controlling the flow, since the rod size and Reynolds number are both variable parameters.

Igbalajobi, McClean, Sumner, and Bergstrom (2013) examined the flow behind a circular cylinder to observe the effects of splitter plate to the flow structure at the $Re=7.4 \times 10^4$. In this study, they utilized four different type of cylinder aspect ratios (AR= 3, 5, 7 and 9) to determine the drag coefficient and the Strouhal number. Throughout the experiment, the cylinder height was kept constant and the splitter plates, which have different lengths (L/D= 1, 1.5, 2, 3, 5 and 7), were situated on the centerline of the wake. Also the relative boundary layer thickness on the ground plane was kept constant as well as cylinder height. Very effective drag coefficient reduction was achieved by the aid of the splitter plate in this experiment for the infinite circular cylinder in comparison with the finite one. They determined that the most effective parameters of the experiment as AR=9 and splitter plate length ratio (L/D) between 1 and 3. The drag reduction ratio that they obtained with the help of these parameters was 12% for the infinite circular cylinder configuration. Consequently they reported that when the splitter plate becomes longer, drag coefficient ascends gradually until the value of those bare cylinder.

Shukla, Govardhan, and Arakeri (2013) placed a flexible splitter plate to the near wake of a circular cylinder and studied the flow behavior and possible effects of that flexible splitter plate. The splitter plate used in the experiment had a conformation that it can change shape due to the unsteady forces of the flow. They defined the splitter plate as flexural and designated flexural rigidity (EI) for the splitter plate. The other designated parameters of the study are the plate length (L) and the flow speed (U). The flexural rigidity exhibit the behavior of travelling wave type deformations of splitter plate. K* stands for the bending stiffness in this study to comprehend the effect of flexural rigidity better and has the formula of $K^*= EI/0,5\rho U^2L^3$. They observed that when the speed is not too high periodic oscillation of plate with the amplitude of 0.5D takes place and it is referred as mode I. When the flow speed becomes higher the splitter plate oscillations is accepted as aperiodic with large changes in amplitude depending on time. After a certain increase in the flow speed, the splitter plate begins to oscillate in a periodic manner and this is known as mode II. The remarkable indication they discovered is that, when the plate oscillation is periodic, Strouhal number has almost same value (0,2) with bare cylinder case while the splitter plate motion frequency is lower in the aperiodic regime. They interpreted from the experimental results that although shorter plates have remarkable differences, the oscillation of splitter plates with varying lengths point out that the plates which are notably larger than the formation length of the cylinder wake have similar indications.

Gozmen, Akilli and Sahin (2013) conducted two separate experimental studies in 2013 for suppression of vortex shedding. One of control method is controlling the flow by means of permeable cylinder and the other one is suppression of vortex shedding by splitter plate. PIV technique was utilized in both study and flow characteristic like streamline topology, Reynold stresses, velocity profiles were scrutinized extensively. But the one with passive control method by means of splitter plate is our concern as we are looking for splitter plate study in this title. Two primary parameters were propounded in this study as the ratio of splitter plate length to the cylinder diameter (L/D) and the ratio of splitter plate height to the water level height (h_p/h_w). The Reynolds number based on the cylinder diameter was to be 6250 in the study. According to their experimental study, they proposed (L/D) =2 and h_p/h_w=1 values to be the most consistent and effective parameters for suppression of vortex shedding separately. However, the value h_p/h_w=1 was not compatible with the different plate length and indicated different behaviors in each case. Although the L/D and h_p/h_w are interrelated and affect each other, they proposed the value of h_p/h_w=0,5 for the case the height ratio and the plate length are taken into consideration together.

An experimental study of vortex shedding formation behind a square cylinder was carried out by Sarioglu (2017). He located a fixed splitter plate to the downstream direction of the cylinder and performed his study in subsonic wind tunnel. The length of the splitter plate and cylinder were chosen to be 30 mm and incidence angle of the cylinder range from 0° to 45°. The Reynolds number in which the experiment was conducted is $3x10^4$. Despite the fact that, he managed to attain the minimum drag coefficient at the approximate value of 13° incident angle, the abrupt increment of Strouhal number took place. However, by arranging incident angle to 0°, he managed to diminish drag coefficient about 20% and made

Strouhal number decrease. He deduced from his experimental study that the minimum drag coefficient takes place at the 13° incident angle, whereas maximum drag coefficient occurs at the 20°.

One of the very recent experimental studies was conducted by Ozkan, Fırat and Akilli (2017). They investigated the influences of splitter plates that have different porosity ratios on the drag coefficient by locating the plates at a specific angle with respect to the flow direction. First they applied dye visualization technique to attain qualitative results and to obtain general flow structure. Than they applied Particle Image Velocimetry technique to acquire the quantitative results like streamline topology, vorticity contours etc. and evaluate the results in a more comprehensive manner. Both the dye visualization and PIV experiments were carried out in water channel. To determine the possible effects of splitter plate porosity ratio to the flow structure in detail, they kept the Reynolds number and diameter of the cylinder constant throughout the experiment. The porosity ratio of the splitter plate (β) was defined as the ratio of permeable gap area to the whole surface area. The porosity ratios (β) were calculated with respect to this definition is to be 0.4, 0.5, 0.6, 0.7 and 0.8. For the porosity ratios of β= 0.4, 0.5, 0.6, although the drag coefficient that is effective on the body increased, the splitter plate was able to suppress the vortex shedding. On the other hand, we cannot accept the porosity ratios of β= 0.7, 0.8 as effective parameters since hindering of vortex shedding has not been accomplished. However, these parameters may justify their utilization by reducing the vibration and fluctuating force acting on the body.

They also conducted the exact same experiments in the wind tunnel to evaluate the drag coefficient that is exerted the cylinder by utilizing all the parameters. The permeability of plate (β) and the angle of splitter plate with respect to the flow direction (θ) were the primary parameters for this experiment that carried out in the wind tunnel. They investigated the effect of splitter plate porosity, angle and presence to the drag coefficient of the cylinder. They observed that the presence of splitter plate has significant effect on suppression of vortex shedding and reduction of velocity fluctuations in the wake region. From the experimental results they deduced that plate porosity of $0.4 \leq \beta \leq 0.6$ and angle of plate that range between $45° \leq \theta \leq 90°$ has notable effect of flow fluctuation reduction, diminished turbulent kinetic energy and also less vortex induced vibrations. They also propounded that in this study, it would be good to utilize this method where the control of vortex induced vibrations is needed. But one should apply the effective parameters, which are $0.4 \leq \beta \leq 0.6$ and $\theta \geq 30°$, to accomplish the desired control of flow. It is also should be taken into consideration that the increment of drag coefficient for some parameters.

2.1.2. Passive Control by Adding Porous Element

Adding porous elements to the flow around bluff bodies has been applied significantly and lots of numerical and experimental studies have been conducted. This flow control technique is a passive control technique, since the unnecessity of energy input or complex actuators/sensors. The aim is to put a permeable structure which allows the flow to pass from the permeable structure in a restrained manner. By the help of porosity of the permeable element, an intermediate flow takes place between the bluff body and permeable structure. Thus flow velocity is reduced and make the drag coefficient diminishes. In literature, porous structure utilized around the bluff body show great diversity geometrically and researchers have always been tried to find the most effective and consistent way of controlling the flow characteristic.

Bruneau and Mortazavi (2004) and Bruneau and Mortazavi (2006) carried out a few numerical studies to provide a controlled flow by using porous elements. They applied a numerical flow simulation that utilizing Navier-Stokes equations. By the help of permeable media around the squared cylinder, they intended to alter the boundary layer structure and vortex shedding mechanism. They designated permeability coefficient (K) and applied it to the Navier-Stokes equations. They also specified three different Reynolds numbers as follows Re = $3x10^2$, $3x10^3$, $3x10^4$ and studied three different flow regimes. From the investigated numerical results they deduced that, for the Re = $3x10^2$, the drag coefficient of the squared cylinder diminishes severely due to the transient regime of the Re = $3x10^2$. With the well-defined permeability coefficient the Reynolds number is affecting-factor for regulating and controlling the flow characteristic when it is at higher values. However they indicated that reducing the drag coefficient and suppressing the vortex shedding downstream of the cylinder is not achievable for all cases. Nevertheless, they concluded that, it is accomplished that in the presence of porous element the reduction of drag coefficient up to 40%, attenuation of vortex shedding and controlling the flow remarkably.

Bhattacharyya, Dhinakaran, and Khalili (2006) conducted a study in a numerical manner to examine the flow characteristic and flow concentration around a permeable cylinder. They designated four different parameters to evaluate the flow mechanisms as follows Reynolds number (Re), Schmidt number (Sc), Darcy number (Da) and porosity (ε). They concluded from the results that, when the drag coefficient (C_D) comes across with the permeable cylinder diminishes for the case when Reynolds number is high and Darcy number is low. For the lower Reynolds numbers, the results indicated that drag coefficient is in tendency to diminish as the permeability of the cylinder increases. In addition to those results, further analysis indicated that when the Darcy number ascends, the separation angle and the wake length reduce.

Bruneau et al. (2008) carried out a numerical study on a square back Ahmed body by utilizing seven distinct types of porous layers between a solid body and fluid. They interpreted the results in terms of vorticity fields, root mean square of the lift coefficient (C_{Lrms}) and drag coefficient. For every single configuration, they obtained very distinctive consequences from this numerical study. To give an example, for the configuration 1, the rear side of the porous layer led to vertical jet flow, hence the drag coefficient ascended as well as the frequency of vortex shedding. When the conformation of porous media becomes transient, from porous to solid structure, the pressure differences and velocity gradients increase. Thus the total drag enhanced nearly 22%.

Zhao and Cheng (2010) carried out a numerical study to look for the effects of porous layer on the lift coefficient and their purpose was to reduce the lift coefficient. They designated the Reynolds number values as follows Re= 10^3, $2.5x10^3$ and $5x10^3$ and finite element method was utilized to investigate the flow structure inside and outside of the permeable structure in this numerical study. And they justified the utilization of the porous layer by reducing the lift coefficient for the proper selection of porous layer. But the quantity of lift coefficient reduction depends heavily on the Reynolds number, the porosity ratio and the Forchheimer coefficient. Moreover they concluded that lower lift coefficient is attainable if the thicker permeable structure is utilized. They also investigated that the existence of critical Darcy number (Da), where the minimum RMS lift coefficient takes place, as it can be seen from Figure 2.2.

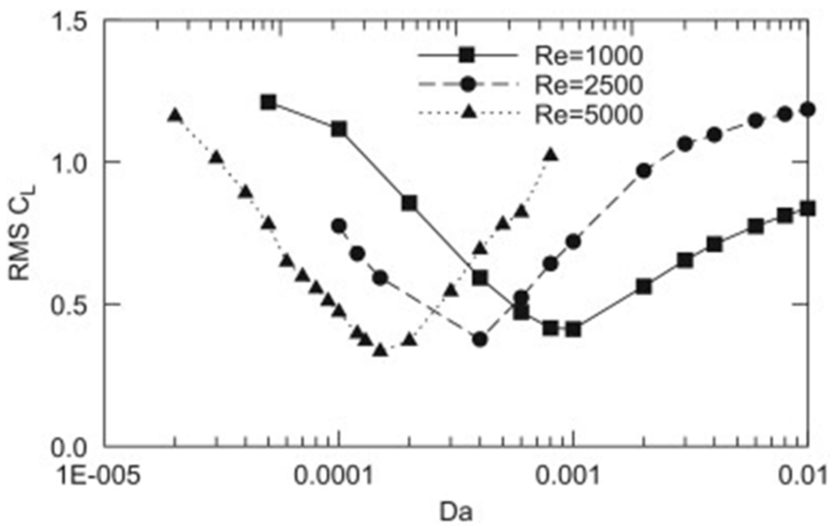

Figure 2.2. Change of RMS lift coefficient with different Darcy number for different Reynolds numbers (Zhao and Cheng, 2010)

Ruck, Klausmann, and Wacker (2012) carried out an experimental study to investigate the drag resistance of a cylinder in a wind tunnel with the aid of porous coating at the range of Reynolds number, Re= 10^4 to $13x10^4$. The porous coating utilized in the experiment was made out of polyester (Poret-Ester-Foam) that had various thicknesses of 3, 5 and 10 mm. The porosity was identified as pores per inch (PPI) in this study and the PPI values of 10, 20 and 30 were investigated. Additionally, they conducted the experiments with "full coating" and "half coating" and investigated their effects to the flow. Consequently, they designated enhanced flow resistance for the case that full coating is utilized. On the other hand, the flow resistance diminished when the half coating was applied.

Ozkan, Oruc, Akilli and Sahin (2012) designed an experimental configuration in order to investigate the influence of porous outer cylinder and its diameter on the flow behavior in the wake region. The diameter of the inner cylinder (controlled cylinder) was kept constant (d=50 mm) throughout the experiments and the diameter of the outer cylinder (control cylinder) varied to the values of D= 60, 70, 90 and 100 mm. Another variable parameter of the experiment is porosity ratio which has the values of β= 0.4, 0.5, 0.6 and 0.7. To make a control case, the bare cylinder (inner cylinder) was investigated to determine turbulence intensity, and the result compared with the other configurations which the porous outer cylinder was used. And for better understanding the diameter ratio is defined as the diameter of the inner cylinder to the diameter of the outer cylinder (d/D). For some diameter and porosity ratios, suppression of vortex shedding was achieved. The results obtained by the PIV technique indicated that the utilization of the outer cylinder affect the maximum values of turbulence intensity positively. In general, the both vortices on the separate side of the cylinder were affected by diameter ratio (d/D), regardless of the porosity ratio of the outer cylinder. They also accepted that the results of drag and lift coefficients provide insight to comprehend the influence of the porous outer cylinder.

Gozmen, Akilli, and Sahin (2013) conducted an experimental study in order to suppress the vortex shedding downstream of a circular cylinder. A permeable outer cylinder that has the constant diameter of 75 mm was used in the experiment. The porosity values of β=0.4, 0.5, 0.6, 0.65, 0.7, 0.75, 0.8 and 0.85 were investigated in order to comprehend the effect of divergent porosities. Such a wide range and close values were utilized for better comprehension of the possible effects of the porosity values over flow structure. The porosity ratio was defined as the ratio of pores area on the body to the whole surface body area. Throughout the experiments, the free stream velocity, Reynolds number and the diameter of the inner cylinder was remained constant. The conclusion that they made, among other porosity ratios, the porosity value of β=0.7 is the most effective ratio for controlling the flow around the cylinder. Compared with the bare cylinder case, almost 70% reduction was accomplished with the help of outer porous cylinder.

Besides experimental studies, numeric studies were also carried out and one of them was conducted by Valipour, Rashidi, Bovand, and Masoodi (2014). They conducted notable analysis numerically for controlling the flow. Their numerical study consists of permeable diamond-square cylinders and two dimensional and steady flow takes place. The numerical experiment results were compared with the wake length according to Darcy number, and the pressure coefficient exhibited a tendency to diminish when the Darcy number increases.

Mimeau et al. (2014) conducted numerical study that utilizes passive control method with porous coating around a two dimensional semi circular cylinder. The Vortex-penalization technique that allows computing concurrently the fluid, porous and solid layers was preferred for this numerical study. They anticipated this numerical study to be successful, to hinder the vortex formation in the boundary layer, to suppress vortex shedding, to reduce the drag coefficient and unsteady forces and lastly to attenuate the vortex induced vibration. They designated the Reynolds number of Re= 550 and Re= 3000 at the transitional flow regime. The first parameter defined in this study is porous layer permeability (λ).

The value of $\lambda = 1$ stands for high permeability, while 10, 10^2 and 10^3 values stand for lower permeability and $\lambda = 0$ means that there is no control. And the second parameter of the study is porous layer thickness (τ). At first, results indicated that higher λ values more effective than lower values of λ. But the most useful and consistent parameters that results were obtained for the drag reduction were those with intermediate porosity and thin layer thickness. They also indicated that intermediate porous ring on the edge of the wall can be applied in real engineering applications easily and in a cheap way.

Pinar et al. (2015) carried out an experimental investigation in water channel and scrutinized the effects of shallow water to the flow around perforated cylinder. They utilized perforated circular cylinders that have various porosity ratios (β) and defined this ratio as the gap area to the whole surface area of the cylinder. In order to understand the effect of the porosity ratio better, they investigated the porosity ratios between $0.1 \leq \beta \leq 0.8$ while they kept the other parameters constant. They regulated the desired Reynolds number according to the free stream velocity (U) and cylinder diameter (D). To scrutinize the effect of porosity, they investigated another cylinder which has the same dimensional properties without porosity. And they compared these results with the permeable cylinder results according to velocity gradients, vorticity contours, turbulence kinetic energy and Reynolds stress values. It was concluded from this experimental study that, porosity ratios of $0.4 \leq \beta \leq 0.8$ is efficient for suppression of Karman Vortex Street. But it should be taken into consideration that the effect of drag coefficient reduction of the perforated cylinder should also be investigated for these parameters.

Oruc, Akilli, and Sahin (2016) carried out an experimental study by utilizing a passive control technique. They investigated the possible effects of perforated cylinder as an external control element to the flow characteristics, regardless of the existence of the inner cylinder. Particle Image Velocimetry technique was utilized to obtain useful results. The experiments were conducted for three different Reynolds number. Consequently, control of the flow was certainly accomplished and also elongation of vorticity layers was observed. Another useful observation they made is that a certain reduction of Turbulent Kinetic Energy and Reynolds Shear Stress takes place in the wake region.

Durhasan et al. (2016) conducted a series of experimental study about the effects of perforated fairing on vortex shedding suppression of a circular cylinder in shallow water by means of PIV technique. They investigated the effect of three different arc angle (α= 120°, 150°, 180°) and porosity ratio of fairing (β= 0.3, 0.4, 0.5, 0.6, 0.7 and 0.8). Turbulent kinetic energy and Reynold shear stress in the wake region were examined at the Reynolds number of $Re=5x10^3$. They concluded that the opposing shear layers weakened remarkably compared with the bare cylinder case. The Reynold shear stress value was diminished up to 75% for the arc angle of α= 180° and location of maximum Reynold stress value was sent away further from the cylinder base. They deduced that the most effective flow control was accomplished for the β= 0.6 and α= 180° case.

Another experimental study carried out by Durhasan et al. (2016) was about perforated circular cylinders. They scrutinized the flow structure around the constant diameter perforated cylinders (100 mm) by means of PIV technique. Reynolds number was also kept constant value of 10000 with respect to perforated cylinder diameter. They examined the different porosity ratios in the range of $0.25 \leq \beta \leq 0.80$ and evaluate the flow structure according to turbulent kinetic energy, stream wise Reynolds stress, transverse Reynolds stress and Reynold shear stress statistics. They realized that by increasing the porosity ratio, β instabilities are significantly reduced in the wake region. Consequently, suppression of Karman Vortex Street was achieved by the aid of perforated cylinders, resulting in elongated and fragmented shear layers and weaker vortices.

Durhasan et al. (2019) carried out an experimental study in order to control the flow around a circular cylinder by locating a permeable cylinder around the inner cylinder concentrically. They designated two determinant parameter as porosity ratio (β) and diameter ratio of inner and outer cylinders (D/D_S). Reynolds number was kept constant at Re=5000 according to the inner cylinder diameter and porosity ratio varied from 0.3 to 0.7 were examined. They also investigated the effect of different diameter ratios (D/D_S = 0.4, 0.5 and 0.6). They observed that the vortex formation appears only in the gap between the cylinders and shroud generates its own wake flow structure for the porosity ratios of $\beta \leq 0.5$. Jet-like flow from the shrouds prevented the interaction of the upper and lower shear layers in the near wake. They also conducted force measurements in an air tunnel to unveil the effects of permeability on the drag coefficient. In comparison with the bare cylinder case, the drag coefficient of the cylinder with perforated outer cylinder was diminished notably. However, when the outer perforated cylinder was taken into consideration with the inner cylinder, the drag coefficient of these two cylinders was higher than the bare cylinder case due to the enhanced areas.

2.1.3. Passive Control by Surface Protrusions

Surface protrusion is a passive control technique that can be regarded as boundary layer control method in literature. The principle of this method is based on modifying the geometrical shape of the bluff body surface. By modifying the surface geometry this method becomes capable of delaying the boundary layer separation. Thus manipulation of vortex shedding formation, unsteady forces, drag and lift coefficients and vortex induced vibrations can be applicable by surface protrusions method. For the applications that surface protrusion is utilized, one should know there is a strong correlation between surface roughness and drag coefficient. Up until now this method have been investigated and utilized broadly by the researcher and countless studies have been carried out in literature. Also easy implementation and consistency make this method noteworthy. Initial investment may be high due to chance of complex surface geometry may be needed, but when it is implemented once, the desired flow control can be achieved.

Achenbach (1971) conducted an experimental study in a wind tunnel to examine the cross flow around a circular cylinder by using surface protrusion and became pioneer for many researchers in this area. He carried out the experiments for a fixed cylinder that has sand grain shape as surface roughness model and Reynolds number of up to Re= $3x10^6$ was investigated in the study. He found out that when the surface roughness increases, flow has a tendency of faster change from laminar to turbulent. He contributed the literature and defined the term "drag crisis" that explained as the sudden drop of drag coefficient when the flow behavior turns from laminar to turbulent at the critical Reynolds number. He concluded that this abrupt reduction could be annihilated by enhancing the surface roughness. In other words, when the boundary layer flow turns to turbulent state from laminar state, the net drag exerted on the cylinder decreases rapidly at the critical Reynolds number. And as the surface protrusion enhances, the effects of drag crisis phenomena can be attenuated.

Another experimental investigation was made by Achenbach and Heinecke (1981) in the Reynolds number range of Re= $6x10^4$ - $5x10^6$ to modify the vortex shedding frequency downstream of a circular cylinder. Surface protrusion pattern utilized in this experiment was chosen to be pyramidal roughness model as can be seen from figure 2.3. The study was conducted in the wind tunnel and they measured the local pressure and drag coefficient with respect to different surface roughness parameters and Reynolds numbers. They realized the fact that enhancing surface roughness gives rise to critical Reynolds number to decrease, hence remarkable reduction in drag coefficient takes place. They also found out this surface roughness has an effect to the flow at the subcritical Reynolds numbers, but these effects are not significant as those at the critical Reynolds number.

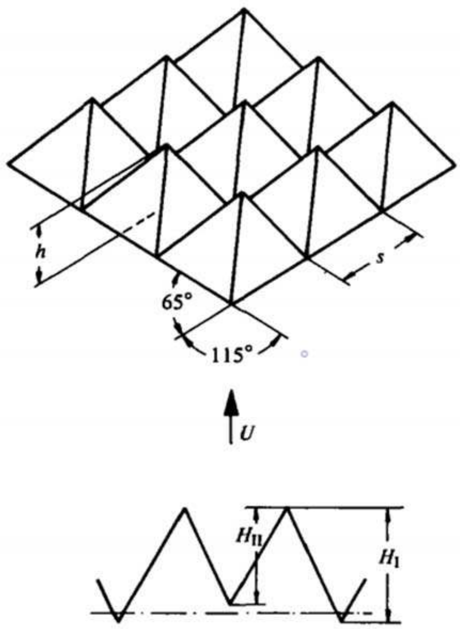

Figure 2.3. Pyramidal surface patterns (Achenbach & Heinecke, 1981)

Kawamura, Takami, and Kuwahara (1986) analyzed the influence of the high Reynolds number to the flow on a circular cylinder in the presence of surface protrusions. They carried out both numerical and experimental study and began the investigation with the Reynolds number, Re= $1.2x10^3$. They obtained the results from both numerical and experimental methods and when they compared these separate results, they realized that the results correspond to each other. Remarkable and abrupt reduction of the drag coefficient was acquired when the Reynolds number had the value of Re= 2×10^4 as shown in figure 2.4. The underlying reason of this reduction of drag coefficient was that the small eddies generated on the surface in the vicinity of the separation points.

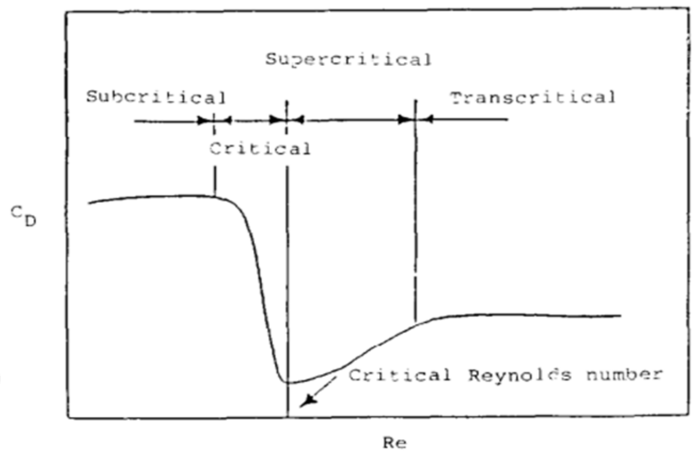

Figure 2.4. Reynolds number changes relevant to the flow a past circular cylinder (Kawamura et al., 1986)

Bearman and Harvey (1993) investigated the relation between surface roughness and drag coefficient and carried out an experimental study on wind tunnel. They applied dimpled pattern as the surface roughness model and Reynolds number varied between Re= $2x10^4$ and $3x10^5$. In comparison with the plain cylinder case, they observed that due to the dimple effect the critical Reynolds number took place at lower values. However, beyond the critical Reynolds number, dimpled cylinder indicated the same flow behavior (same drag coefficient) as plain cylinder, regardless of the dimples. In addition, dimpled cylinder had a lower drag coefficient than plain one at the Reynolds number range between Re= $4x10^4$ and $3x10^5$. Consequently, they reported that they did not utilize different type or scale dimples, so by the aid of applying different type of dimples reduction of drag coefficient can be attained on a larger scale.

Being aware of the accomplishment on reducing the drag coefficient of bluff bodies Merrick and Bitsuamlak (2008) conducted both numerical and experimental study. They carried out the study at high Reynolds numbers in order to have more controlled flow around a circular cylinder by the aid of surface protrusion that is applied to the exterior surface of the cylinder. According to experimental results they obtained, they could not find ideal roughness model for retarding the separation point of the flow and concluded that further investigation must be carried out for the aim of scale model testing.

From all the studies that were carried out, it is deduced that utilization of the surface protrusions to the bluff bodies can change the pressure distribution and the drag coefficient downstream of the cylinder in a positive manner. Up until now, the surface protrusion studies mentioned above were conducted in the wind tunnel and this method associated with drag coefficient. Due to the present study is concerned with the vortex shedding downstream of a circular cylinder in deep waters to eliminate vortex induced vibration, experiments that were carried out in the water channel should also be investigated.

Allen and Henning (2001) conducted an experimental study to understand the effects of surface protrusion to the vortex induced vibration and the coefficient of drag around a circular cylinder with a large aspect ratio at the critical and supercritical Reynolds numbers. Surface roughness was designated as k/D (k is the height of average peak from trough of the surface protrusions and D is the cylinder diameter) and it became the key parameter for the investigation as well as Reynolds number. Experimental results indicated that the plain cylinder is more efficient for suppression of vortex induced vibrations than the other one in general. And when turbulent flow took place the drag coefficient of plain cylinder has a lower value. Moreover, up to a certain point, when the surface roughness increases the displacement is also increases and there is a correlation between the displacement and drag coefficient. Consequently, they determined that the surface protrusions model is determinant for this method.

Bernitsas and Raghavan (2008) investigated the surface protrusion effects to the vortex induced vibration of a circular cylinder. They applied protrusion to the surface by the aid of sandpaper strip and conducted the experiments in a free surface water channel at low turbulence. Several parameters were examined in this study. The first one is the reduction rate of vortex induced vibration (VIV) of the cylinder. Latter is the beginning and ending of protrusion and the last parameter is the thickness of the sandpaper base and grit size. They concluded that if the surface protrusions well-distributed in a homogeneous way, the VIV can be attenuated or even suppressed. They carried out an experiment similar to this study to reduce VIV (Bernitsas et al., 2008) with only one difference which is the Reynolds number. Their experimental consequences were almost the same for both study and their method was able to reduce the VIV.

Chang et al. (2011) studied experimentally flow around a circular cylinder in a water channel at high Reynolds number, which range between $3x10^4<Re<12x10^4$. To understand the effects of surface protrusions, they carried out the experiments with a plain cylinder and protrusive cylinder. They investigated the effects of roughness to the vortex induced vibration and how roughness modifies the vortex induced motion. According to experimental results, they deduced that the rough surface is more efficient for reduction of VIV and vortex induced motion than the smooth surface. They also concluded that the cylinder with surface roughness sheds five vortices per cycle, whereas cylinder with smooth surface sheds seven vortices per cycle.

Kiu et al. (2011) investigated the effects of uniform surface protrusion to the vortex induced vibration of towed cylinder at underwater. They made a conclusion from the experimental results, that the surface roughness has a significant effect on the hydrodynamic effects. As the surface roughness enhances, the maximum mean drag coefficient has a tendency to diminish. Another consequence of the study was that, Strouhal number has lower value for the case which smooth cylinder is used than the case that surface roughness was utilized.

When a flow passes around a cylinder, it exerts time-dependent drag and lift forces to the cylinder between a certain ranges of Reynolds number. The cylinder may be exposed to vortex induced vibration if it is not fixed properly like marine cables and underwater pipelines. The lift force generally induces cross-flow

(CF) vibration, while the drag force induces inline (IL) vibration and with a more general definition this is called VIV. Gao et al. (2015) investigated experimentally on these phenomena of VIV with the help of surface protrusions on a circular cylinder. To comprehend the effects of surface roughness, they designated displacement response, drag/lift and vibration frequency as the determinant parameters in their study. The observation that they made was, the displacement response diminishes as well as vibration frequency and the vortex shedding frequency ascends with the increment in the surface roughness. And according to their study, the drag coefficient diminishes remarkably with small surface roughness value beyond a certain value of Reynolds number.

Another experimental investigation about drag and lift coefficient according to different surface roughness was conducted by Zhou, Wang, Gho, and Tan (2015). They utilized two distinct surface protrusion models for their experimental study. In both methods, the cylinder covered with a uniformly distributed material. These methods are the netting and dimples as it can be seen from Figure 2.5. The experimental Results indicated that for the case which the dimpled cylinder is used, the reduction of drag coefficient by 30% is achieved compared with plain cylinder case. In addition to these results, they also determined that the root mean square lift coefficient of both rough surfaces is lower than those of plain cylinder case.

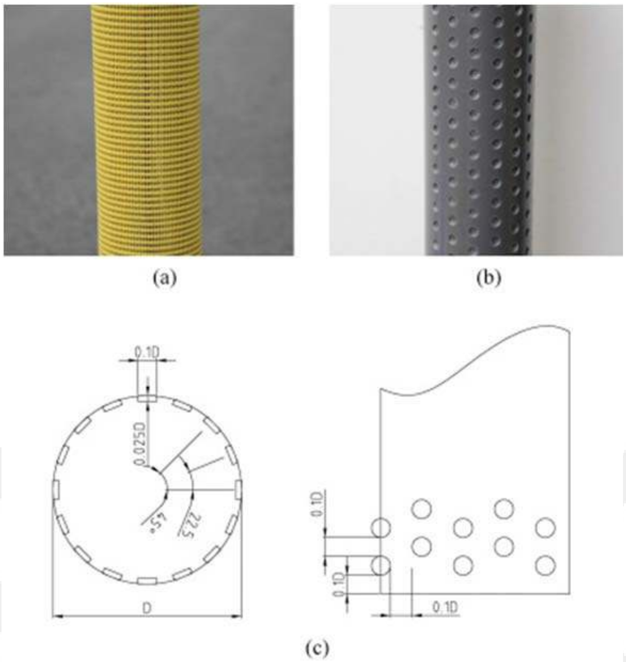

Figure 2.5. The rough cylinders with (a) netting (b) dimples. (c) details of the dimples (Zhou et al., 2015)

Rodríguez et al. (2016) carried out a numerical flow simulation to examine the surface roughness of cylinder with sand grain type surface roughness. Their intention was to determine the influences of this sand grain type surface roughness to the boundary layer of the circular cylinder and to the wake structure downstream of the cylinder. They made the comparison between the cylinders with and without protrusion to comprehend the effects to the flow and Reynolds number was determined as Re= $4.2x10^5$. They indicated that instabilities due to the roughness on the cylinder surface bring about an early transition to turbulent state. For this reason, the drag coefficient value of C_D= 1.122 was obtained which is higher than those of plain cylinder.

As indicated above in this title, the surface protrusion brings about abrupt and observable drag coefficient reduction of bluff bodies at subcritical Reynolds number. Another effect of the surface protrusion technique is that the delay of flow separation in the boundary layer. Consequently, it can be concluded that surface protrusion method can be applied for many engineering applications and it is worth to investigate in detail to control the flow characteristics.

2.2. Active Flow Control Techniques

2.2.1. Active Control by Feedback Control Method

This is an active control method based upon the idea of utilizing an actuator feedback by the help of convenient sensor. There are numerous investigations of this method as an earlier study, for instance Williams and Zhao (1989) applied feedback control method by the aid of experimental arrangement they designed. They obtained feedback of acoustic signals from hot-wires situated in the wake of a circular cylinder. Another early period feedback control method study was carried out by Park et al. (1994). Their investigation is based on the principle of feedback method, and they utilized two dimensional Naiver Stokes equations to carry out this study. And their purpose was to control Karman vortices at low Reynolds number around the cylinder. They stated that they suppressed the vortex shedding completely, under the circumstances of Reynolds number value of Re=60 and by the usage of single feedback sensor. They also concluded that when the location of feedback sensor is stationary, the vortex shedding can be suppressed by increasing the feedback gain (α). However further increase of the feedback gain endangers the flow consistency and beyond Reynolds value of 80 it is not possible to control the vortex shedding.

Roussopoulos and Monkewitz (1996) applied feedback control method in order to control Karman vortices by utilizing a nonlinear model. They determined the critical Reynolds number value as Re=47 according to the cylinder diameter. They reported that for relatively long cylinders, despite the fact that the actuation takes place on an equal basis over the entire span, suppression of vortex shedding can only be accomplished for span wise location.

Tao, Huang and Chan (1996) carried out visualization techniques to comprehend the flow behavior of the cylinder wake and flow behind the cylinder for the case that feedback method applied. They observed that the vortex shedding takes place for the no control case and it can be suppressed when the feedback method is utilized. Moreover, they indicated that the wavy character of the streak lines can be converted almost a straight line. Consequently, they concluded that the peak points indicated by the monitor probe are diminished by the aid of feedback control method.

Fujisawa et al. (2001) investigated the vortex shedding mechanism downstream of a circular cylinder at the intermediate values of Reynolds number. The experimental study they carried out is based on the principle as follows. First a feedback signal is obtained from the velocity gradients of the cylinder wake, than the rotary cylinder oscillations are controlled by the feedback signal. From the experimental results they concluded that the velocity fluctuations and fluid forces diminish in comparison with the uncontrolled case.

Fujisawa and Nakabayashi (2002) conducted a series of experiments to suppress the vortex shedding downstream of a circular cylinder with the aid of feedback control method with rotational oscillation. As being an active control method, this method utilizes a neural network model. Their purpose was to enhance the performance of the feedback method by using rotational oscillation. As being one of the most practical feedback control method, it was able to attenuate the lift force by 70% and the drag force by 16% on contrary to plain cylinder case which no control method applied.

2.2.2. Active Control by Generating Secondary Flow

Seal and Smith (1999) investigated experimentally the influence of steady suction to the turbulent flow. They utilized Particle Image Velocimetry (PIV) to determine the flow pattern by means of quantitative results and investigated the downstream and cross stream plane. They indicated that, surface suction provides, to diminish instantaneous turbulent vortex and its corresponding surface interactions in the symmetry plane, to annihilate the turbulent necklace vortex formation in the symmetry plane, and attenuate downstream vortex extensions. Moreover, it was reported that suction diminishes the frequency of the Reynolds-stress in symmetry plane and trailing edge, and provides more stable flow behavior.

Tensi et al. (2002) tried to control the flow around a circular cylinder by using unsteady blowing method (synthetic jet) at the Reynolds number value of Re=105 according to cylinder diameter. Synthetic jet productivity was evaluated according to delaying the flow separation and modifying the drag coefficient. Consequently, they made the conclusion that it would be appropriate to utilize zero-mass-flux type actuator (needs very little energy input) for further investigations and to control the flow around different type of bodies.

Glezer and Amitay (2002) indicated that when the synthetic jet located on a certain position over the cylinder, it can delay the flow separation at various Reynolds number (both in a turbulent or laminar boundary layer). They concluded that this delay is based upon enhanced interfering within the boundary layer. Additionally, the interactive relation between the synthetic jet and the cross flow has a significant influence on the separated shear layer and on the wake. The Reynolds stress values were diminished and this situation signify that the delay of flow separation not only stem from a transition in the boundary layer.

Feng et al. (2010) carried out a study in order to control the flow around a circular cylinder by an authentic synthetic jet located at the rear stagnation point. The suction duty cycle factor (k) designated as the ratio of the time duration of suction cycle to the blowing cycle and it is utilized as determinant to qualify the synthetic jet signal. They concluded that, when the suction duty cycle factor enhances, the momentum coefficient increases, and a more powerful synthetic jet vortex pair is created and it can arrive further downstream. This particular feature has a remarkable effect on the wake and vortex shedding of the cylinder.

Chen et al. (2013) studied experimentally in order to attenuate the vortex induced vibration (VIV) of a circular cylinder by applying the suction technique. Experiments were carried out in a wind tunnel that has a test chamber whose dimensions are 4 m width, 3 m height and 25 m length. The circular cylinder made out of acrylic has spring mass system and four suction holes (10 mm diameter) located at the lower side of it utilized for the experimental study. In a flow around bluff body, vortex induced vibration and corresponding dynamics are quantified in terms of pressure coefficient and aerodynamic force coefficients acting on the body, regardless of flow control. For this reason, corresponding flow parameters, the suction flow rate and the productivity of control method can be determined quantitatively. In the experiment, various suction flow rates applied to the flow and control of the flow could not be achieved at very low and very high flow rates. Alternatively, the maximum performance was obtained at the optimal suction rate on contrary to these values. Consequently, from the experimental results, it can be concluded that the steady suction flow control is a productive technique to diminish and suppress vortex induced vibration.

2.2.3. Active Control by Electrical Methods

Artana, Sosa, Moreau, and Touchard (2003) utilized a simple cylinder model and carried out an experimental study about time averaged flow parameters of the near wake by the aid of electro hydrodynamic actuator. This study was conducted for the cases which the flow is perturbed continually and the Reynolds number varied between $2300 < Re < 58000$. A wind tunnel was utilized to perform the experiments and electrodes that are parallel to the cylinder axis were used for this study. They made the deduction from the experimental results, although utilization of the actuator at the lower Reynolds numbers has remarkable influence on the near wake of the flow. However, for the case of higher Reynolds number, the actuator was not effective for delaying separation of the boundary layer.

Hyun and Chun (2003) performed an experimental study and applied ion wind method which is an active flow control technique. Their purpose was to control the vortex generation caused by the flow that in contact with the cylindrical surface. This technique is simply based on the utilization of electrical momentum that is obtained from ions and transferring this momentum to the flow. First the ions are generated in the strong electrical fields, than the electric momentum of these ions is transferred to the adjacent fluid. Thus fluid movement of the flow can be manipulated and this procedure is called ion wind method. H is one of the parameter they designated and it can be defined as the distance between the electrode wire and the cylinder. The second parameter is θ that stands for the angle and it is defined as the angular value measured in clockwise direction from front stagnation point. In the experiment two wires were utilized except the one case that the angle (θ) is 180°. Consequently, this method proved itself and they concluded from the experiment, that the ion wind is an efficient technique to control the wake region, vortex shedding and flow separation.

Thomas, Kozlov, and Corke (2008) carried out a study in order to control the flow around the cylinder, unsteady vortex shedding and to reduce the noise by using single dielectric barrier discharge plasma actuators (main characteristics of this type of actuator is well defined in the study of Enloe et al. (2004)). In this study Reynolds number was kept constant value of $3.3x10^4$ and both steady and unsteady actuators were investigated. They reported that for both steady and unsteady actuators, vortex shedding is suppressed, the wake turbulence level remarkably reduces and the sound level is reduced by 13.3 dB. They indicated that the unsteady actuator is capable of reducing total shedding pressure by 25%.

Mertz and Corke (2011) applied single dielectric barrier discharge plasma actuators (this actuator is explained in detail in the study carried out by Enloe et al. (2004)) to control flow structure, vortex shedding and to diminish the noise. They developed a flow control technique to attain the dynamic structure of the local air ionization and vector dispersion for unsteady body force. They carried out a numerical study to simulate the SDBD plasma actuator model. In order to suppress the Karman Vortex Street, they applied two flow simulations. First one was the utilization of impulsively started plasma actuator in still air and the other one is flow around a circular cylinder in which plasma actuators were utilized. From the results of the study carried out, it can be seen that the experimental and numerical study are consistent with each other.

2.2.4. Active Control by Magnetic Field

Mutschke et al. (1998) conducted a numerical study to control the wake structure of a circular cylinder by means of magnetic field control method. They applied stability analysis by means of numerical simulation method at different Reynolds number and tried to control the two and three dimensional flow regime. According to the numerical results they concluded that, two-dimensional flow regime can be stabilized and the vortex shedding can be attenuated or even annihilated with respect to magnitude of the magnetic field utilized.

Chen and Aubry (2005) carried out a study of controlling by magnetic field and created an effective active control algorithm in order to modify the wake structure of solid cylinder in an electrically low conductive fluid (e.g. seawater). They conducted the study with the aim of vortex shedding suppression, delaying flow separation in the boundary layer and remarkable reduction of the drag coefficient. They generated a Lorentz force in the azimuthal direction by the aid of an array that consists of permanent magnets and electrodes situated on the solid body. And by the help of this Lorentz force they were able to attenuate the vortex shedding downstream of the cylinder and eventually they manage to annihilate the vortex shedding thoroughly when the Lorentz force is notably high.

Zhang et al. (2010) carried out a numerical study to control cylinder wake by electromagnetic field based on a nonlinear adjacent optimal control approach. They designated Lorentz force as N, and made an observation that when optimal Lorentz force N(t) takes place, the flow separation is attenuated completely. Also mean drag coefficient diminished significantly. For the different adjacent flow fields, efficiency of the flow control may indicate differences because of different optimal values are needed for each case.

Another study of active control by means of magnetic field was carried out by Sintu Singha (2011). His purpose was to control the vortex shedding behind a circular cylinder by utilizing imposed transverse magnetic field, at the Reynolds number range varying from 50 to 250. According to their study, they made the conclusion that when the applied magnetic field is sufficiently high, vortex shedding can be annihilated completely at higher Reynolds numbers.

3. MATERIAL AND METHODS

When a fluid flow around a bluff body, the fluid and bluff body interact with each other and complicated flow mechanisms take place like flow separation, vortex formation etc. Therefore, a researcher needs a flow visualization technique to scrutinize the flow structure and these complex flow mechanisms. And increasing technological advancement, especially in electric and electronic area, paved the way for some flow visualization techniques (high resolution camera etc.). However, measuring some values at a single point or small region may be inadequate for some applications such as visualization of vortex formation or flow around a bluff body. For this reason a versatile and comprehensive measurement technique have been developed like Particle Image Velocimetry (PIV). Among the other Measurement techniques, Particle Image Velocimetry is a non-intrusive method that measures an instantaneous two or three dimensional velocity vector field of desired area. Its principle is based upon measuring the displacement of small particles, in the presence of laser light.

3.1. Water Channel System

The present study was carried out in order to see the flow characteristics downstream of a circular cylinder in deep water. To accomplish deep water effect for the desired situations and to examine the related parameters in this effect, the experiments were carried out in a large scale closed-loop water channel in the Mechanical Engineering Laboratory at Çukurova University. The channel has a width of 1000 mm, a length of 8000 mm and a depth of 7500 mm from the free surface. And the water channel length is approximately 15 m. The general layout of the water channel is shown in Figure 3.1. The test section of the water channel is made up of 15 mm thick optically transparent Plexiglas to observe the flow thoroughly.

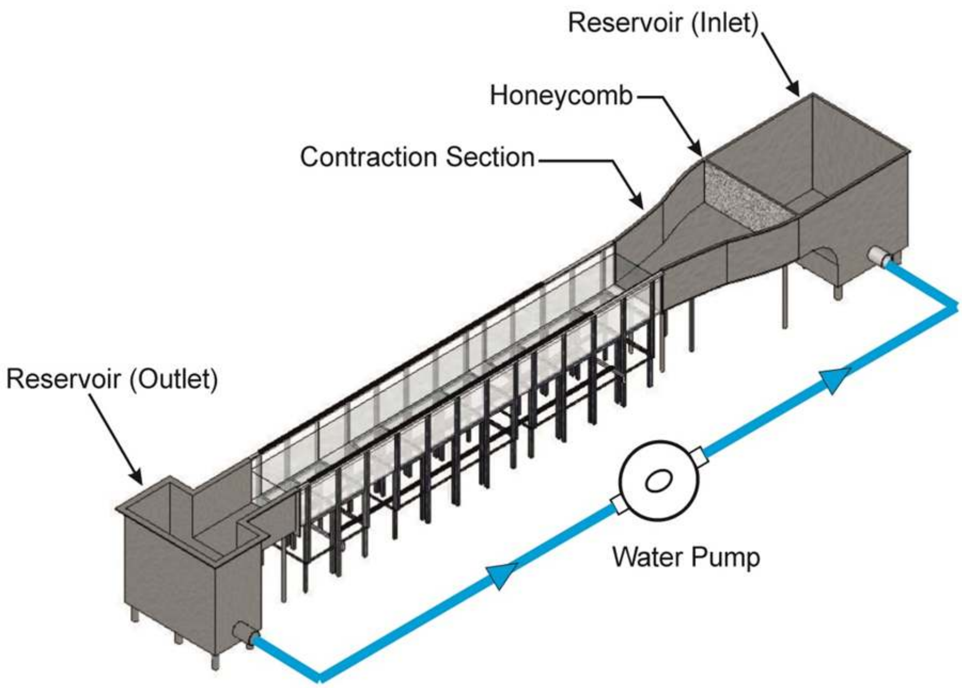

Figure 3.1. The Layout of the water channel

For the test section, steady flow without any interruption of flow is needed and to provide this steadiness, water channel has two different reservoirs at the inlet and the outlet of the test section. Water is driven by a pump, which can work at variable speeds by the aid of speed control panel, between the inlet and outlet reservoirs. The water then flows from the inlet reservoir to the honeycomb set and then to the contraction zone with a ratio of 2:1. The design of honeycomb and contraction zone is the key to ensure the uniform flow and to maintain the turbulence intensity lower than 0.5 %.

A platform which is shown in Figure 3.2 was placed in the water channel and it was utilized to attach the inner cylinder, perforated outer cylinder and splitter plate. The dimensions of the platform were 2300, 980 and 220 mm and these dimensions are length, width and height respectively. The platform was not just used for to hold the cylinders and splitter plate together; it also provided us to create a deep water affect and to regulate the desired Reynolds number.

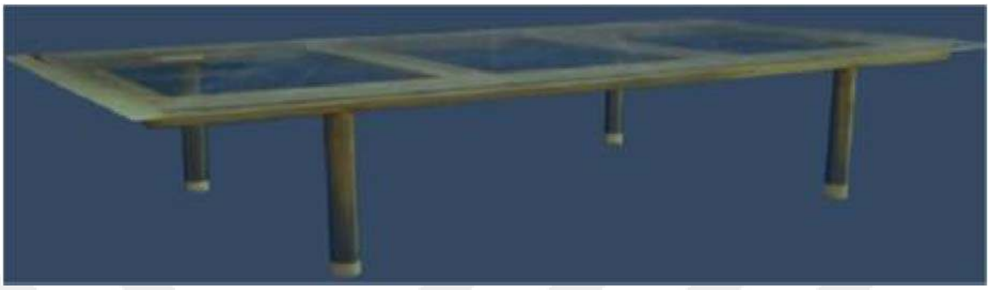

Figure 3.2. The Platform used for creating the deep water effect

3.2. Measurement and Visualization techniques

3.2.1. Dye Visualization Technique

There are several ways to visualize the flow and to analyze it according to different aspects. Some visualization techniques like PIV give us numerical results and make it possible to study the flow elaborately. However it might be helpful to have basic information about the subject for subsequent steps. Therefore dye visualization technique was used in the present study to determine the distinctive flow behavior. In contrast with PIV, dye visualization technique doesn't provide numerical information, but it gives preliminary and distinctive information about the flow. This technique makes it possible to obtain results quickly, since it is easy to implement and does not require any extra data processing. To visualize the flow in water channel a solution which contains water and Rhodamine (Rhodamine 6G or Rhodamine B can be used) is used. This solution is almost invisible in daylight, but when it is brightened by the continuous laser sheet in dark environment, it becomes apparent and flow can easily be observed. Spectra Physics continuous laser source shown in Figure 3.3, which has 532 nm wavelengths, was used for the illumination.

Figure 3.3. Spectra Physics Continuous Laser Source

A container full of dye solution was placed about 75 cm above the free surface of the water channel and dye was drained by 3 mm diameter plastic tube to visualize the flow. SONY HD-SR1 Video Camera was utilized to record the flow pattern for about 3 minutes. After analyzing video footages elaborately, instantaneous images of flow were taken by software which is called Play Memories.

3.2.2. Particle Image Velocimetry (PIV)

Many measurement techniques in fluid mechanics provide time-dependent information at a single point of flow. But to analyze the flow in detail in a certain region, it is necessary to have a comprehensive measurement technique which we can perform simultaneous measurements at multiple points in the studied area. This necessity led to the development of the PIV method and allowed us to perform simultaneous measurements at multiple points and to analyze the flow structure in detail. Particle Image Velocimetry (PIV) method allows us to perform 2 and 3 dimensional analysis in the selected region in the flow. PIV method allows the researcher to examine the presence of small flow structures and their influence, obtain vorticity fields quantitatively and, finally, obtain mean velocities, turbulence level and stresses at desired region. This method is a powerful diagnostic tool for solving problems, and provides unique insight into the nature of flow and the ability to improve the performance of fluid machinery and systems. Instantaneous or mean velocity field, vorticity contour, streamlines and turbulent statistics can also be attained by PIV.

PIV principle was first propounded by Landreth and Adrian (1988) in the late 1980s. Just after this theoretical study, Keane and Adrian (1990) carried out the first implementation of PIV technique experimentally. At that time, because of hardware restrictions, a single photograph frame was analyzed by the aid of auto-correlation technique. Afterwards, development of speed photographic recording enabled capturing two separate frames and these frames analyzed by cross-correlation techniques. The first appearance of digital camera technology in PIV facilitate the direct recording of particle images (Willert et al., 1991), to the detriment of resolution, ending up with the development of digital PIV (Westerweel et al., 1997). Besides those hardware innovations, some new algorithms have been improved in the last decades, developing the consistency and speed of PIV technique. One of the crucial advantages of the PIV method contrary to other traditional methods such as hotwire anemometry is that the capability of obtaining instantaneous flow-field information, and this enabled to investigate the turbulent flow field structure (Meinhart and Adrian, 1995; Westerweel, Draad, Van der Hoeven, and Van Oord, 1996).

PIV applications are usually carried out in wind and water tunnels. In the present study closed loop water channel is preferred. The principle of PIV can be defined simply as adding reflective material to the fluid, illuminate the particles by a light source and record the flow in a certain time period. To determine the velocity vector distribution of the flow we need 2 separate frames at a certain time interval. Laser source is not continuous and it provides intermittent illumination in a certain plane. First strike of laser source illuminates the particles and camera detects the first frame simultaneously. Second frame is obtained just like the first one. A synchronizer is used to make laser pulse and camera capture time overlap. If the time interval between first and second frame is known, than the velocity profiles of the particles can be obtained. Figure 3.4 shows the general principle of the PIV.

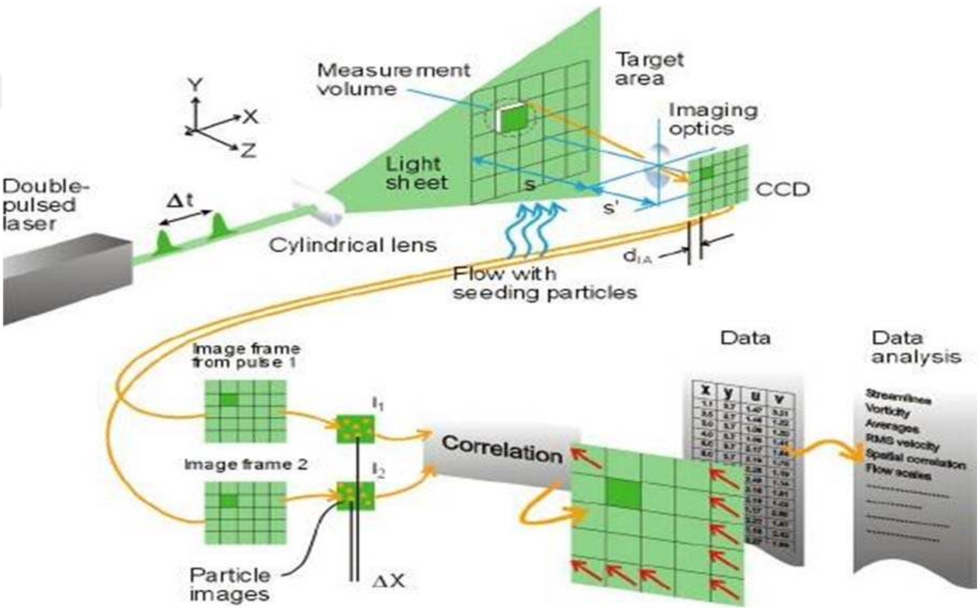

Figure 3.4. PIV Measurement Principle (Dantec Dynamics, 2019).

Illumination, particle seeding, image acquisition and image processing can be counted as indispensable steps of PIV process. To create a proper illumination and make particles reflect the sufficient amount of light to the camera a Nd: YAG Laser (Neodymium-Doped Yttrium Aluminum Garnet) was used in the present study. The laser beam has 120 mj energy and it strikes 15 times in a second. A CCD (Charged Couple Device) camera, which has resolution of 1600×1200 pixels, synchronized with the laser source to capture the images. Adequate laser light and tracer particles should be used to provide accurate images. But adjusting the laser source timing and light intensity at desired levels is not the only necessity; researcher must add the right amount of tracer particles. For seeding process, 10 micron diameter silver coated glass spheres are used. Sufficient amount of particles are mixed with water and poured into the water channel. To have the homogeneous and uniform particle distribution throughout the water channel, centrifugal pump was operated at almost full speed about 3-5 minutes. Tracer particles should also be reflective, noncorrosive, nonpoisonous, and nonabrasive and clean enough. Density of the tracer particles must be close enough to water density to move with the water; otherwise the particles may descend or ascend due to buoyancy forces. When the right amount light illuminates the flow field and the channel is seeded with right amount of particles (25-35 particles for each interrogation areas), the raw images are taken by the camera. Interrogation arear are shown in figure 3.5. The size of these interrogation areas is 32x32 pixels, which can be obtained 7227 vectors from an image with a resolution of 1600 x 1200 pixels.

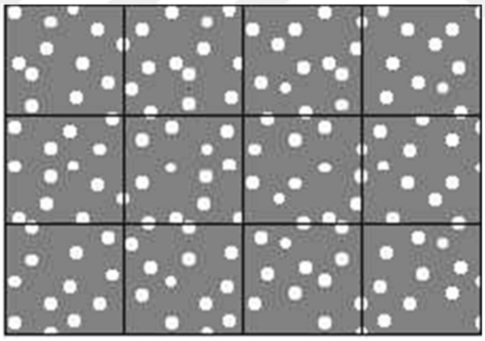

Figure 3.5. Interrogation Areas

The cross-correlation technique is used to designate the displacement by using related interrogation areas for every single image. This method is a complete and it ensures valid results. Throughout the experiment for every single run 1000 raw images were taken. Dantec flow grabber digital PIV software employing frame-to-frame adaptive correlation technique was used to calculate the raw displacement vector field from the particle image velocimetry data. Then to attain the velocity field, the cross-correlation technique, with 32x32 interrogation areas, was applied, with an overlap of 50% (Dantec Dynamics Software Manual). CLEANVEC software written by Meinhart and Soloff (1999) was used to eliminate the spurious vector from every single instantaneous raw image. To compensate the deleted vectors, bilinear interpolation with least squares fit was used.

3.3. Experimental Parameters

In the present study, flow control over a circular cylinder (inner cylinder) was investigated by means of a splitter plate and perforated semi circular cylinder (outer cylinder). To perceive the experimental setup completely, experimental parameters must be defined properly. Inner cylinder was made up of acetyl polymer which is optically transparent and its diameter is 50 mm. Due to its transparency laser beam can pass the other side of the cylinder. Outer semi circular cylinder has diameters of 125 mm, and it has 10 mm diameter holes on it to provide the desired porosity. Both outer cylinder and splitter plate are made out of chrome metal sheet. Also splitter plate has different porosities. Porosity of the outer cylinder and splitter plate are one of the most determinants for this study. By reason of the effective porosities of cylinder and splitter plate were investigated in the present study. To evaluate the porosities of cylinder and plate the formula in the figure 3.6 was used.

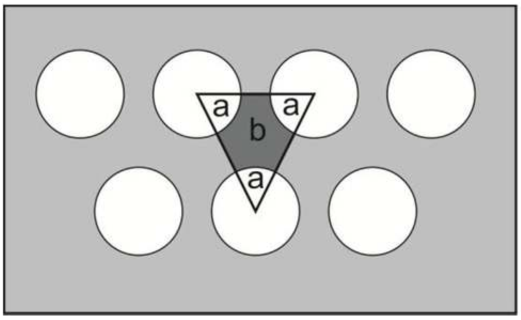

$$\beta = \frac{3a}{3a+b}$$

Figure 3.6. Porosity calculations of outer cylinder and splitter plate.

As it can be seen from the figure above, porosity (β) can be defined as the ratio of the blank area to the surface area of the whole body. Since we have two porosity values, β_c for the porosity of outer cylinder and β_p for the splitter plate were designated. D_i/D_o is another dimensionless parameter to define the diameters of inner and outer cylinder easily and it refers to the ratio of the inner cylinder diameter to the outer cylinder diameter. Since perforated outer cylinder is half cut, layout of the outer cylinder is important. Figure 3.7 shows the general layout of the experimental system (inner cylinder, outer cylinder and splitter plate), and it is seen that outer semi circular cylinder is located downstream of the inner cylinder.

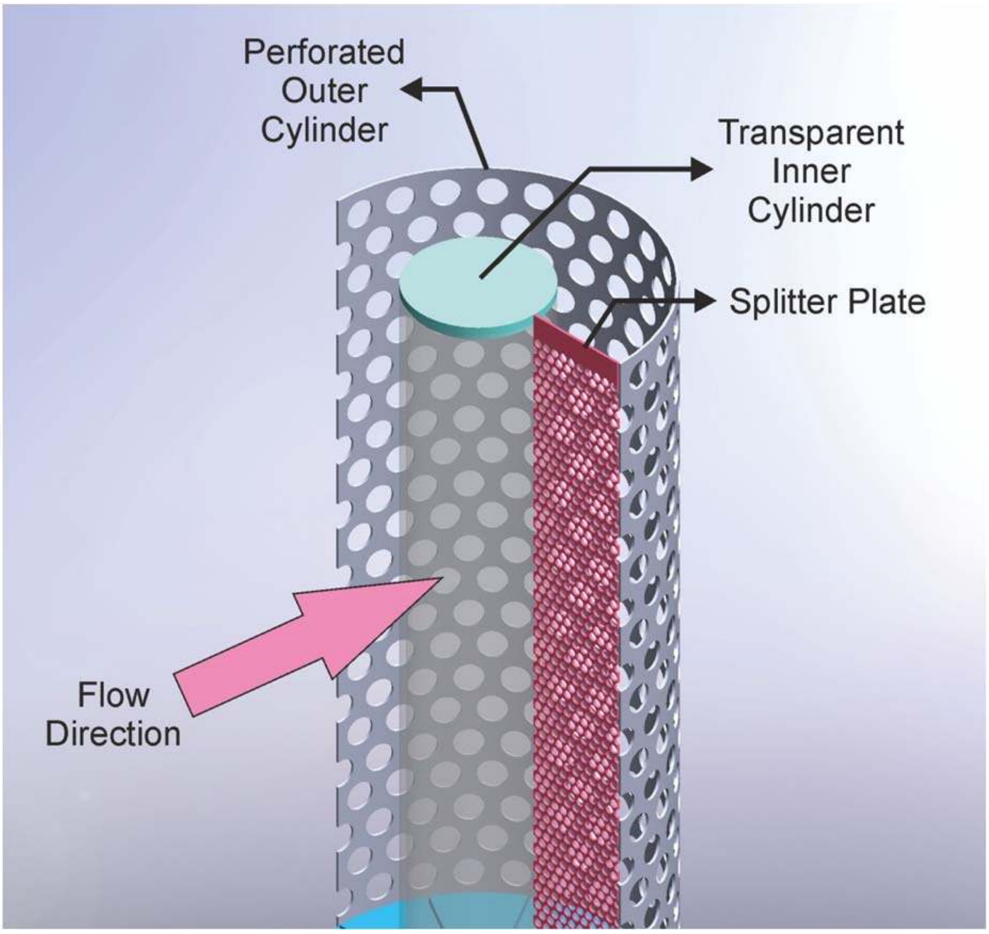

Figure 3.7. Layout of the components according to the flow direction

To accomplish the deep water effect, the depth of the water in the base of the channel was kept 55 cm. In this study the experiments were carried out at Re=5000, which was based on the inner cylinder diameter (50 mm). Free stream velocity of the flow was kept constant both in PIV and Dye Visualization experiments at 97,5 mm/s. Both PIV and Dye Visualization Experiments were conducted according to Plan View, as shown in Figure 3.8.

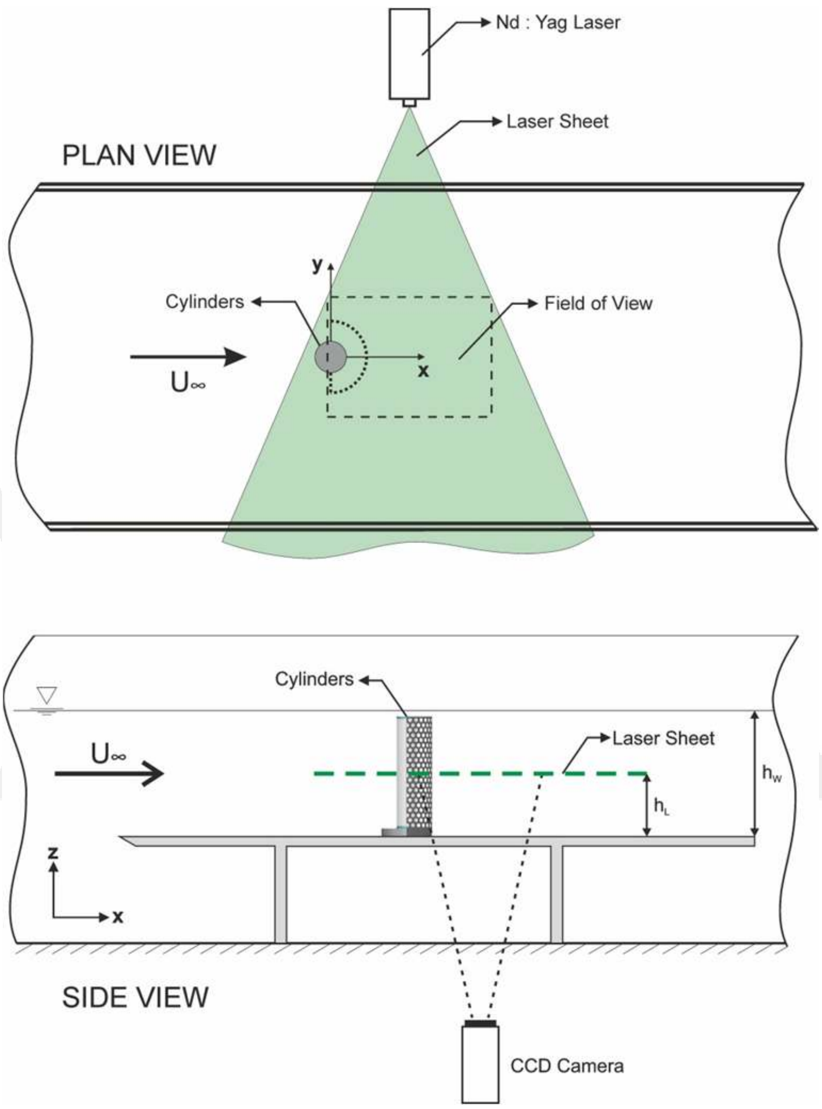

Figure 3.8. General Layout of the experimental setup

The aim of the present study was to examine the flow around a circular cylinder and to control the flow in the annular region and downstream of the circular cylinder. To control the flow, two passive control methods were applied together. As mentioned before three dimensionless parameters were defined (D_i/D_o, β_c, β_p). For this study D_i/D_o were designated as D_i/D_o =0,4 and it was kept constant throughout the study. The results were studied one by one, but also comparisons were made according to the different parameters. β_C values were chosen as β_C =0.3 , β_C =0.5 , β_C =0.7 to determine the effects of different cylinder porosities. Also four different β_P were designated to make comparison as β_P= 0, β_P= 0.3, β_P= 0.5, β_P= 0.7. The last parameter to investigate is the location of the splitter plate with respect to flow direction. This location was symbolized as α and it is the angle between splitter plate and the flow direction. Plate angle values of α=90˚, α=120˚, α=150˚ and α=180˚ were examined in this study and comparison between these angles were made.

4. RESULTS AND DISCUSSIONS

In the present study, the perforated circular cylinders were cut into half and located downstream of a circular inner cylinder concentrically in order to prevent or attenuate the vortex shedding downstream of the cylinders as a passive control technique. Another passive control device, splitter plate was also utilized between inner and outer perforated cylinders to control the flow in the annular region and to prevent the interaction of vortices in between inner and outer cylinders. Both splitter plate and perforated cylinder have different porosity ratios and the effect of these different porosity ratios were scrutinized and compared with each other. In this chapter, the time averaged vorticity contours <ω>, the time averaged streamlines <ψ> and instantaneous dye visualization results were introduced to visualize and comprehend the corresponding flow structure.

4.1. Bare Cylinder Case

When analyzing the flow structure of control elements (perforated semi circular cylinder and splitter plate around circular inner cylinder), a control case is needed to comprehend the effectiveness of these control elements. For this reason, flow around the circular cylinder (bare cylinder with the diameter of 50 mm) was investigated without splitter plate and perforated cylinder in order to take it as a reference point and to make comparison with the other experimental results.

To form a reference point and comprehend the basic flow behavior around a circular cylinder, the time average streamlines <ψ> and the time average vorticity contours <ω> are indicated in figure 4.1. By the aid of PIV technique, 1000 instantaneous images were taken and these two images were acquired. As it can be seen from the figure 4.1, the time average streamlines constitutes focal points F_1 and F_2 in the wake region of the cylinder. They appear in a symmetrical order as it is anticipated and they are getting closer to each other. From figure 4.1, it is also can be seen that symmetrical time average vorticity contours <ω> takes place and it is in accordance with streamline topology result.

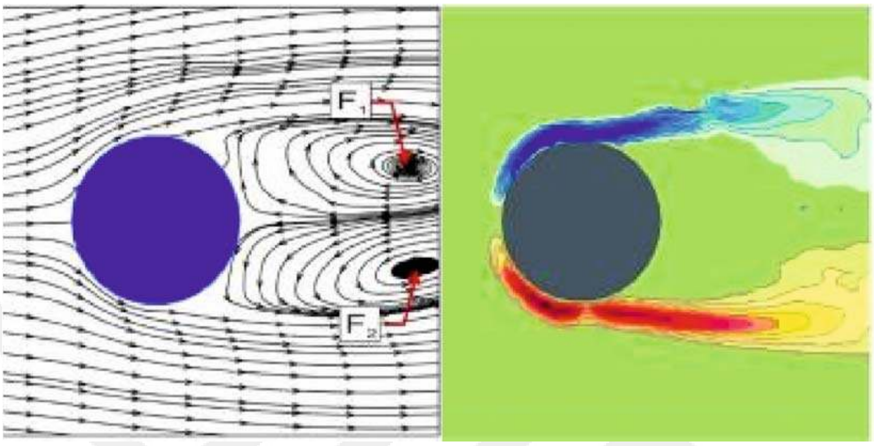

Figure 4.1. Time averaged streamlines <ψ> and time averaged vorticity contours <ω> of the inner cylinder

4.2. Effects of Perforated Semi Circular Cylinder with Different Diameter and Porosity Ratios

In the present study, three determinant and variable parameters are designated initially to investigate the flow structure according to their presence. These are the porosity of outer semi circular cylinder, the porosity of splitter plate and the splitter plate angle with respect to flow direction. However, investigation of these parameters simultaneously might be difficult for comprehension of individual characteristics of these parameters. Accordingly, in the first step, flow behavior of inner cylinder and outer perforated semi circular cylinder configuration was examined thoroughly. But, more far-reaching investigation was carried out in this stage to determine the most effective parameters. Three different diameter ratios (D_i/D_o= 0.4, 0.5, 0.6) and five different porosity ratios (β_C= 0.3, 0.4. 0.5, 0.6, 0.7) were examined and the flow characteristic of these configurations were interpreted according to time averaged streamlines <ψ>, time averaged vorticity contours <ω> and instantaneous dye visualization results.

In figure 4.2, 4.3 and 4.4; time averaged streamlines $<\psi>$, time averaged vorticity contours $<\omega>$ and instantaneous dye visualization results are indicated respectively. In the first, second and third columns; D_i/D_o= 0.4, D_i/D_o= 0.5 and D_i/D_o= 0.6 are presented respectively and in each rows different porosity ratios are indicated incrementally. In figure 4.2, F symbols stand for the circulating flow structures and they indicate the complicated flow structure. For D_i/D_o= 0.4 in the first columns, upper and lower shear layers generated by the inner cylinder, interact with each other up to the outer cylinder and give rise to unsteady flow in the annular region as well as downstream of the cylinders. This situation can also be seen from time averaged vorticity contours $<\omega>$ in figure 4.3. Upper and lower shear layers get blocked initially by the perforated cylinder wall, generating circulation pairs and then they are dispersed in downstream of the cylinders for $0.3 \leq \beta_C \leq 0.6$. Although it is seen from figure 4.2 that some circulation points (F) take place in downstream of the cylinders, suppression of Karman Vortex Street is achieved for D_i/D_o= 0.4 and $0.3 \leq \beta_C \leq 0.6$ parameters. In figure 4.3 and 4.4, time averaged vorticity contours $<\omega>$ and instantaneous dye visualization results confirm the suppression of Karman Vortex Street. In figure 4.3, it is seen that jet-like flow takes place for lower porosity ratios. And also in figure 4.4 there is no evidence that Karman Vortex Street takes place for D_i/D_o= 0.4 and $0.3 \leq \beta_C \leq 0.6$. For porosity ratio of β_C=0.7, more fluid flow can pass through the perforated cylinder according to lower porosity cylinders and perforated cylinder cannot dispersed the flow structure caused by the flow separation, thus generating Karman Vortex Street as it can be seen in figure 4.4. This situation is valid in all diameters ratio for β_C=0.7 and this porosity ratio might be regarded as ineffective for controlling the downstream of the cylinders. Herein, β_C=0.6 can be regarded as the transient parameter for controlling the downstream region. Consequently, for the case D_i/D_o= 0.4 and $0.3 \leq \beta_C \leq 0.6$, there is a control situation downstream of the cylinders, yet high magnitude vortex pairs and unsteady flow take place in the annular region between inner and outer cylinder.

The second columns in figure 4.2, 4.3 and 4.4 indicate the results of D_i/D_o= 0.5 and these results show similarities to D_i/D_o= 0.4 case. However, in this case, vortices generated from the inner cylinder encounter with the perforated cylinder wall in shorter range stemming from smaller diameter of outer cylinder. Transition parameter in this case can be noted as β_C=0.5, because unsteady flow behavior such as vortex shedding and Karman Vortex Street arise due to higher porosity ratios. Especially for the porosity ratio of β_C=0.7, as it can be seen from the instantaneous dye visualization results, Karman Vortex Street takes place in wider range as compared with lower porosity ratios.

The last columns in the figure 4.2, 4.3 and 4.4 present the results of D_i/D_o= 0.6 by means of time averaged streamlines $<\psi>$, time averaged vorticity contours $<\omega>$ and instantaneous dye visualization results and these configurations reveal another situation. Vortex pairs generated by the inner cylinder can pass through the shrouds easier as the porosity ratio enhances. And flow structure exhibits oscillations for porosity ratio in the range $0.3\leq \beta_C \leq 0.5$. Besides, in the case of $\beta_C\geq 0.6$, large scale Karman Vortex Street comes into existence downstream of the cylinders. For this reason, it is not anticipated that this configuration becomes successful for controlling the flow even if a splitter plate is utilized. Because in this diameter ratio, the inner and outer perforated cylinder tend to exhibit single cylinder (bare cylinder) behavior. Accordingly, D_i/D_o= 0.6 configuration are not presented in the present study with splitter plate.

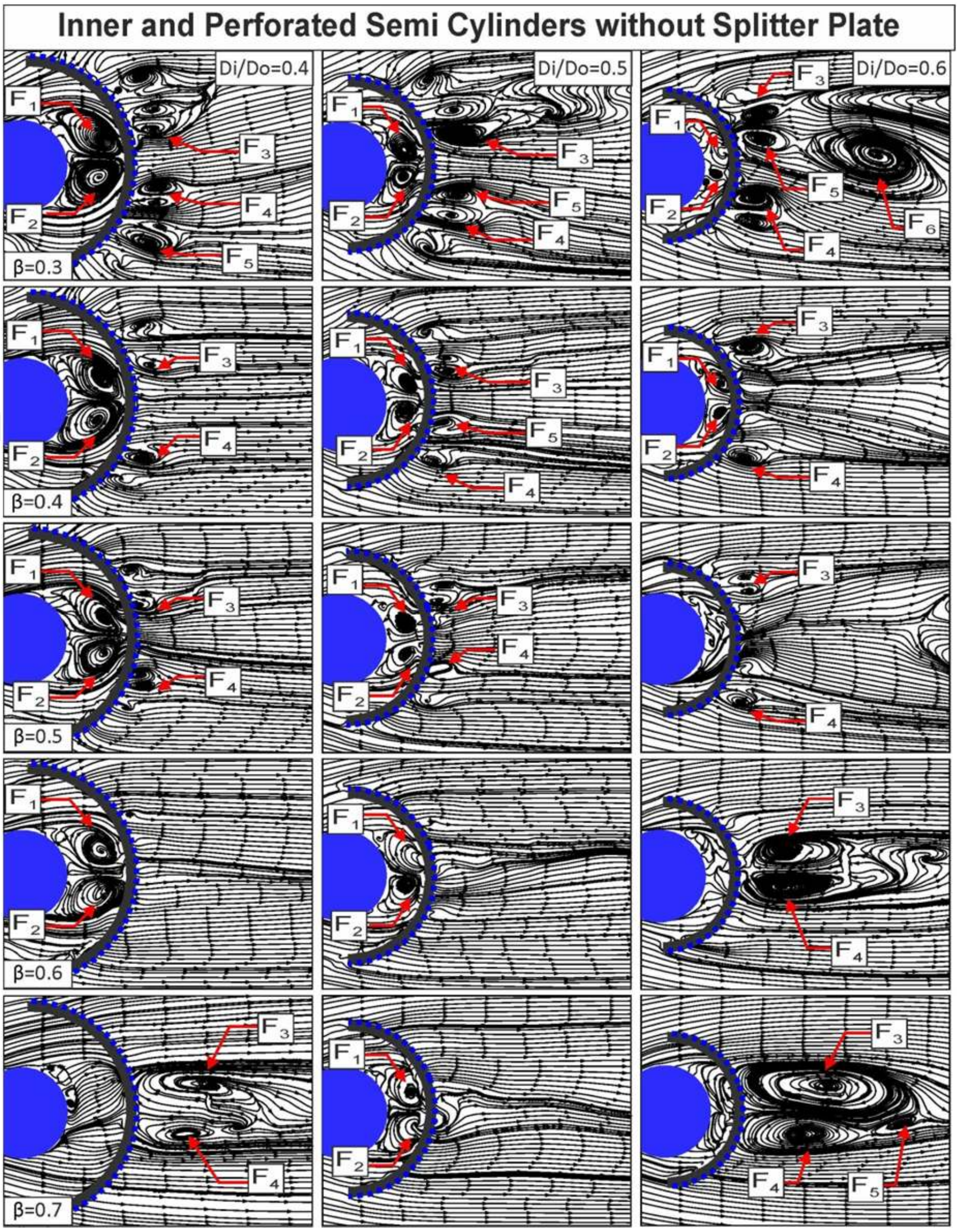

Figure 4.2. Time averaged streamlines <ψ> of inner and perforated semi circular cylinders without splitter plate in the wake region

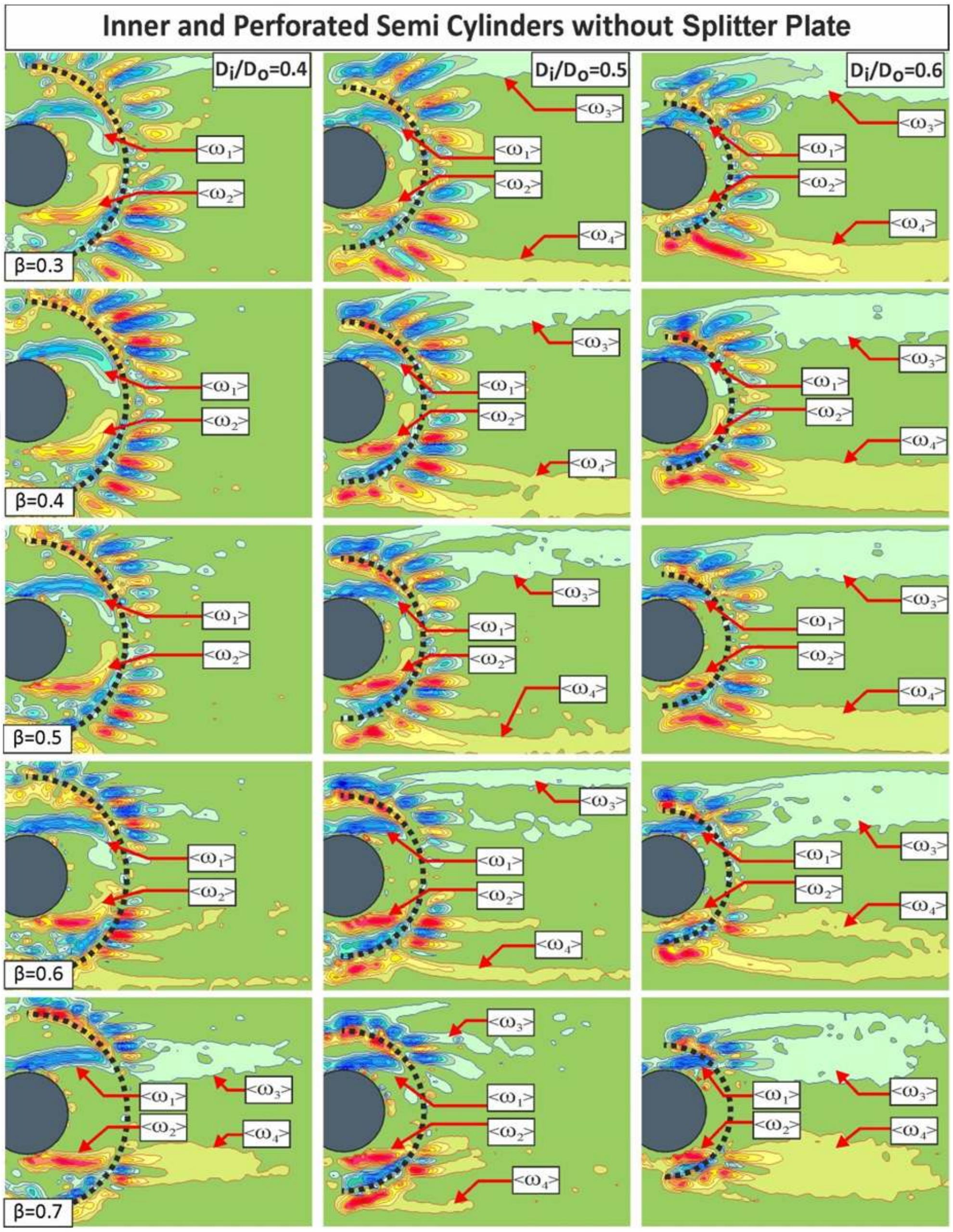

Figure 4.3. Time averaged vorticity contours <ω> of inner and perforated semi circular cylinders without splitter plate in the wake region

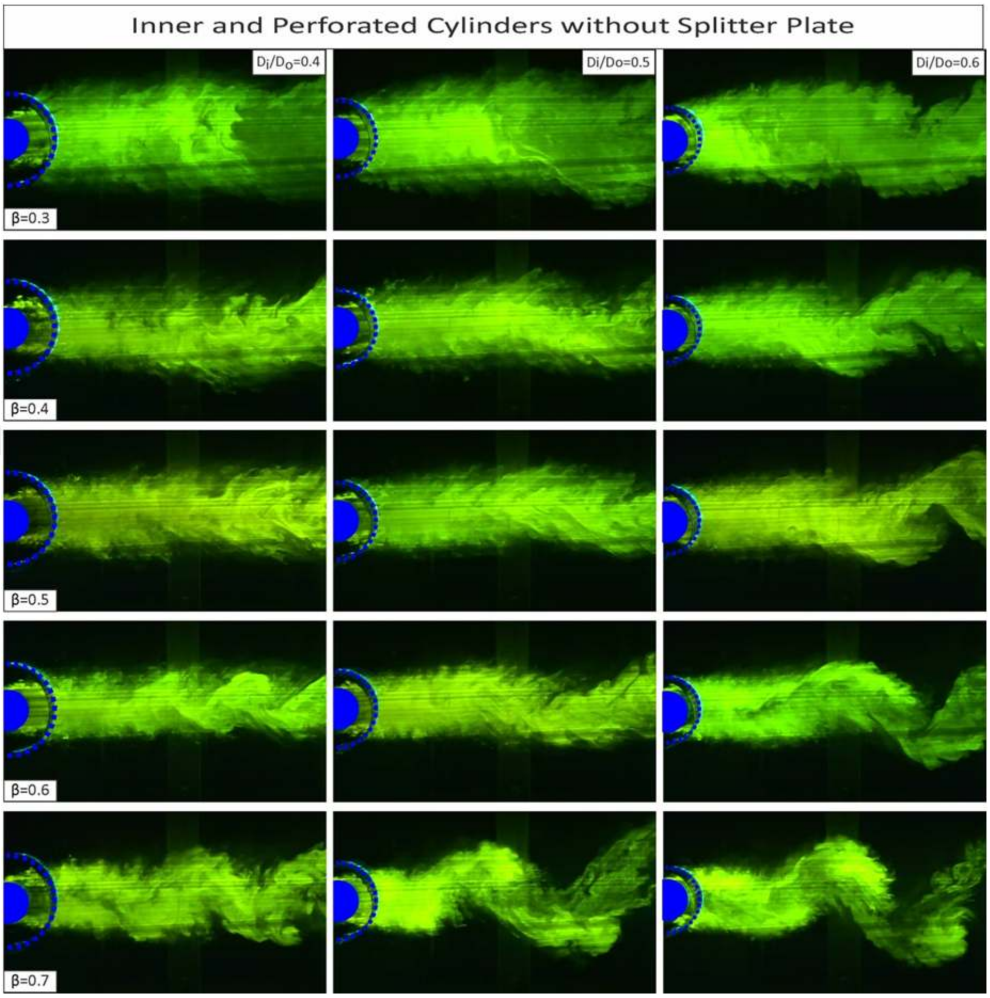

Figure 4.4. Instantaneous dye visualization results of inner and perforated semi circular cylinders without splitter plate in the wake region

4.3. Dye Visualization Results

In the previous title, perforated semi circular cylinders, which have different porosity and diameter ratios, were located concentrically downstream of the inner cylinder and flow behavior around this configuration were scrutinized. After analyzing time averaged streamlines <ψ>, time averaged vorticity contours <ω> and instantaneous dye visualization results of this configuration, efficient parameters were determined as D_i/D_o= 0.4, 0.5 and β_C=0.3, 0.5. Since D_i/D_o= 0.4

and D_i/D_o= 0.5 indicated very similar behaviors, it was decided that keeping the diameter ratio constant as D_i/D_o= 0.4 for following investigations. Subsequent to outer cylinder investigation, splitter plate utilization took place in this chapter. As mentioned earlier four different splitter plate porosity as β_P=0, 0.3, 0.5, and 0.7 were examined with different β_C ratios. Although it was regarded as ineffective parameter in the previous title, β_C=0.7 were investigated with the splitter plate configuration as well as β_C=0.3 and 0.5.

In order to comprehend the general flow behavior of the corresponding parameters, dye visualization experiments were conducted initially. Dye visualization technique is very practical method to examine the flow behaviors in a qualitative manner and it allows the researcher to make preliminary study in a short time interval. So the flow was recorded for about 2-3 minutes and these videos were watched a few times to scrutinize and comprehend the general flow characteristic. Then, one distinctive and descriptive image was determined for visualize the every single flow configuration and they were presented in this title.

In figure 4.5 dye visualization images were presented. As it can be seen from figure, cylinder porosity has a constant value of β_C=0.3 in this case and splitter plate porosity ratios are indicated in the first and second columns as β_P=0 and 0.3. In each row, splitter plate angle are shown from 90° and 180° with the increment value of 30°. At first glance, more extended wake region draws attention for 90° and 120° in both splitter plate porosity cases. This situation stems from the blocking effect of splitter plates. Flow encounters with the splitter plate and compelled to flow upper side of the inner cylinder and lower side of the splitter plate. So on the upper side of the outer cylinder jet-like flow takes place and it is also can be seen in figure 4.3 for β_C=0.3. Porosity of the outer cylinder also causes the extended wake region. Due to lower porosity ratio of the cylinder, the flow compelled over upper side of the inner cylinder cannot pass through outer cylinder and circulates in the annular region. Then, it encounters with the low porosity splitter plate and compelled to flow through the outer cylinder. Besides, some of the flow can pass through the upper side of the outer cylinder and jet like flow takes place, resulting extended wake region. Meanwhile, lower shear layer get blocked by splitter plate and pass through the lower side of the splitter plate and outer cylinder, ending up with jet like flow. Therefore, vortex shedding in the annular region and near wake is attenuated, but in approximately $2D_i$ distance big scale vortex formation occurs. The only difference between β_P=0 and 0.3 for 90° and 120° is that, reduction in the vortex scale for β_P=0.3. It should also be taken into consideration that the low porosity splitter plates are exposed to high amount of momentum.

When we look at α=180° configuration, narrower wake region and more stable flow draw attention. This condition is valid for both β_P=0 and β_P=0.3 cases and no Karman Vortex Street takes place. It can be said that the control of downstream region of the cylinders are achieved. In this configuration, fluid comes from upper and lower shear layers cannot pass through outer cylinder and generates vortex pair in the upper and lower side of in the cylinder. However, this vortex pair cannot interact with each other due to the splitter plate utilization. That means more stable and controlled flow exists in both annular and wake region. Plate angle of α=150° should also be examined since it affect the flow around inner cylinder in the same way as α=180° configuration. For both plate porosity ratios, β_P=0, 0.3 and plate angle of 150° provide controlled flow in annular and wake region. The only difference between 150° and 180° configurations, α=180° provides slightly narrower wake region than α=150° configuration. In conclusion, for porosity ratios of β_P=0, 0.3 and the plate angle of 150° and 180°, flow control in both annular and wake region is accomplished.

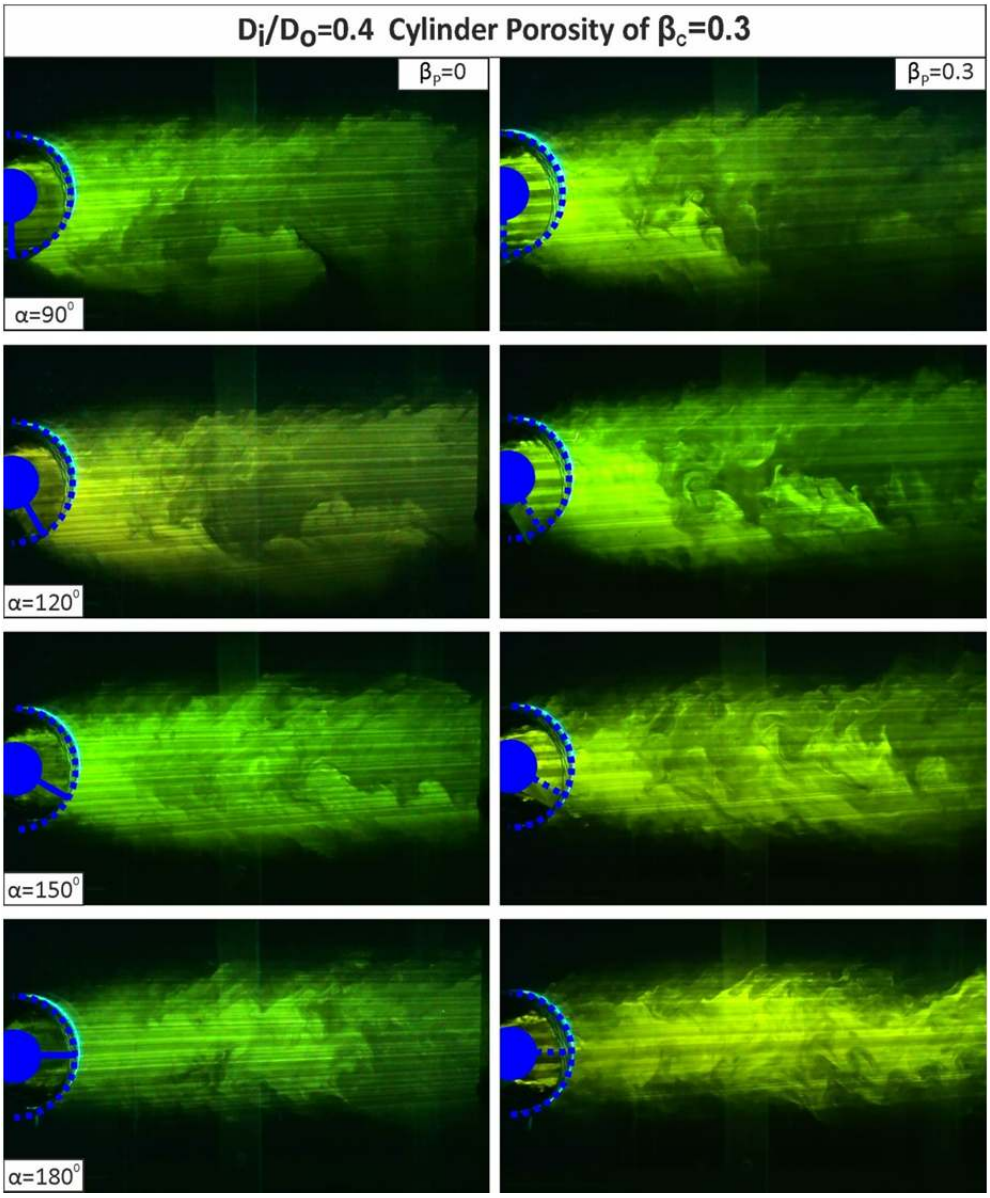

Figure 4.5. Instantaneous dye visualization results of cylinder porosity, β_C= 0.3 and plate porosity of β_P= 0, 0.3 for different plate angles

Instantaneous dye visualization results of cylinder porosity, β_C= 0.3 and plate porosity values of β_P= 0.5 and 0.7 are presented in the figure 4.6. Porosity values of β_P= 0.5 and 0.7 are indicated in the first and second columns respectively.

And four different plate angles are shown in corresponding rows in an incremental way. In this case splitter plate porosities are enhanced and same configurations in figure 4.5 are applied for β_P= 0.5 and 0.7. Higher porosity ratios of splitter plate means that more amount of fluid can pass through the plates according to previous case.

For the plate angle of 180°, flow in the annular region and wake region can be regarded as controlled by means of higher porous splitter plates. When compared with the β_P= 0 and 0.3, both plate porosity ratios of β_P= 0.5 and 0.7 are capable of preventing the interaction of vortex pair in the annular region. Also more porous plates enable to scatter the vortex formation as well as preventing interaction of them. So these splitter plates can be regarded as effective to control the flow in the annular and wake region. Just like 180° configuration, plate angle of 150° prevent interaction of vortex pair in the annular region and control the flow downstream of the cylinders for both porosity ratios. And plate angle of 150° can be regarded as a special case, since its location is in the vicinity of separation point and this configuration enables the splitter plate to scatter the vortex formation just before it exists. Because of this specialty, plate angle of 150° can inhibit the interaction of vortex pair in the annular region and give rise to more stable wake region.

When we compare the β_P= 0.5 and 0.7 with the lower porosity ratios according to 120°, it can be realized that the scattering effect of the high porous plates enable more stable and controlled flow with small scale vortices as can be seen from figures 4.5 and 4.6. In contrast with the very low porosity ratios, β_P= 0.5 and 0.7 allow flow to pass through the plate as well as preventing interaction of vortex pair. So we can say plate angle of 120° has a significant amount of control over suppression of Karman Vortex Street, yet still time averaged streamlines $<\psi>$ and time averaged vorticity contours $<\omega>$ should be investigated to determine the efficiency of configuration. Lastly, for the plate angle of 90°, larger scale vortex formation is detected relative to angle of 120°. However, when it is compared with the β_P= 0 and 0.3 case, it can be seen β_P= 0.5 and 0.7 arrangement attenuates the vortex formation better.

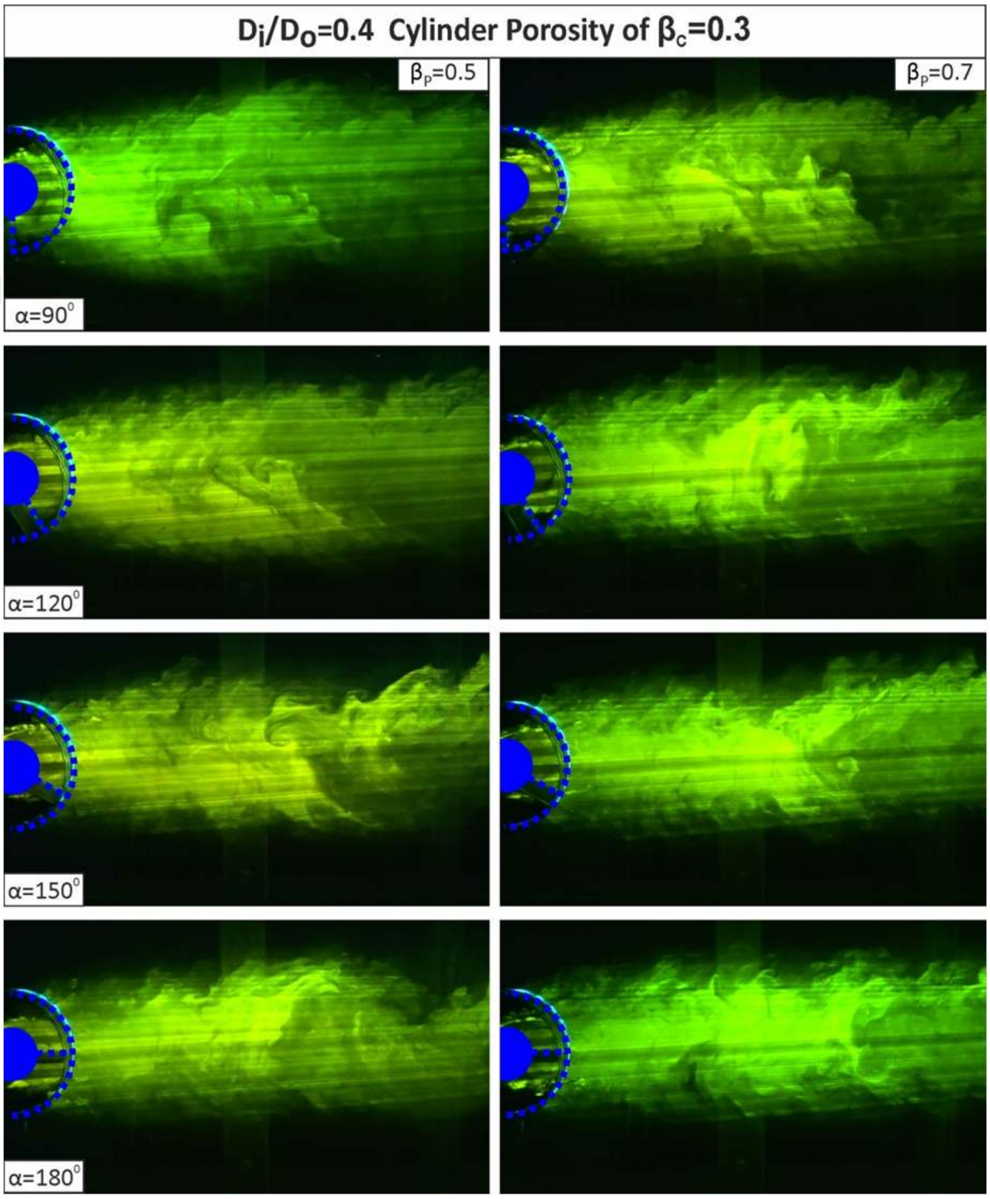

Figure 4.6. Instantaneous dye visualization results of cylinder porosity, β_C= 0.3 and plate porosity of β_P= 0.5, 0.7 for different plate angles

In figure 4.7, cylinder porosity of β_C= 0.5 and plate porosity of β_P= 0 and 0.3 are presented with different plate angles. For D_i/D_d= 0.4, cylinder porosity of β_C=0.5 was defined as an effective parameter to suppress the vortex formation and inhibit the Karman Vortex Street in figure 4.4. It was also mentioned that it is needed to control the vortex pair in the annular region in addition to wake region. In order to obtain fully controlled flow, splitter plate was utilized with variable porosity ratios. For the plate angle of 180°, both plate porosity ratios are influential to control the wake region and disengage the interaction of vortex pair in the annular region. Therefore plate angle of 180° can be regarded as the most effective parameter for this arrangement. For α=90° and 120°, there is a circulation in the annular region for both plate porosity ratios. Splitter plate with porosity ratio of 0.3, allows a little flow to pass through it and provide reduction in the magnitude of vortex formation generated in the wake region. Even if vortex formation takes place in the wake region occasionally, plate angle of 90° and 120° cannot be described as inefficient to control the flow. Since Karman Vortex Street doesn't take place in these configurations.

Due to its proximity to separation point, plate angle of 150° has a significant effect on controlling the flow characteristics of annular region and wake region. This arrangement also exhibit similar flow behavior to α=180° case and can be regarded as effective parameter. It not only prevents the Karman Vortex Street, but also enables the more steady flow around the inner cylinder.

When we compare the figure 4.5 and 4.7, sharper circulations in figure 4.7 attract notice for plate angles of 90° and 120°. When the low porous splitter plates are used with low porous outer cylinder (β_C=0.3), blockage effect of splitter plate is less significant, because flow directed to the upper shear layer cannot pass through outer cylinder easily, resulting lower scale vortex formation. However, when low porosity splitter plates are utilized with higher porous outer cylinder (β_C=0.5), blockage effect of splitter plate comes into prominence. The flow directed to upper shear layer can pass the outer cylinder easily and jet like flow occurs on the upper side of the outer cylinder and flow moves very slowly on the lower side of the outer cylinder, thus circulation takes place, resulting large scale vortex formation.

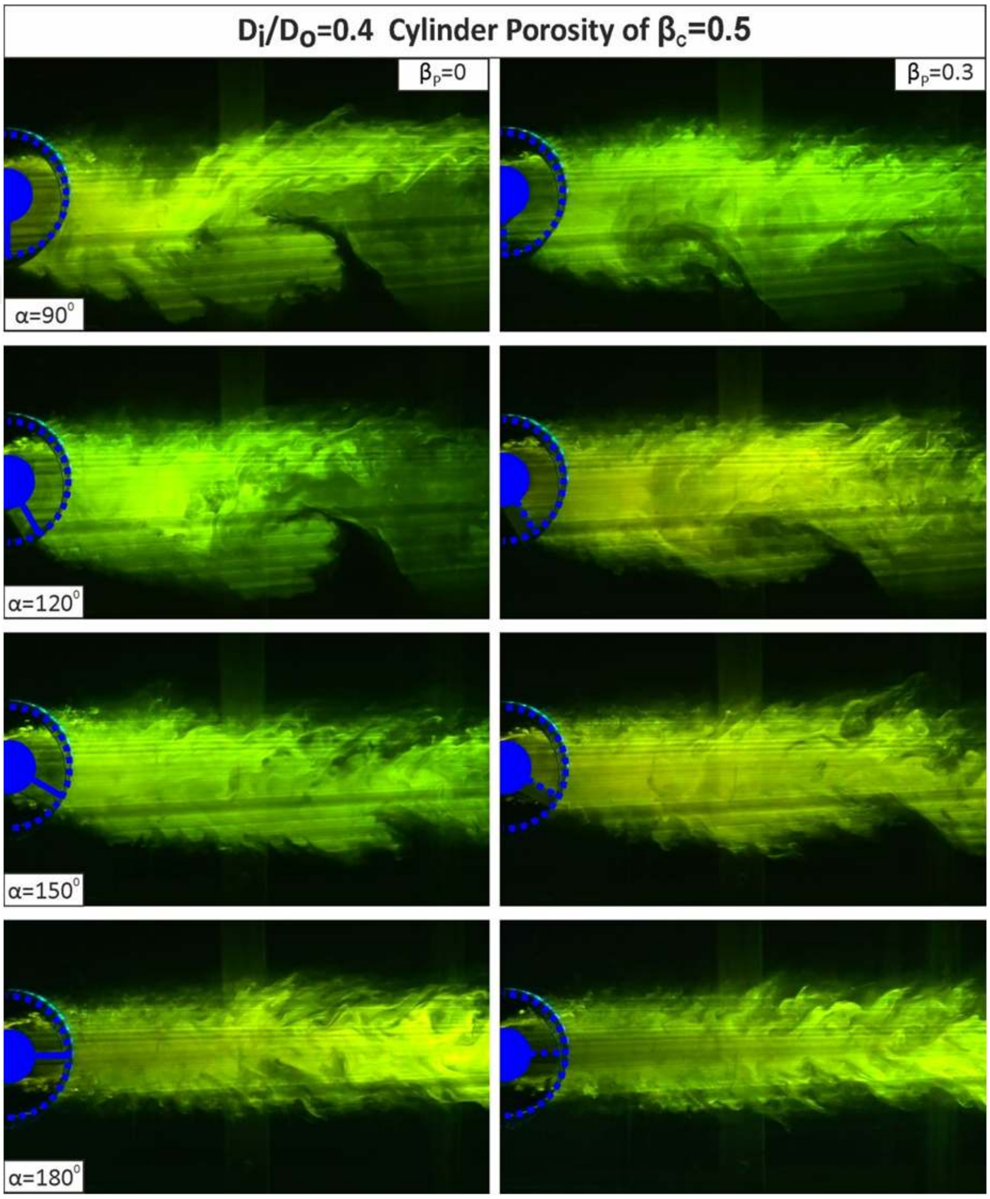

Figure 4.7. Instantaneous dye visualization results of cylinder porosity, β_C= 0.5 and plate porosity of β_P= 0, 0.3 for different plate angles

Instantaneous dye visualization results of cylinder porosity, β_C= 0.5 and plate porosity values of β_P= 0.5 and 0.7 are presented in the figure 4.8. Higher splitter plate porosity ratios enable the flow to pass through the plate easily, hence more stable flow structure can be realized from figure. The most effective parameter of this arrangement can also be regarded as the plate angle of 180°. Because splitter plate in this arrangement provide elongated and narrow wake region without slightest Karman Vortex Street indication. Plate angle of 150° for both plate porosity ratios also procures very effective control in the annular and wake region.

In contrast with the β_P= 0 and 0.3 case, porosity ratios of β_P= 0.5 and 0.7 enable to control the flow and inhibit the Karman Vortex Street. This configuration also procures controlled flow behavior in the annular region by annihilation of the interaction between vortex pair. In previous figures, it is indicated that the arrangement of 90° plate angle is not efficient relative to other plate angles. However, cylinder porosity ratio of β_C= 0.5 and β_P= 0.5 and 0.7 values seem to have sufficiently high control indication for plate angle of 90°.

Up until now, among the other dye visualization results, β_C= 0.5 and β_P= 0.5 and 0.7 parameters can be regarded as most effective ones at the first glance. The underlying result of this situation might be the accordance and consistency between splitter plate and cylinder porosity ratios. Both porosity ratios of β_C= 0.5 and β_P= 0.5 have same effect under the flow conditions. They allow the flow to pass through almost in half and additionally have and sufficient blockage effect. And when they are utilized together, their consistency and efficiency come into prominence and they achieve flow control in both annular and wake region for almost every plate angles. This combination is useful even for the plate angle of 90°, because of the blocking effect and sufficient permeability. β_P= 0.7 value has almost identical dye visualization results with β_P= 0.5 for the wake region. But investigation of time averaged streamlines $\langle\psi\rangle$ and time averaged vorticity contours $\langle\omega\rangle$ might be needed for analyzing the annular region thoroughly.

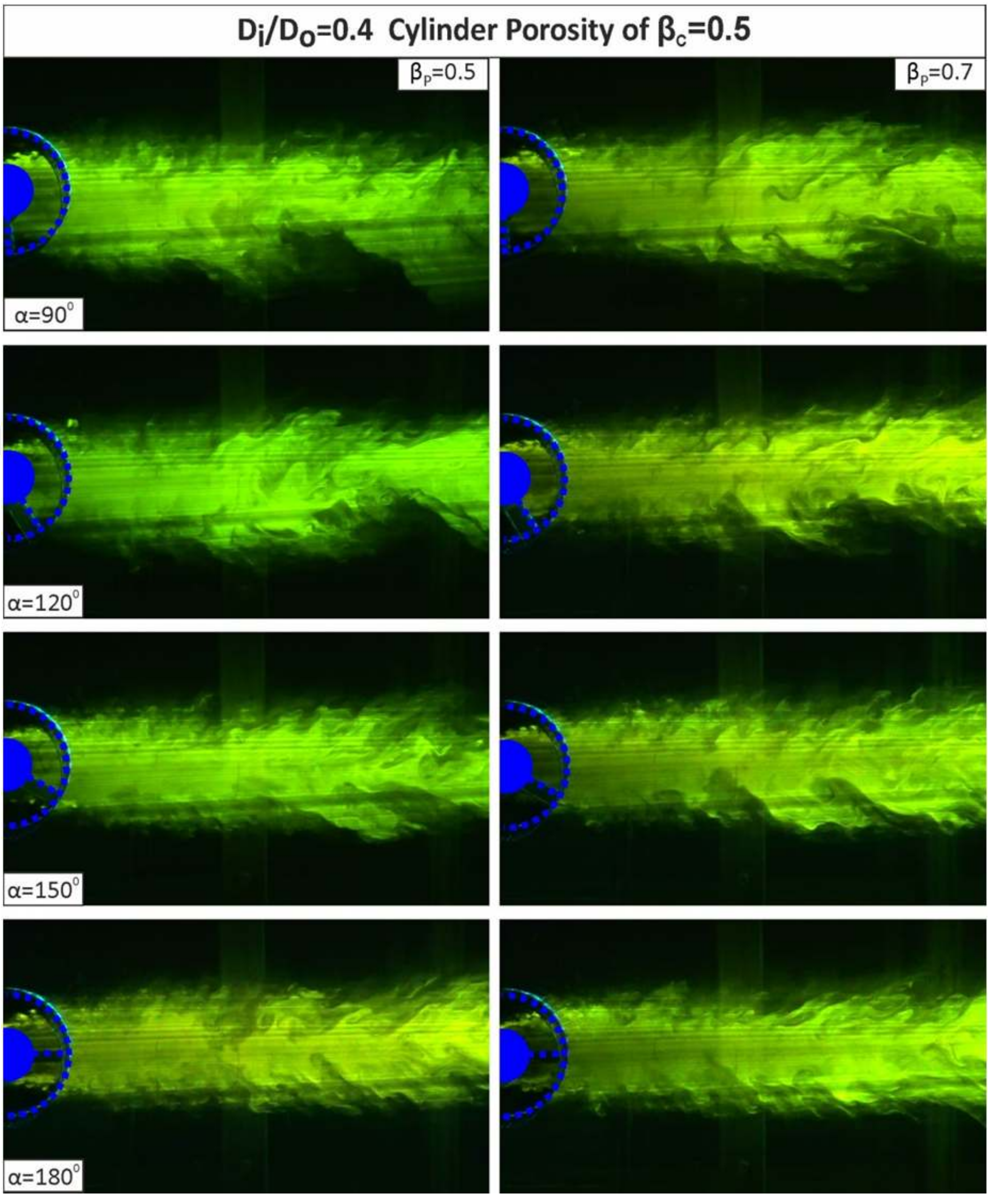

Figure 4.8. Instantaneous dye visualization results of cylinder porosity, β_C= 0.5 and plate porosity of β_P= 0.5, 0.7 for different plate angles

Momentary dye visualization images of cylinder porosity, β_C= 0.7 and plate porosity values of β_P= 0 and 0.3 are exhibited in the figure 4.9. When the figure is examined in detail, it is explicit that β_C= 0.7 has not much control effect over inner cylinder. This is because, the flow directed to the inner cylinder is separated and constitute upper and lower shear layers, then these shear layers directed to the outer cylinder and can pass the outer cylinder easily due to high porosity ratio. Therefore for β_C= 0.7 case, due to absence of the blockage effect, the shear layers cannot generate significant scale vortex pair. In contrast with β_C= 0.3 and 0.5 cases, β_C= 0.7 configuration cannot accomplish effective control on the wake region even with the presence of splitter plate angle of 180°. Normally, 180° plate angle was one of the most efficient parameter for low cylinder porosities, but Karman Vortex Street takes place even for the 180° case and this plate angle can be regarded as inefficient. The arrangement with plate angle of 150° has slightly better results than 180° and there is no significant Karman Vortex Street formation.

Splitter plate utilization comes into prominence for the β_C= 0.7 case and splitter plate becomes dominant in this arrangement. It should also be stated that when very low porous splitter plate is utilized with very high porous cylinder, this situation give rise to incompatibility between splitter plate and outer cylinder. For the low plate angles of 90° and 120°, very low porous splitter plate blocks the flow almost wholly and flow is directed to upper side of the cylinder. This flow moves with a higher momentum and can pass through the outer cylinder easily. Even though β_C= 0.7 allow the high momentum flow to pass through, it also has a small dispenser effect that resulting more extensive wake region. Therefore, as can be seen from figure 4.9, 90° and 120° configurations has a little control effect on the inner cylinder relative to 150° and 180°. There is no Karman Vortex Street presence for these cases, but occasionally large scale vortex formation takes place in the wake region.

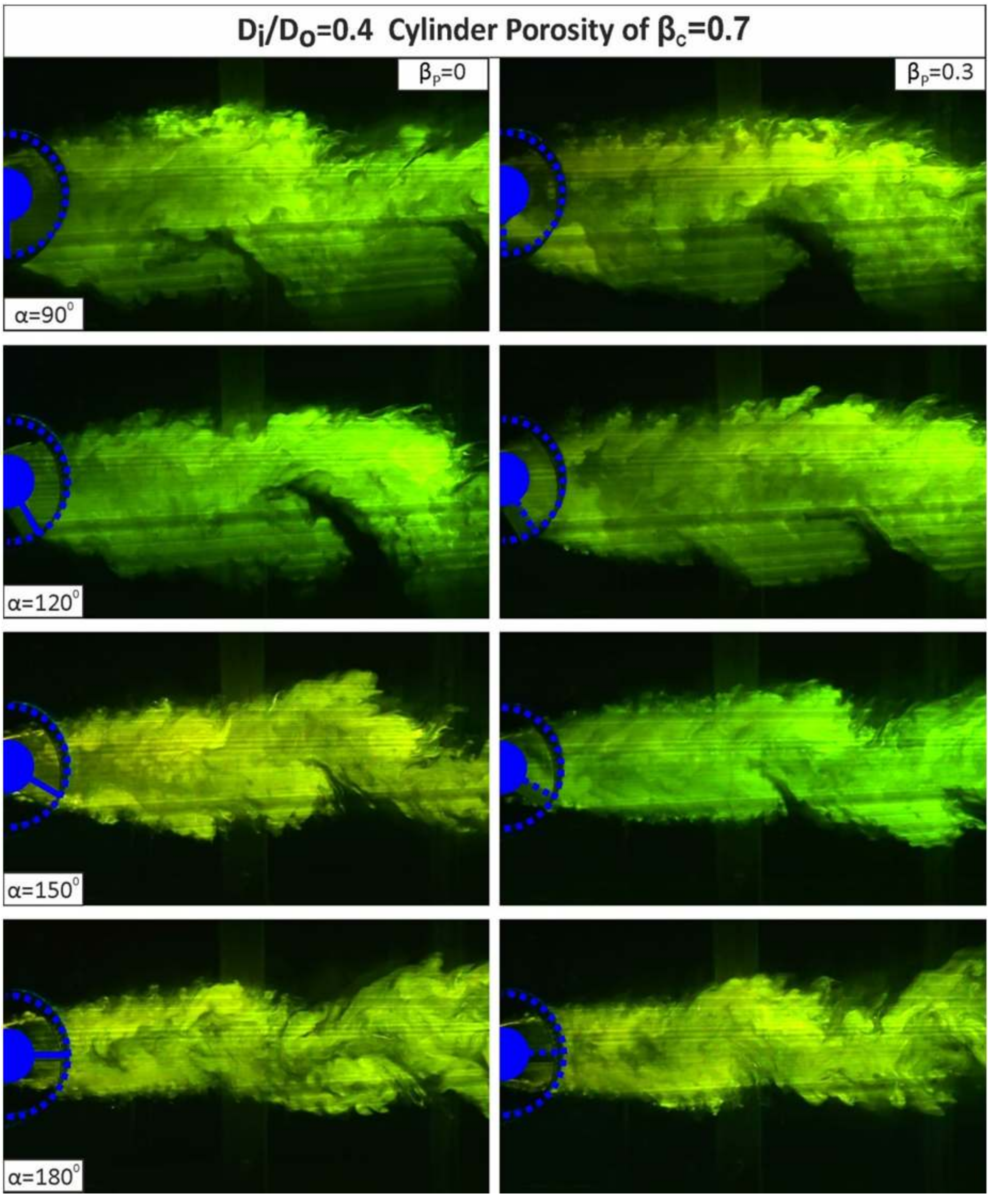

Figure 4.9. Instantaneous dye visualization results of cylinder porosity, β_C= 0.7 and plate porosity of β_P= 0, 0.3 for different plate angles

Momentary dye visualization images of cylinder porosity, β_C= 0.7 and plate porosity values of β_P= 0.5 and 0.7 are exhibited in the figure 4.10. Higher porosity values of both cylinder and splitter plate give rise to the flow to pass through easily and they have not blockage effect as β_P= 0 and 0.3. In the relevant figure it can be seen that the 180° plate angle cannot control the flow in the wake region and resulting the small scale Karman Vortex Street. However this Karman Vortex Street is not intense as in the bare cylinder case. If the figure is analyzed in detail, it can be seen the vortex formation in the wake initiates in far away from cylinder pair. Therefore it can be stated that very little control over the inner cylinder takes place even for the 180° plate angle. The plate angle of 150° has almost same effect with the 180° over the inner cylinder and cannot be mentioned from a fully controlled flow.

When the figure 4.9 and 4.10 compared with each other, narrower and more controlled wake region attract notice for the plate porosities of β_P= 0.5 and 0.7. It is because the plate porosity ratio is in accordance with the porosity of the outer cylinder and there is a certain consistency between them when they are utilized together. The compatibility between splitter plate and outer cylinder porosities came into prominence in this case just like in other cases.

For the plate angle of 90°, the flow seems to be controlled remarkably; only occasional vortex formation takes place in the wake region. Besides, plate angle of 120° draws attention in this arrangement as well as 90°. Because more stable and more consistent wake region takes places in this configuration. However, in general β_C= 0.7 application cannot be regarded as efficient as β_C= 0.5 application.

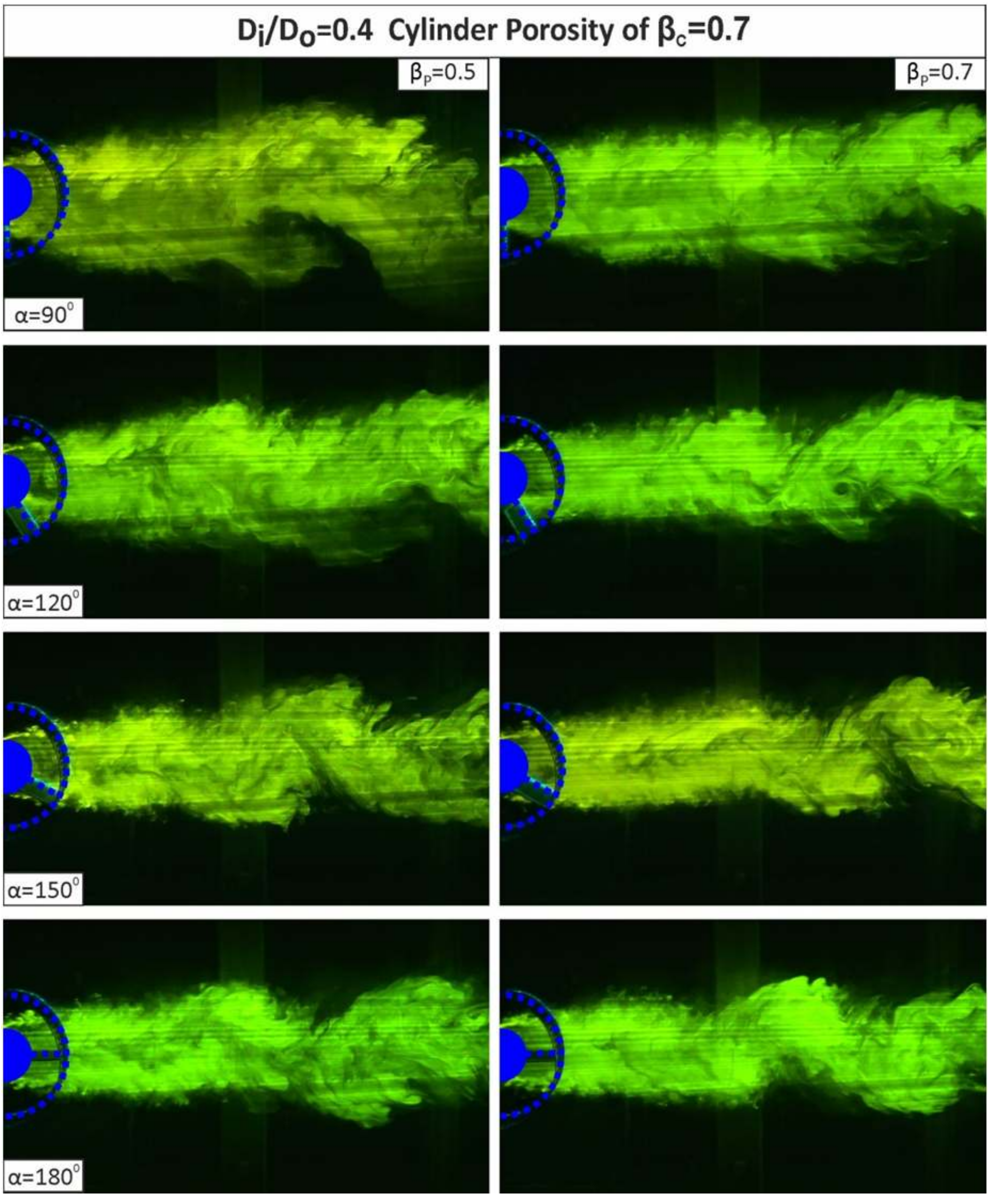

Figure 4.10. Instantaneous dye visualization results of cylinder porosity, β_C= 0.7 and plate porosity of β_P= 0.5, 0.7 for different plate angles

4.4. PIV Experiments Results

Up to this time, cylinder pair (inner and perforated outer cylinders) application without splitter plate was investigated by means of time averaged streamlines $<\psi>$, time averaged vorticity contours $<\omega>$ and instantaneous dye visualization results and dye visualization technique was applied to understand the flow structure in a qualitative manner for the splitter plate application. The purpose of the dye visualization experiments was to have a preliminary consideration about the flow, and comprehension of the splitter plate and cylinder effects to the flow structure. But for investigating the flow structure thoroughly and to determine the effective control parameters much better, quantitative and far-reaching PIV technique was applied. Therefore, all parameters and configurations that were examined by dye visualization method will be presented in this section by means of PIV technique in order to scrutinize the flow characteristics of the desired control parameters.

In figure 4.11 and 4.12, time averaged streamlines $<\psi>$ and time averaged vorticity contours $<\omega>$ were presented respectively, for cylinder porosity of β_C= 0.3 and plate porosity of β_P= 0, 0.3 with different plate angles. β_C= 0.3 and plate porosity of β_P= 0, 0.3 are the lowest porous medias for the present study. From the dye visualization images the blockage effect of these porosities were observed and for the streamlines $<\psi>$ and vorticity contours $<\omega>$, complicated flow structure can be seen from the corresponding figures as it is anticipated. And the most salient feature of this β_C= 0.3 configuration is that the jet like flow that takes place just on the downstream side of the outer perforated cylinder, can be seen in figure 4.12 for all plate angles. So even if the outer cylinder is used as semi circular cylinder, β_C= 0.3 porosity hinder the vortex pair from passing through the outer cylinder in the annular region and prevent large scale vortex generation in the wake region. Figure 4.11 is compatible with the figure 4.12 and this jet like flows, resulting circulating flow structure, is indicated as F_3 and F_4 in figure 4.11. The circulating flow structure developed out of jet like flow on the outer cylinder can be explained as follows. There are circular holes on the outer cylinder to obtain the desired porosity ratio and the distance between these holes are remarkably high. These high distances between the holes bring about dead flow regions between the jet streams. Then between the jet streams and dead flow regions, strong shear layers come into existence and reverse flows developed out of these shear layers around the jets. Thus, the circulating flow structure just behind the outer cylinder comes into existence.

In figure 4.11 and 4.12, there is no interaction of vortex pair generated by inner cylinder and both streamlines $<\psi>$ and vorticity contours $<\omega>$ are in accordance with each other for the plate angle of 180°. The only difference between plate porosity of β_P= 0 and β_P= 0.3 is that plate porosity of 0.3 bring about lower scale of vortex pair. When we look at the α=180° configuration, the narrow wake region and absence of Karman Vortex Street draws attention. So these PIV results match up with dye visualization results and this configuration can be regarded as successful to control the flow. For the plate angle of 150°, there is no indication of vortex pair interaction according to vorticity contours $<\omega>$, but there is a small scale vortex pair formation just in downstream of the outer cylinder symbolized by F_3-F_4 and $<\omega_3>$ in the corresponding figures. However this configuration also seems to be effective control case as well as 180° application. Therefore, β_P= 0 and β_P= 0.3 can be considered effective flow control parameters for α=150° and 180°.

For the plate angles of α= 90° and 120°, upper shear layer intensified by the blockage effect of the splitter plate get blocked by low porous outer cylinder and it is compelled to flow to the splitter plate. This effect can easily be seen from figure 4.12. On the other hand, because of low porous splitter plate blockage intensified upper shear layer give rise to larger jet like flow on the upper side of the outer cylinder whereas there are very small jet like flow on the lower side of the outer cylinder for 90° and 120° cases. Vortex pair formation in the upper side of the outer cylinder is valid for all four configuration in figure 4.11 and 4.12 and symbolized as F_3-F_4 and $\langle\omega_3\rangle$ in the relevant figures. In addition to these, large scale vortex generation and high momentum flow that encounters with the splitter plate may bring about unsteady and severe force on the splitter plate. Although there are no vortex pair interaction in the annular region and deficiency of large scale vortex formation for these plate angle values, we cannot consider 90° and 120° as effective parameters for β_C= 0.3 and β_P= 0, 0.3.

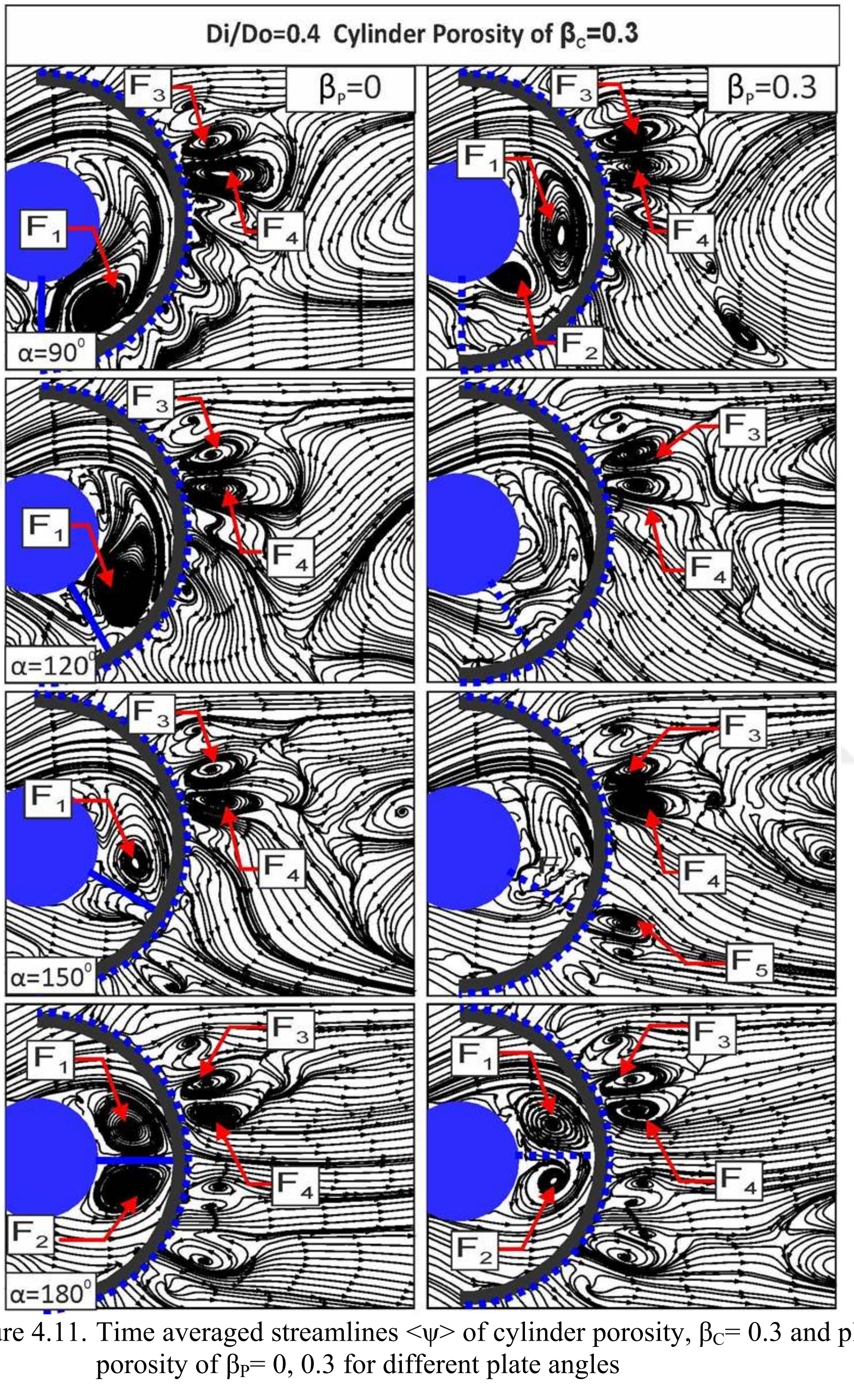

Figure 4.11. Time averaged streamlines <ψ> of cylinder porosity, β_C= 0.3 and plate porosity of β_P= 0, 0.3 for different plate angles

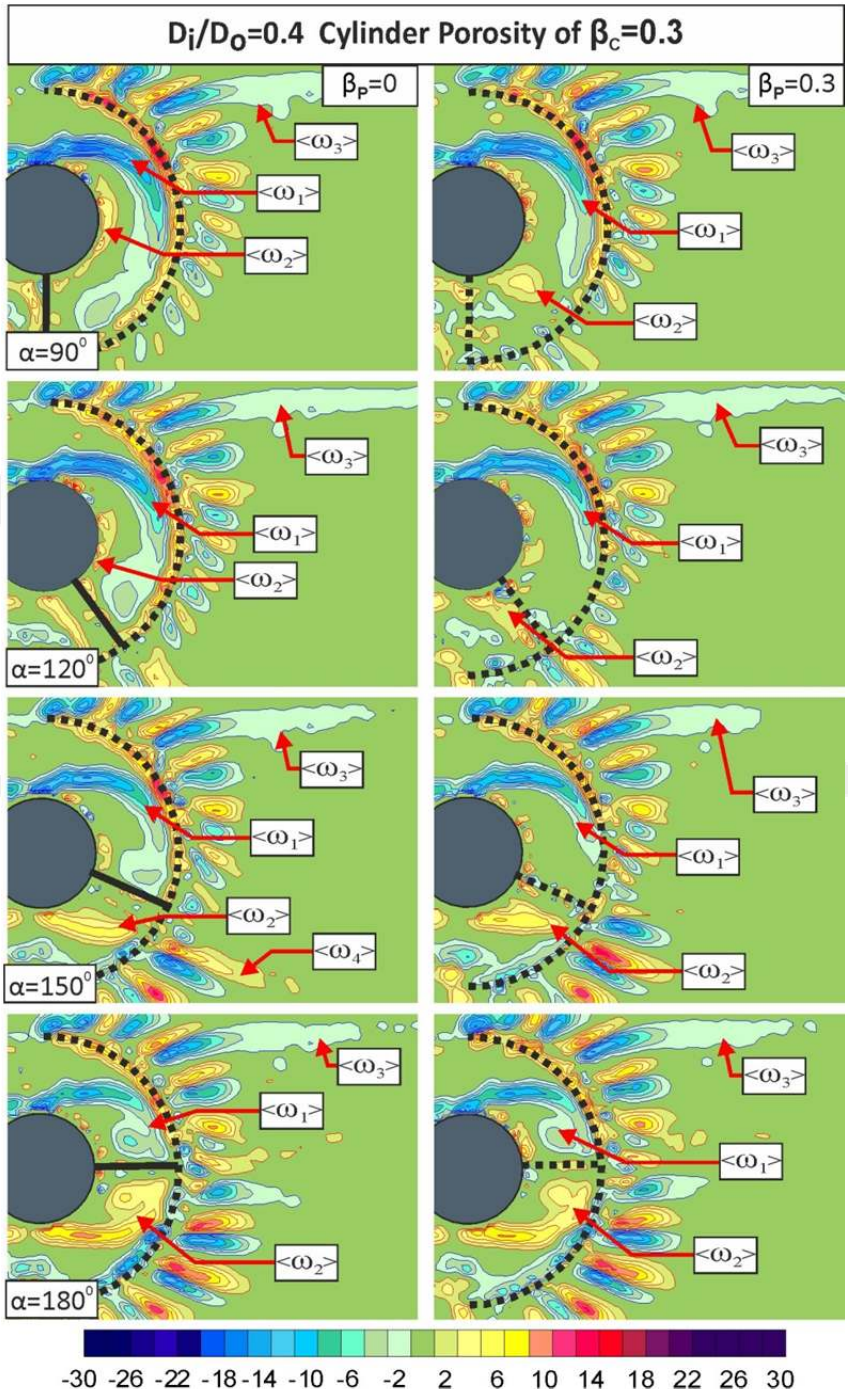

Figure 4.12. Time averaged vorticity contours <ω> of cylinder porosity, β_C= 0.3 and plate porosity of β_P= 0, 0.3 for different plate angles

The results obtained from the plate porosity of β_P= 0 and 0.3 for α= 90° and 120° were not efficient enough to control the flow and higher porous splitter plates (β_P= 0.5 and 0.7) are applied for the β_C= 0.3 configuration. The relevant time averaged streamlines <ψ> and time averaged vorticity contours <ω> were presented in figure 4.13 and 4.14. As can be seen in figure 4.13, three different vortex pair formation (F_1-F_2, F_3-F_4 and F_5-F_6) takes place for most of the configuration. It can be concluded that, this vortex pair formation is developed out interaction of reverse flow and jet streams due to the low porosity of the outer cylinder. Also, increasing the splitter plate porosity gives rise to the vortex pair formation of F_5-F_6, that is not takes place in the previous case with plate porosity of β_P= 0, 0.3. When we look at the time averaged vorticity contours <ω> in figure 4.14, both plates are able to disperse the vortex formation generated by lower shear layer partially, but they cannot prevent the interaction of vortex pair generated by lower and upper shear layers. Besides, $<w_1>$ and $<w_2>$ vorticity contours are getting closer each other in almost all plate angles except 150°. Plate angle of 150° is in the vicinity of the flow separation point, thus vortex formation in the lower shear layer is scattered just before the initiation, and momentum of the flow passing through the plate holes is diminished. Therefore, plate angle of 150° can be considered effective parameter to hinder the unsteady vortex shedding in the annular region. Another efficient parameter is the plate angle of 180° and increasing the plate porosity reduce the vortex pair interaction on a variable scale. Although the presence of the vortex pairs of F_3-F_4 and F_5-F_6 in the wake region, plate angle of 180° can be regarded as an effective control parameter for both plate porosity ratios. Instantaneous dye visualization results also justify this efficiency.

In figure 4.13, there are large scale vortex formation which can be seen partially at the end of the field of view, for β_P=0.5, α≤150° and β_P=0.7, α=90°. Even they cannot be seen in the vorticity contour <ω> figure, they are indicators of small scale vortex shedding. This vortex formation caused by low porosity of the outer cylinder may give rise to Karman Vortex Street in the far wake region.

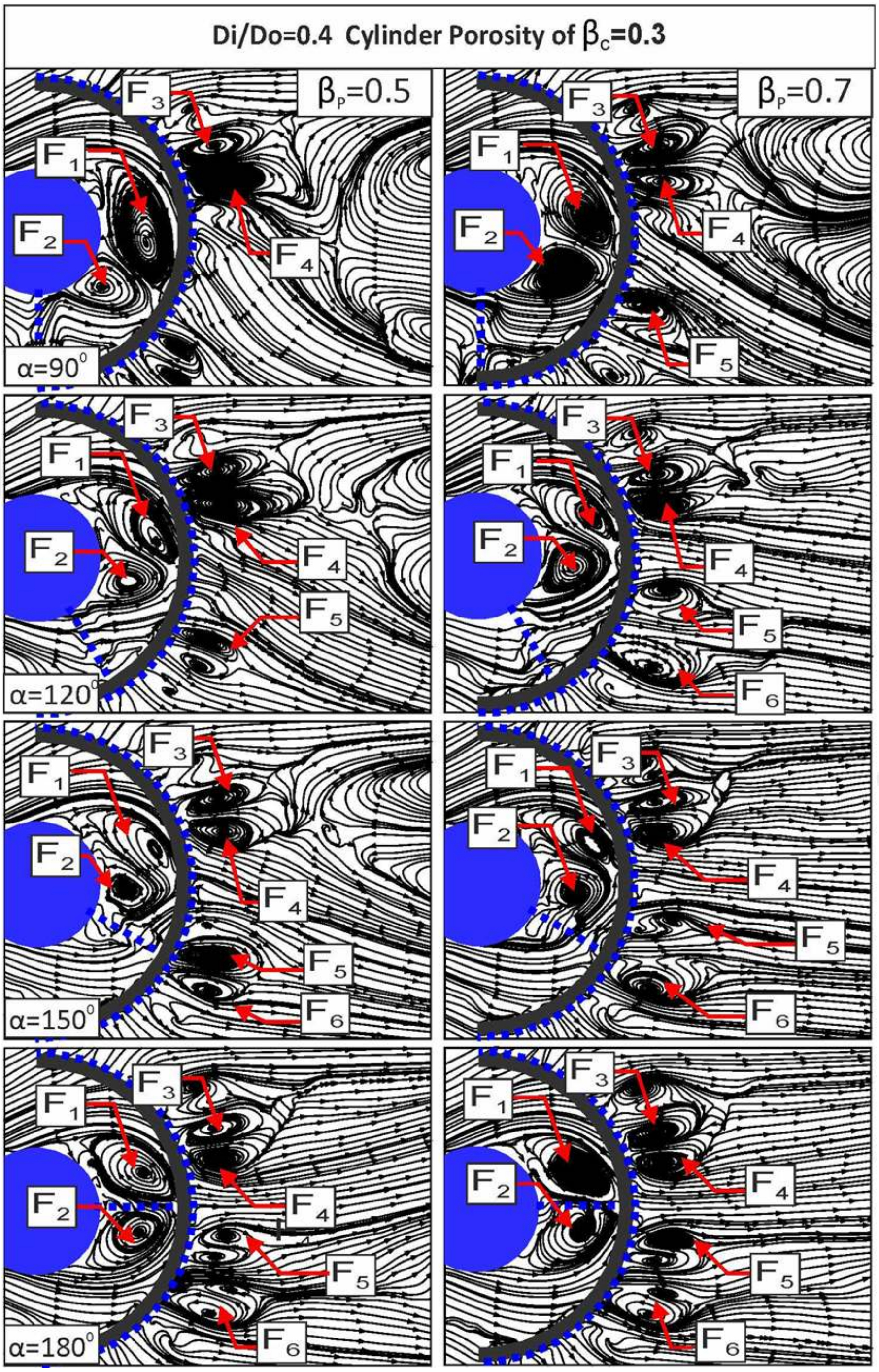

Figure 4.13. Time averaged streamlines <ψ> of cylinder porosity, β_C= 0.3 and plate porosity of β_P= 0.5, 0.7 for different plate angles

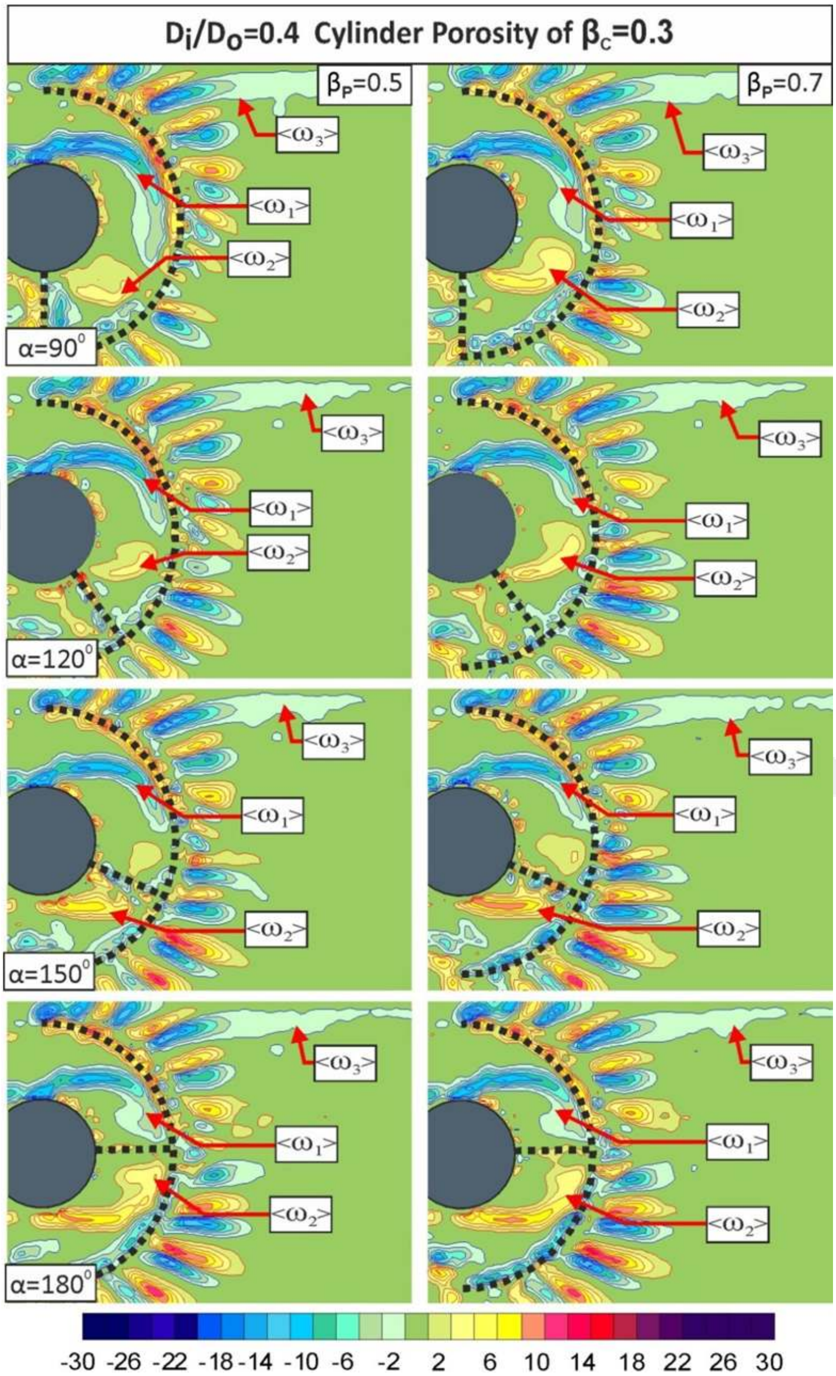

Figure 4.14. Time averaged vorticity contours <ω> of cylinder porosity, β_C= 0.3 and plate porosity of β_P= 0.5, 0.7 for different plate angles

It was stated before, for Di/Do=0.4, β_C= 0.5 is an effective parameter for suppression of the vortex shedding and for prevention of the Karman Vortex Street, according to the inner and outer perforated cylinder configuration in figure 4.2-3-4. And it was also proposed that vortex pair generated from the inner cylinder needs to be controlled to prevent the interaction of them and to eliminate the unsteady vibration and forces. And to annihilate the unsteady effects of vortex pair interaction, various porosity of splitter plates was also utilized and investigated for the cylinder porosity of β_C= 0.5 application. In figure 4.15 and 4.16, time averaged streamlines $\langle\psi\rangle$ and time averaged vorticity contours $\langle\omega\rangle$ were exhibited. At the first glance, plate angle of 180° seems to suppress the vortex interaction and Karman Vortex Street formation in both annular and wake region for either plate porosities. Thus for this case, plate angle of 180° can be presumed as the most effective plate angle.

Plate angle of 90° and 120° bring about the circulating flow structure in the annular region. When we look at the plate porosity of β_P= 0.3, the flow generated by the lower shear layer pass through the plate and create small scale vortex, and then this small scale vortex interact with other large scale vortex that is generated by the upper shear layer, resulting an unsteady flow structure. According to streamlines $\langle\psi\rangle$ (see the figure 4.15), this unsteady flow gives rise to large scale vortex formation in the far wake region, which may cause vortex shedding in farther wake region. For this reason 90° and 120° plate angles can be presumed as low efficient for controlling the flow behavior with low porous splitter plates.

Among the other plate angles, 150° plate angle should be commentated discretely. Because according to vorticity contours $\langle\omega\rangle$, it exhibit distinctive flow behavior. The vortex formation generated by the lower shear layer gets blocked by the splitter plate and pass through the outer cylinder, resulting elongated vortex formation indicated as $\langle\omega_4\rangle$ in figure 4.16. So 150° plate angle can be presumed as transition parameter and it can be concluded that remarkable flow control is achieved for the plate angle of 150° according to figure 4.15.

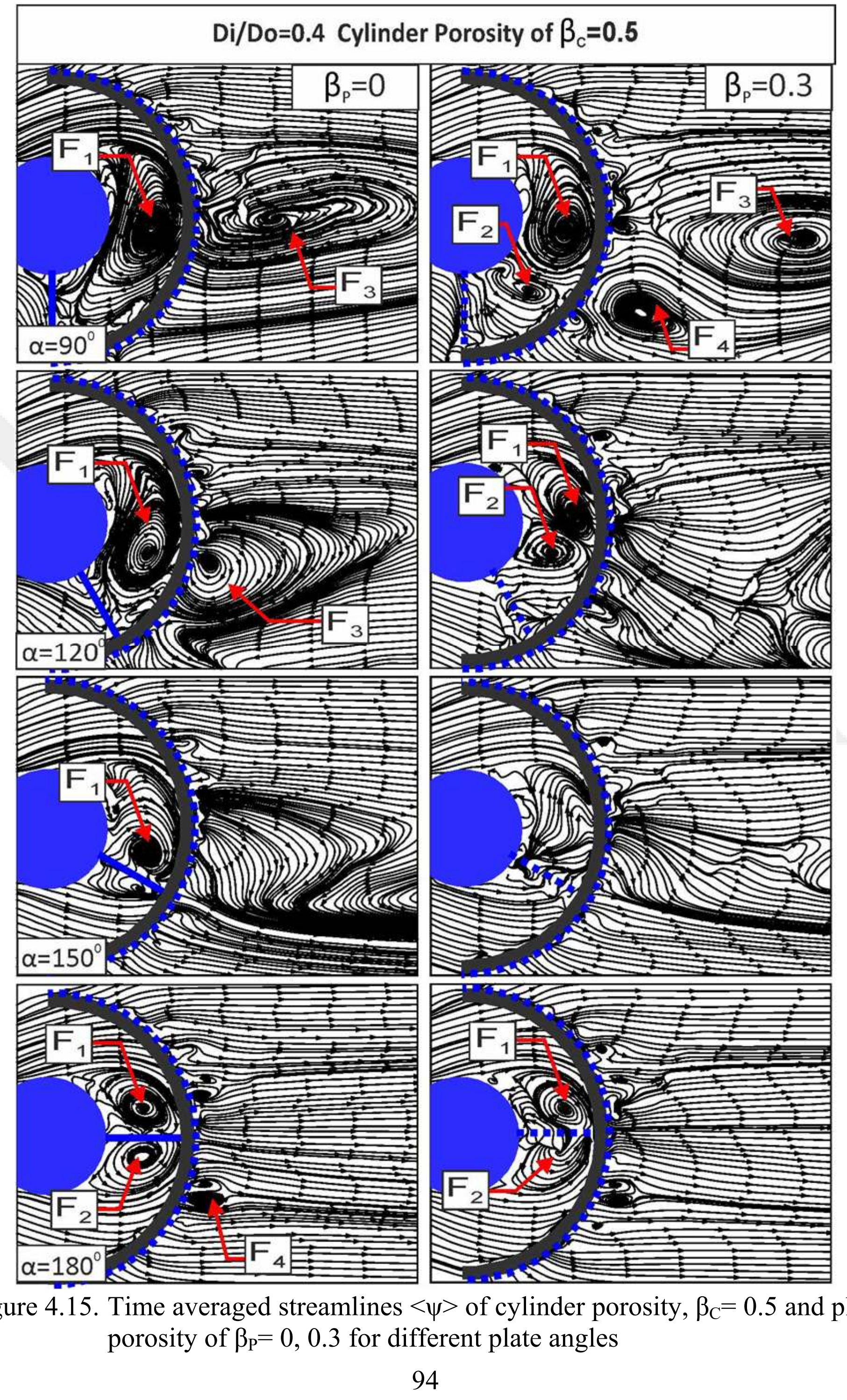

Figure 4.15. Time averaged streamlines <ψ> of cylinder porosity, β_C= 0.5 and plate porosity of β_P= 0, 0.3 for different plate angles

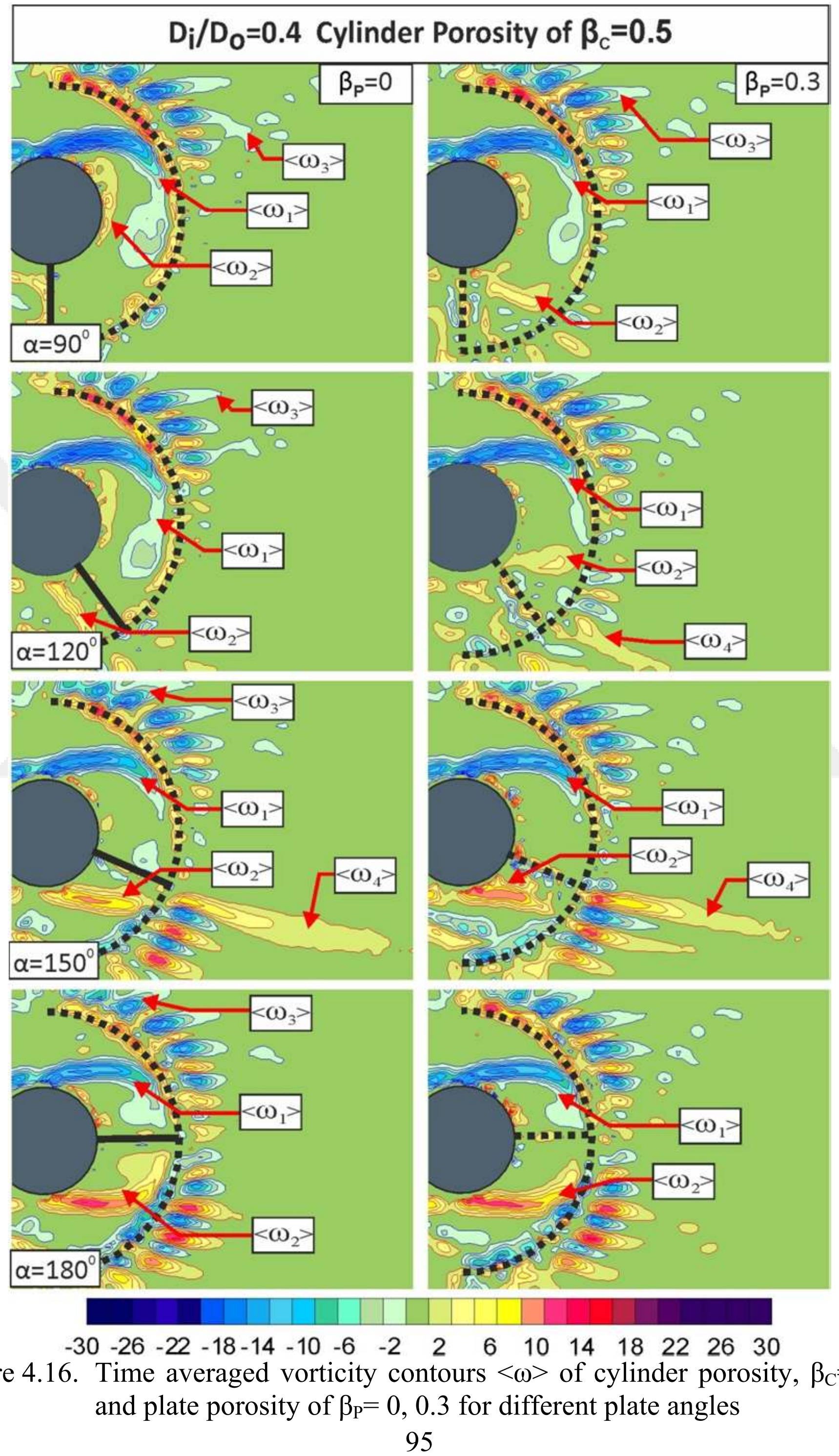

Figure 4.16. Time averaged vorticity contours <ω> of cylinder porosity, β_C= 0.5 and plate porosity of β_P= 0, 0.3 for different plate angles

In figure 4.17 and 4.18, time averaged streamlines $\langle\psi\rangle$ and time averaged vorticity contours $\langle\omega\rangle$ results were exhibited for cylinder porosity of β_C= 0.5 and plate porosity values of β_P= 0.5, 0.7. When plate porosities increase to 0.5 and 0.7 values, even for low plate angles (90° and 120° plate angles) vortex pair interaction takes place in the annular region. Vortex pair that is getting closer to each other can be seen from streamlines $\langle\psi\rangle$ and vorticity contours $\langle\omega\rangle$ in figure 4.17 and 4.18. Because high porous plates allow the flow to pass through from the lower shear layer to annular region, ending up with vortex formation and vortex pair interaction. Even if the flow behaviors show similarities, the vortex formation generated by the lower shear layer has larger scale for β_P= 0.5 and 0.7 relative to β_P= 0 and 0.3. Nevertheless, the dye visualization results indicate that almost perfectly controlled wake region for general β_C= 0.5 and β_P= 0.5, 0.7 case. And time averaged streamlines $\langle\psi\rangle$ and time averaged vorticity contours $\langle\omega\rangle$ are compatible with corresponding dye visualization results. Additionally, jet like flow occurred in this case for β_C=0.5 are substantially small relative to those take place in β_C=0.3 case and no vortex pair formation (F_3-F_4, F_5-F_6) appear as it can be seen from time averaged streamlines $\langle\psi\rangle$ in figure 4.17. Therefore, up until now, all of the configurations for cylinder porosity of β_C=0.5 and for plate porosity of β_P= 0.5, 0.7 can be presumed as the most effective case by virtue of the fact that prevention of the Karman Vortex Street and controlling the wake region. However, because of the interaction of vortex pair in the annular region and its effect to the inner cylinder, that high porous plates may not be presumed as totally efficient to control the annular region remarkably for this case. According to vorticity contours, $\langle w_1\rangle$ and $\langle w_2\rangle$ vorticities head towards each other for almost all plate angles and they interact with each other. Nonetheless, according to streamlines $\langle\psi\rangle$, vortex pair interaction seems to be prevented for the 180° plate angle in both plate porosities. Consequently, plate porosity of β_P= 0.5 and 0.7 can be regarded as efficient control parameters for 180° plate angle, to prevent the Karman Vortex Street and to control both annular and wake region.

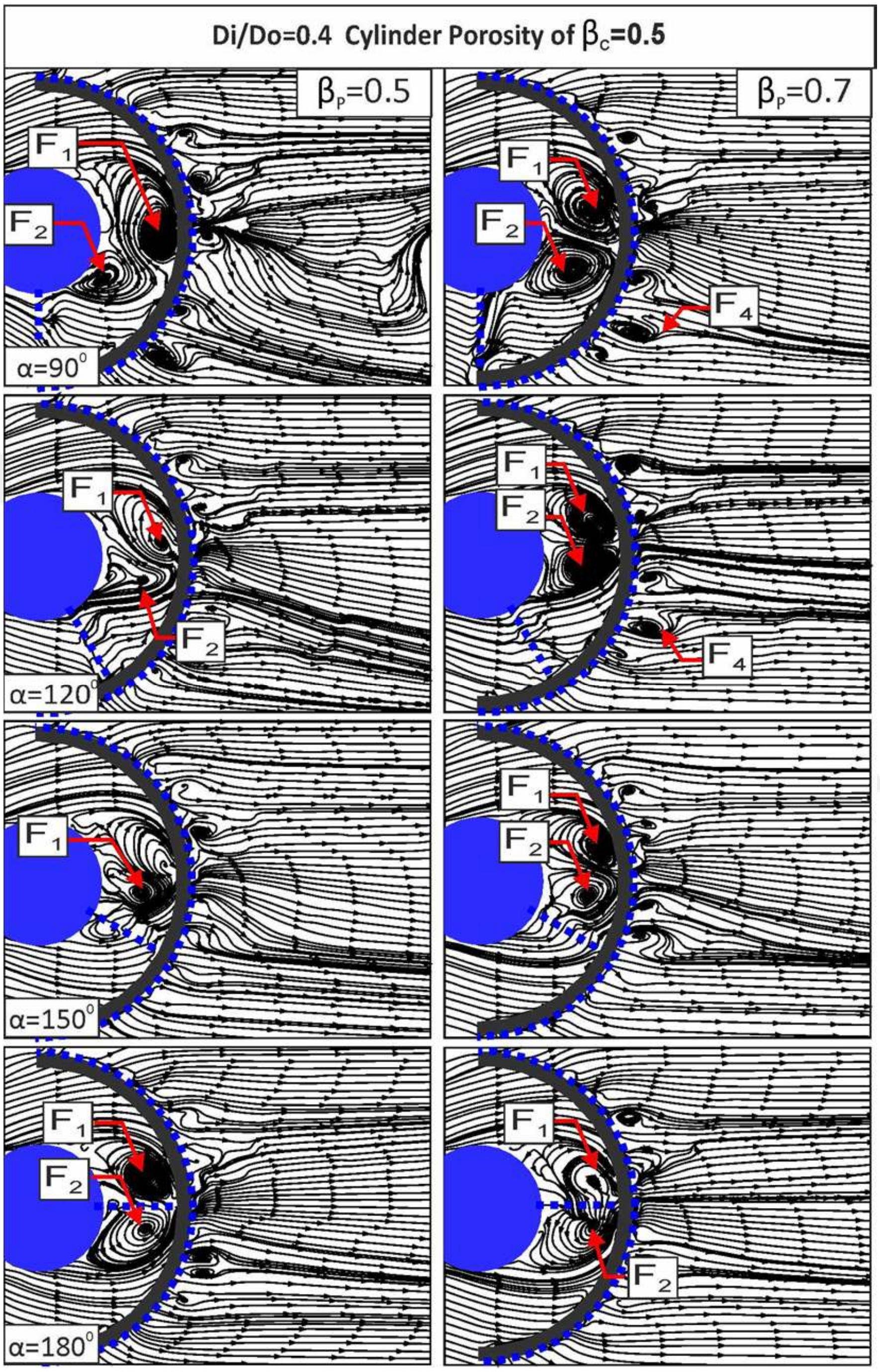

Figure 4.17. Time averaged streamlines <ψ> of cylinder porosity, β_C= 0.5 and plate porosity of β_P= 0.5, 0.7 for different plate angles

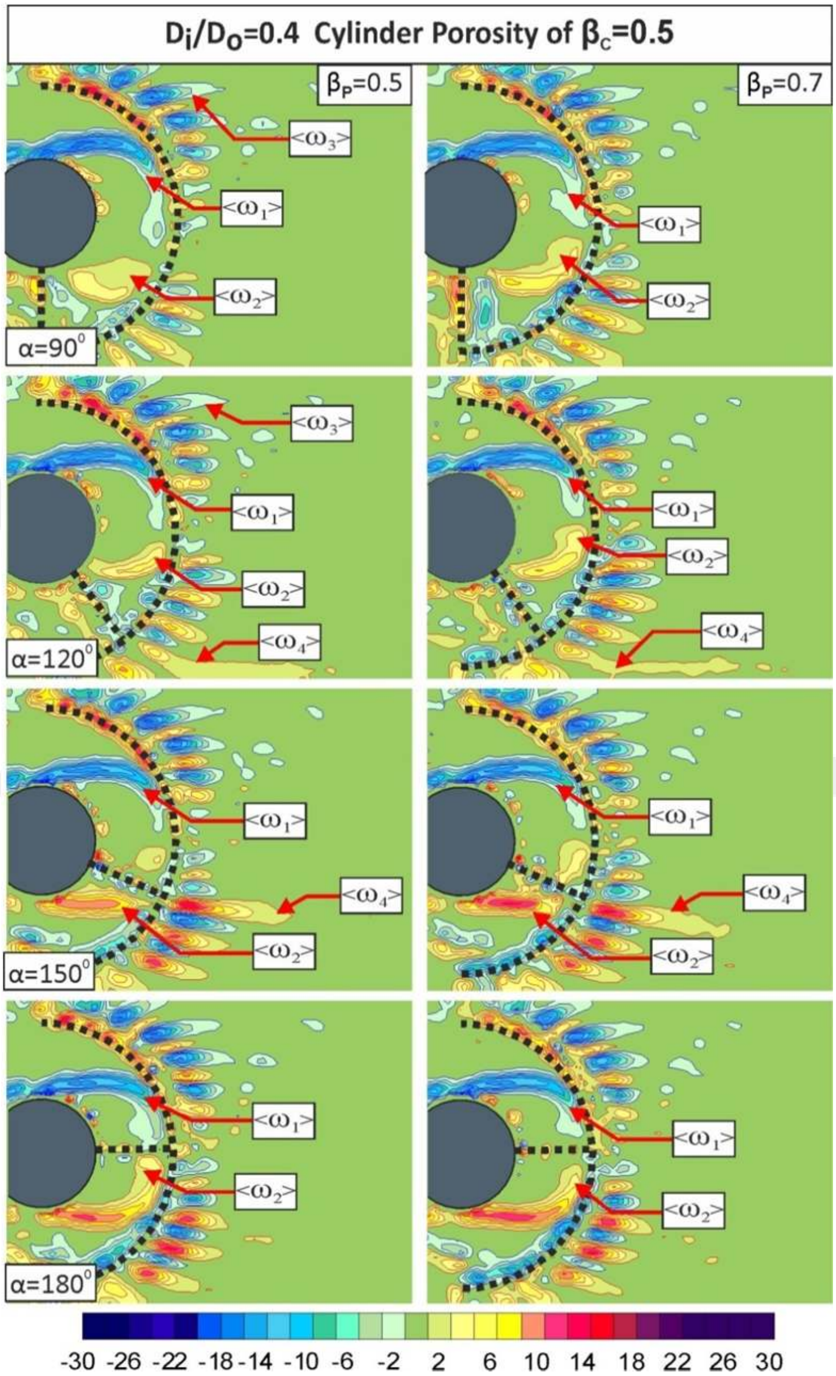

Figure 4.18. Time averaged vorticity contours <ω> of cylinder porosity, β_C= 0.5 and plate porosity of β_P= 0.5, 0.7 for different plate angles

The relevant time averaged streamlines $<\psi>$ and time averaged vorticity contours $<\omega>$ of β_C= 0.7 and β_P= 0, 0.3 case were presented in figure 4.19 and 4.20. Increasing outer cylinder porosity brings about the high momentum flow generated by shear layers pass through the outer cylinder easily and gives rise to more complicated flow structure. This complicated flow behaviors can be seen streamlines $<\psi>$, vorticity contours $<\omega>$ and dye visualization images clearly. For all plate angles, vortex shedding occurs in the wake region and ends up with Karman Vortex Street presence. As the plate angle increases wake region becomes narrower in the vertical direction and smaller scale vortex formation takes place.

According to the figure 4.19, it can be observed that no effective flow control is achieved and time averaged vorticity contours $<\omega>$ and dye visualization results confirm this situation. The vortex pair formation in the wake region is indicated by F symbol and its extent decreases as the plate angles increase. Additionally, for some parameters (β_P= 0.3 and α= 90° and 120°), saddle points, which are the indicators of vortex shedding, appear in the wake region and that means there is no flow control in the wake region. It can also be seen that the distance between the vortex pairs (F_3-F_4) in the wake region diminishes as the plate angle enhances, resulting narrower wake region. Although there is no complete control in the wake region, vortex pair interaction in the annular region is suppressed and unsteady forces that the inner cylinder is exposed to be prevented, especially for the plate angle of 180°. Besides, it can be observed from the dye visualization records that vortex shedding frequency downstream of the outer cylinder is diminished.

When time averaged vorticity contours $<\omega>$ in figure 4.20 are examined in detail, unusual flow structure in the downstream of the outer cylinder takes place due to the high cylinder porosity. Particularly for the $\alpha \geq 150°$, the pair of vortices, which are little or no contact with the plate, are subjected to some distortion by the outer cylinder, forming a pairs of vortices ($<w_3-w_4>$) aligned with the upper and lower layers of the inner cylinder. As a matter of fact, this vortex pair develops downstream direction, breaking each other and forming the vortex street. Therefore, it can be said that β_C= 0.7 is not sufficient to control the flow structure downstream of the outer cylinder. Compared to the inner-outer cylinder case where the plate was not used, flow control was provided in the annular region for β_P= 0 and α= 180°, and the vortex formation and vortex breakdown distance increased on the horizontal axis in the downstream of the outer cylinder.

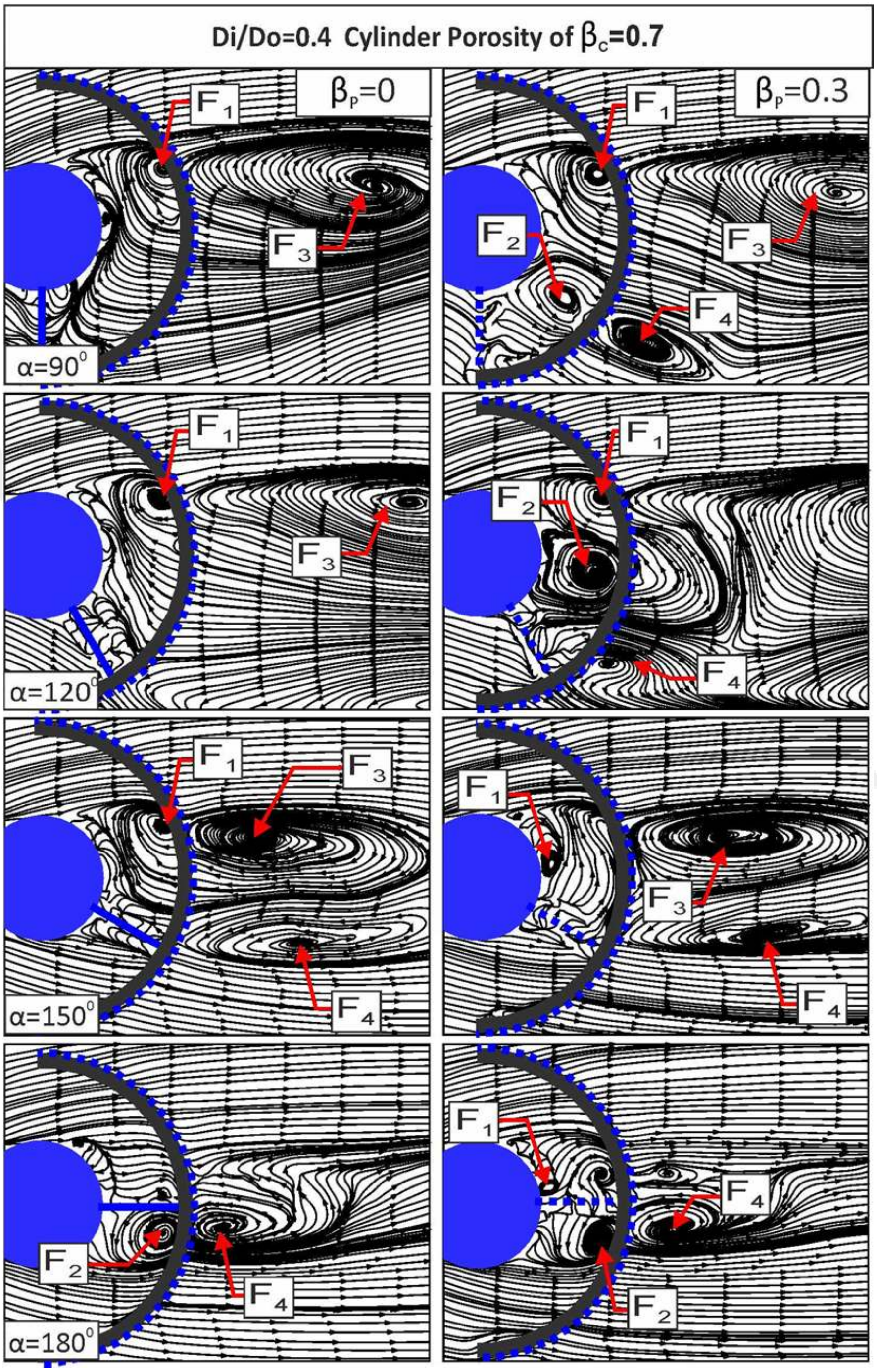

Figure 4.19. Time averaged streamlines <ψ> of cylinder porosity, β_C= 0.7 and plate porosity of β_P= 0, 0.3 for different plate angles

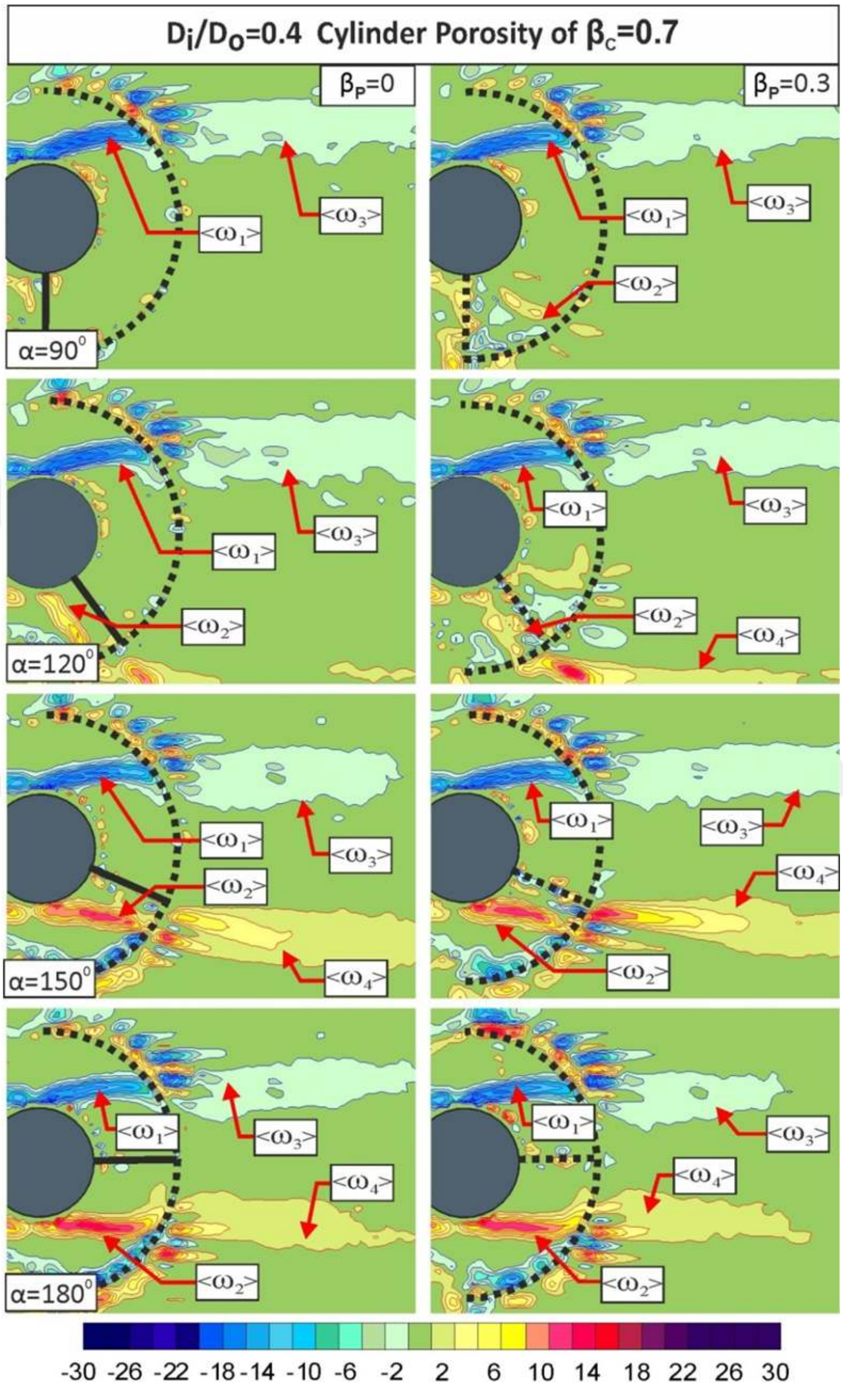

Figure 4.20. Time averaged vorticity contours <ω> of cylinder porosity, β_C= 0.7 and plate porosity of β_P= 0, 0.3 for different plate angles

The relevant time averaged streamlines <ψ> and time averaged vorticity contours <ω> of β_C= 0.7 and β_P= 0.5, 0.7 case were presented in figure 4.21 and 4.22. The increase in the permeability of the plate results in an increase in the strength of the eddy structure compared to the lower permeability of the plate. And as can be seen from the time averaged streamlines <ψ>, both in the annular and the wake region vortex formation takes place. This results in the formation and breakout of the vortex in downstream of the outer cylinder, as can be seen from the respective dye visualization results. This situation is clearly can be observed in both plate porosities for almost all plate angles. When the results obtained are compared with the non-plate state, there is a slight increase in the vortex shedding. It cannot be said clearly about the effect of the vortex pairs formed in the annular region on the inner cylinder, and it is seen that these vortex pairs also continue to affect the downstream of the outer cylinder. The variation between the elongation amounts of the vortex pair is particularly evident in the transition from α= 150° to α= 180°, due to the fact that α= 150° is located in the vicinity of the flow separation point.

When time averaged vorticity contours <ω> in figure 4.22 compared with the figure 4.20, there is no significant change especially for the 150° and 180° plate angles and unusual flow structure in the downstream of the outer cylinder takes place for these plate porosities as well. And vortices pair <w_3-w_4> formation can be seen in figure 4.22 take place as the same way those in figure 4.20.

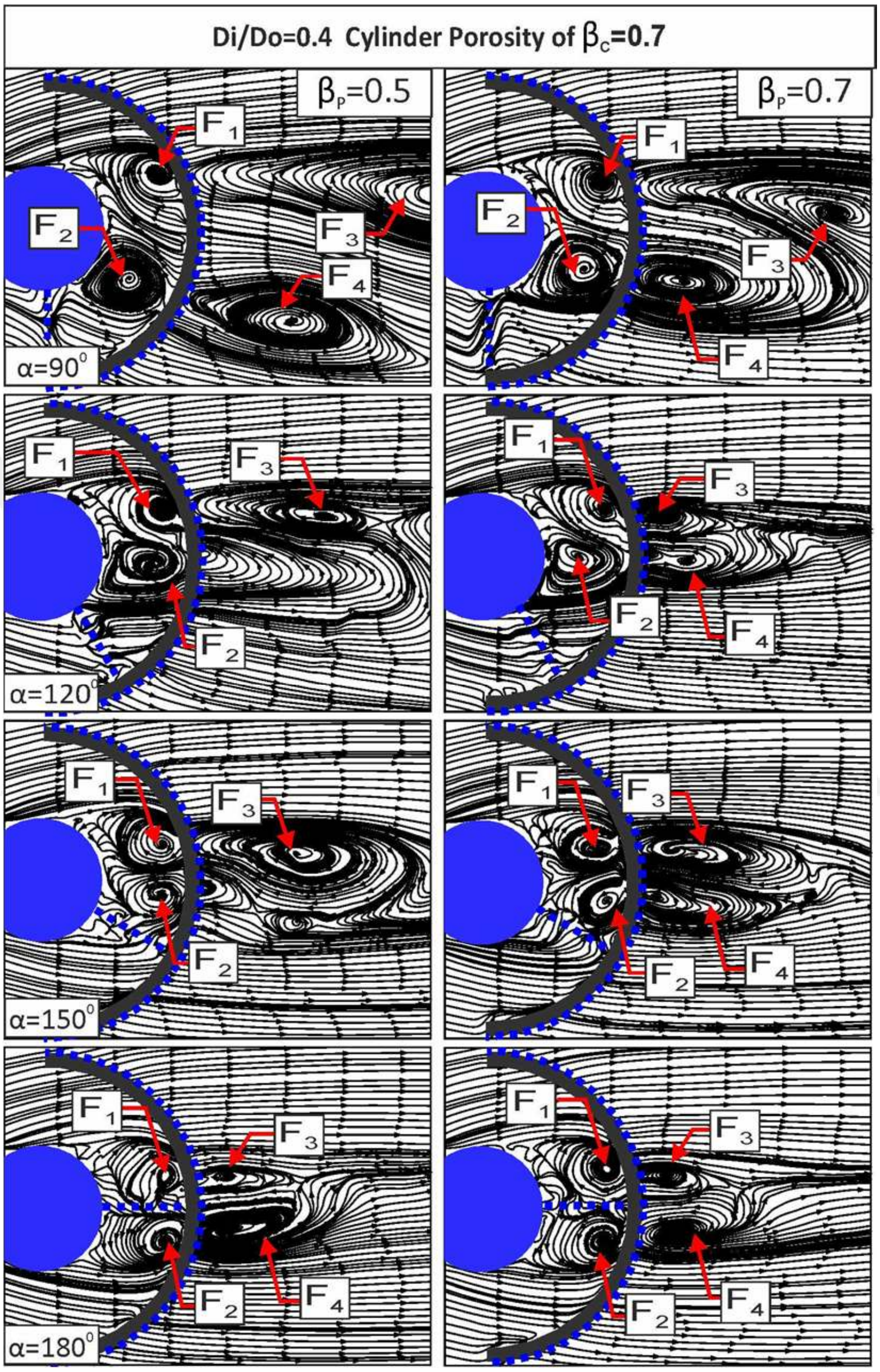

Figure 4.21. Time averaged streamlines <ψ> of cylinder porosity, β_C= 0.7 and plate porosity of β_P= 0.5, 0.7 for different plate angles

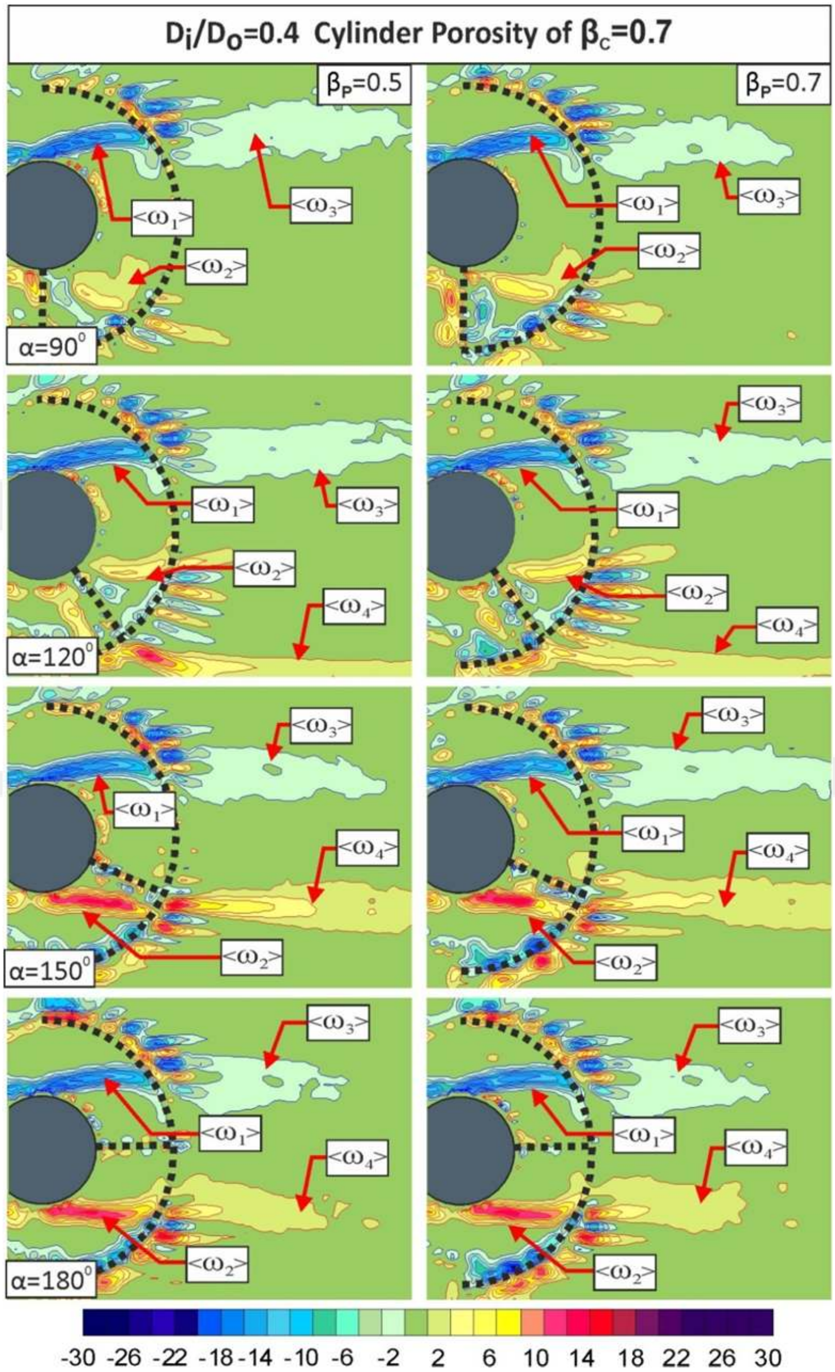

Figure 4.22. Time averaged vorticity contours <ω> of cylinder porosity, β_C= 0.7 and plate porosity of β_P= 0.5, 0.7 for different plate angles

4.5. Turbulent Kinetic Energy Results

The dye visualization and PIV experiments results were interpreted according to time averaged streamlines <ψ>, time averaged vorticity contours <ω> and dye visualization images for all control configurations in a qualitative manner previously. However it was mentioned before that by the help of PIV technique quantitative results can be acquired. Accordingly, to have solid ideas about the flow control for the applied control methods and relevant parameters, and to affirm the validity of the previous interpretations, the turbulence level of the flow for all configurations were investigated thoroughly. As the control of downstream of the circular cylinder both in annular and wake region is the main concern of the present study, it is indispensable to diminish the Turbulence Kinetic Energy (TKE) level especially in the annular region due to its proximity to the inner cylinder. It may not be adequate and appropriate to commentate about the flow control only according to streamlines, vorticity contours and dye visualization images. Because even if vortex pair formation takes place in the annular region, the TKE values may indicate a sufficient decrease. Accordingly, further qualitative investigation was carried out by means of TKE values to compare and discuss the effectiveness of the control parameters. To that end the general formula of the TKE is presented below as;

$$TKE = \frac{1}{2}\left[< u'u' > + < v'v' > + < w'w' >\right]$$

The third fluctuating velocity component can be computed by a 2D approximation when assuming the flow is isotropic (Sheng et al., 2000), in such a way that the third component has been supposed to be equal to the half of $[< u'u' > + < v'v' >]$, in that case the TKE can be computed by the help of formula given below;

$$TKE = \frac{3}{4}\left[<u'u'> + <v'v'>\right]$$

In the figures presented below, maximum TKE values (TKE_{max}) in the annular region were determined for every single configuration and two dimensional graphs were generated to make comparison of the results according to the bare cylinder case. TKE_{max} values are indicated with respect to plate angles and plate porosity values are shown as discrete symbols and lines that have distinct color. The dashed lines represent the TKE_{max} value for the bare cylinder case and it is utilized in the graphs to compare the results obtained from every single configuration. TKE_{max} for the bare cylinder case calculated as 0.044 that is the reference point of the study and the values below the 0.044 can be regarded as effective control parameters.

In figure 4.23, TKE_{max} values of β_C=0.3 case is presented according to the relevant plate angles and different plate porosity ratios. The maximum turbulence level diversity can be seen from the graph and every single parameter represents its own qualification. In comparison with the streamlines topology, vorticity contours and dye visualization results, the maximum turbulence kinetic energy results indicate perfect consistency and compatibility. The plate angle of 180° was stated earlier one of the most effective plate angle value with respect to streamlines and vorticity contours and for the case of β_C=0.3, all the plate porosity ratios justify this statement. Because the TKE_{max} values of all plate porosity ratios, even for the β_P=0, are just below the TKE_{max} value of bare cylinder. And these TKE_{max} values indicate remarkably high control in the annular region for the plate angle of 180°. For the β_P=0 TKE_{max} value of 0.0356 is obtained and this correspond to 19% TKE_{max} reduction for the case 180° plate angle. And for the β_P=0.5 and 180° plate angle, TKE_{max} value was found to be 0.029 and corresponding TKE_{max} reduction was found as 34%. This reduction is also the highest reduction among the all parameters.

When we look at the figure 4.23, the TKE_{max} descends as the plate angle enhances. This situation stems from the blockage effect of the lower splitter plate angles. As the plate angle diminish, it becomes more perpendicular to the flow direction and ending up with more blockage effect especially for lower porous plates. And blocked by the splitter plate the flow is directed to the upper shear layer and brings in higher momentum to the upper shear layer, then due to the low porosity of the outer cylinder the flow cannot pass through and circulates in the annular region. This high momentum and circulating flow is the main reason for high TKE_{max} value as can be seen from the figure. For the plate porosity values of β_P=0 and 0.3, the TKE_{max} values are even higher than the bare cylinder case except the 180° plate angle. As the porosity ratio enhances, the momentum level of the upper shear layer decreases as well as TKE_{max} value. This effect can clearly be perceived from the graph, it can be seen that as the porosity ratio increase the TKE_{max} value decrease almost gradually. Plate porosity ratios of 0 and 0.3 indicate almost identical trend, the only difference is that the plate porosity ratio of β_P=0.3 has lower TKE_{max} values in general.

Plate porosity ratios of β_P=0.5 and 0.7 are need to be commentated separately, by virtue of the fact that they are capable of control the annular region regardless of the plate angle. There is a complete control in the annular region for β_P=0.5 and 0.7 at all plate angles. Another remarkable result is that the plate porosity ratio of β_P=0.5 exhibits almost linear decrease as the plate angle enhances, and reaches its maximum TKE_{max} reduction at the 180° plate angle. As it is mentioned before according to streamlines topology and vorticity contours β_P=0.5 is the most effective plate porosity ratio and that statement was validated by the TKE results. It is because the plate with β_P=0.5 ratio allows sufficient amount of flow to pass and blocks the sufficient amount of flow. Lastly, the β_P=0.7 ratio exhibits a reduction only from 90° to 120° and remain nearly constant at the range of 120°≤ α ≤180°. Except for the 180° plate angle, β_P=0.7 ratio has little bit lower

TKE_{max} values than those of β_P=0.5 ratio. Consequently, the plate porosity ratio of β_P=0.7 can be regard as effective and coherent control parameter as well as β_P=0.5.

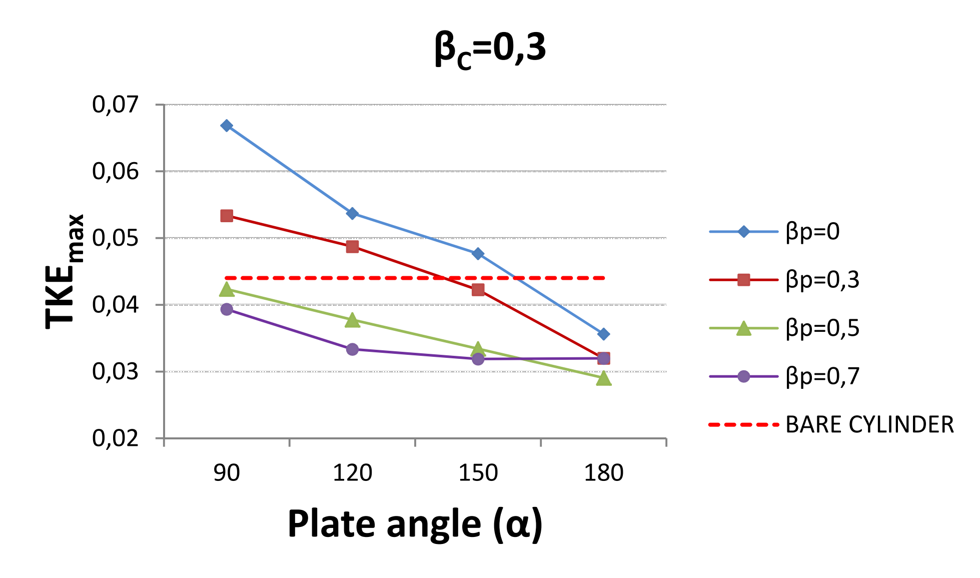

Figure 4.23. TKE_{max} distribution according to different plate angles and splitter plate porosity ratios, for β_C = 0.3

The maximum turbulence kinetic energy levels for the β_C=0.5 case were introduced according to different plate angles and plate porosity ratios in figure 4.24. When compared with the figure 4.23, as the cylinder porosity enhances, the plate porosity ratio comes into prominence. This effect can be perceived easily from the figure 4.24, the difference between TKE_{max} distribution for β_P=0 and 0.3 are greater than the β_C=0.3 case. Another difference between β_C=0.3 and 0.5 is that for the β_P=0 the highest TKE_{max} value is lower than the β_C=0.3 case. Even if the maximum reduction of TKE_{max} was accomplished for the β_C=0.3, the general TKE_{max} distribution of β_C=0.5 can be regarded as slightly more efficient than those of β_C=0.3. By reason of the higher cylinder porosity ratio enables more flow to pass through the outer cylinder at sufficient amount, reducing the upper shear layer momentum for the lower plate angles. When we look at the β_P=0.3 ratio, there is a flow control in annular region except the plate angle of 90°, and the efficiency of this control is almost the same as those of β_P=0.5 and 0.7 at 150° and 180° plate angles. So β_C=0.5 has better effect on flow control for β_P=0.3 ratio and due to this effect β_C=0.5 can be considered slightly more efficient than β_C=0.3. Another noticeable consequence is that the β_P=0.5 and 0.7 ratios have almost identical TKE_{max} distributions according to plate angles. And even for the 90° plate angle, β_P=0.5 and 0.7 have remarkable flow control. When the plate angle ranges between 120°≤ α ≤180° there is no significant change in the TKE_{max} values for β_P=0.5 and 0.7 ratios. Therefore, as in the previous case for β_C=0.5, β_P=0.5 and 0.7 can be regarded as the most effective porosity ratios. In this arrangement for β_C=0.5 ratio, the peak value of TKE_{max} reduction is 22% when the plate porosity is β_P=0.5 and at 180° plate angle. Additionally, for β_P=0.5 and 0.7, when the plate angle ranges between 120°≤ α ≤180°, TKE_{max} reduction is about 21% and almost remain constant. Even for β_P=0.3, at 150° and 180° plate angles, the TKE_{max} reduction of nearly 20% was obtained. Besides, plate angle of 180° must be highlighted as the most effective plate angle again for this cylinder porosity as the all TKE_{max} values clustered around same value even for β_P=0.

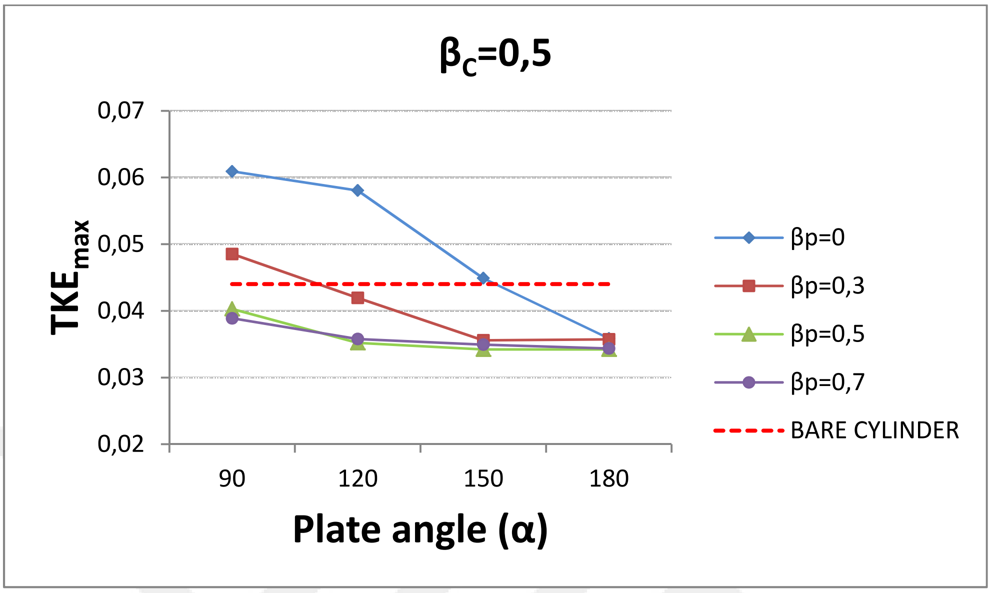

Figure 4.24. TKE_{max} distribution according to different plate angles and splitter plate porosity ratios, for $\beta_C = 0.5$

When the cylinder porosity enhanced up to 0.7, the time averaged vorticity contours <ω>, the time averaged streamlines <ψ> and instantaneous dye visualization results indicated that there is no significant flow control in both annular and wake region. By reason of high cylinder porosity, excessive amount of flow can pass through the outer cylinder and the momentum of upper and lower shear layers cannot be reduced at sufficiently, resulting uncontrolled flow downstream of the inner cylinder. The TKE_{max} distribution of the β_C=0.7 was presented in figure 4.25 according to relevant plate angles and plate porosity ratios. At first glance the distributions of different plate porosity ratios attracts notice, because they all exhibit almost same increment and decrease, at the relevant plate angles except β_P=0.5 at 150°. And as it is anticipated, lowering the splitter plate porosity ratio diminishes the TKE_{max} values. However, there is an exception that the plate porosity of β_P=0.5 has the lowest TKE_{max} values in general. Its TKE_{max} values are even lower than the β_P=0.7. This might be caused from that β_P=0.7 is not as efficient as the previous cases when it is utilized with the cylinder porosity ratio of β_C=0.7. Additionally, as it can be seen from figure 4.25 the β_C=0.7 ratio is not efficient to control the flow for almost all plate porosity ratios and plate angles except for the β_P=0.5 at 120° and 180°. And this cylinder porosity was already determined as inefficient for controlling the flow according to the time averaged vorticity contours <ω>, the time averaged streamlines <ψ> and instantaneous dye visualization results earlier. Consequently, the TKE_{max} graphs are in accordance with interpretations of previous streamlines topology, vorticity contours and dye visualization results.

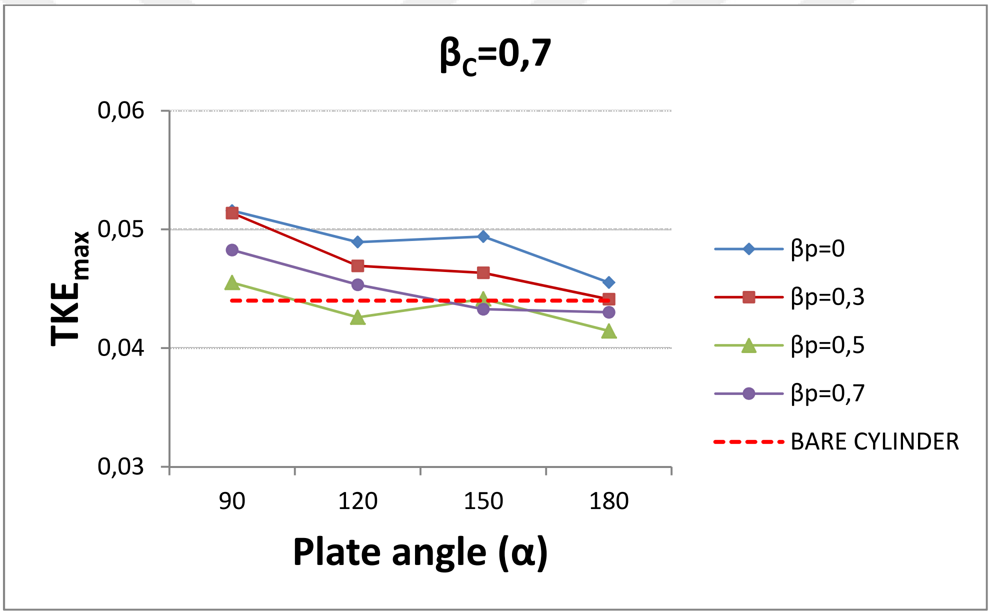

Figure 4.25. TKE_{max} distribution according to different plate angles and splitter plate porosity ratios, for β_C = 0.7

5. CONCLUSIONS

In the present study, the main purpose was to control the flow around a circular cylinder (inner cylinder) and eliminate the formation of Karman Vortex Street in the wake region by two passive control methods, splitter plate and perforated semi circular cylinder. Inner and outer cylinder diameters were kept constant throughout the experiments as 50 mm and 125 mm respectively. Also Reynolds number was kept constant as 5000 and it was evaluated with respect to inner cylinder diameter. Three variable parameters were designated as β_C, β_P and α, and their effects to the flow behavior were observed. Cylinder porosity values were determined as β_C=0.3, 0.5 and 0.7. Four different plate porosities were chosen as β_P=0, 0.3, 0.5 and 0.7. And finally, four plate angles were chosen as α=90°, 120°, 150° and 180°. To have a preliminary comprehension about the flow, dye visualization method was utilized first to the whole configurations. Later, PIV technique was applied to have quantitative results such as time averaged streamlines $<\psi>$ and the time average vorticity contours $<\omega>$ and Turbulence Kinetic Energy (TKE) level.

Dye visualization reveals that, 180° plate angle was the most efficient parameter for all plate porosities and for β_C=0.3, 0.5 to annihilate the Karman Vortex Street in the wake region. Plate angle of 150° also was an efficient parameter to attenuate the vortex shedding for all plate porosities and for β_C=0.3, 0.5. It is because when the plate angle is 150°, splitter plate is located in the vicinity of separation point and plate prevents the possible vortex formation for the relevant shear layer. When the plate location becomes vertical to the flow direction, especially for the lower porous plates, flow cannot pass through the plate and it is directed to the upper shear layer, resulting higher momentum flow. Thus, the plate angle values of 90° and 120° could not achieve the desired flow control especially for lower plate porosities. Cylinder porosity of β_C=0.7 can be regarded as inefficient to control the wake region for almost all configurations.

For quantitative investigation, PIV technique was utilized and annular region was analyzed in detail. And PIV results indicated that, vortex pair interaction is prevented in the annular region for almost all configurations with 180° plate angle regardless of the plate porosity. 150° plate angle also can be presumed as efficient control parameter due to its proximity to the separation point. 90° and 120° plate angles exhibited inefficient flow control performance for lower plate porosities. To have a complete quantitative results, TKE_{max} values in the annular region were scrutinized. According to these results, plate porosity ratio came into prominence and results indicated that as the plate porosity ratio ascends, the TKE_{max} values indicate a remarkable reduction. Besides, cylinder porosity has also an effect on TKE_{max} values and it was determined that as the plate porosity diminishes the TKE_{max} values decreases. And the most notable configuration was found to be β_C= 0.3 and 0.5 with plate porosities of β_P= 0.5, 0.7. Additionally, the peak value of TKE_{max} reduction of 34% was obtained for β_C= 0.3 and β_P= 0.5 at 180°. According to TKE_{max} graphs there is a complete flow control in the annular region at 150° and 180° plate angles for almost all plate porosity ratios except for cylinder porosity of β_C= 0.7. However, for 90° and 120° plate angles there is not complete control in the annular region due to the vortex pair interaction and higher momentum shear layer. β_C= 0.7 cannot be presumed as effective to control the flow for almost all configuration according to dye visualization and PIV results. Additionally PIV results, TKE_{max} values and dye visualization results are compatible with each other. Consequently, the most efficient and salient parameters of the present study can be regarded as β_C= 0.3 and 0.5, β_P= 0.5 and 0.7 with plate angles of 150° and 180°.

In the present study, near wake region was investigated by PIV technique, hence for further investigation it may be useful to scrutinize the far wake region by means of PIV technique. Investigation of the drag coefficient also may be carried out to analyze the flow structure in a comprehensive way.

REFERENCES

Achenbach, E. (1971). Influence of surface roughness on the cross-flow around a circular cylinder. *Journal of Fluid Mechanics, 46*(2), 321-335.

Achenbach, E., and Heinecke, E. (1981). On vortex shedding from smooth and rough cylinders in the range of Reynolds numbers 6×10^3 to 5×10^6. *Journal of Fluid Mechanics, 109*, 239-251.

Akilli, H., Karakus, C., Akar, A., Sahin, B., and Tumen, N. F. (2008). Control of vortex shedding of circular cylinder in shallow water flow using an attached splitter plate. *Journal of Fluids Engineering, 130*(4), 041401.

Akilli, H., Sahin, B., and Filiz Tumen, N. (2005). Suppression of vortex shedding of circular cylinder in shallow water by a splitter plate. *Flow Measurement and Instrumentation, 16*(4), 211-219.

Allen, D., and Henning, D. (2001). *Surface roughness effects on vortex-induced vibration of cylindrical structures at critical and supercritical Reynolds numbers.* Paper presented at the Offshore Technology Conference.

Anderson, E., and Szewczyk, A. (1997). Effects of a splitter plate on the near wake of a circular cylinder in 2 and 3-dimensional flow configurations. *Experiments in Fluids, 23*(2), 161-174.

Apelt, C., and West, G. (1975). The effects of wake splitter plates on bluff-body flow in the range $10^4 < R < 5\times 10^4$. Part 2. *Journal of Fluid Mechanics, 71*(01), 145-160

Apelt, C., West, G., and Szewczyk, A. A. (1973). The effects of wake splitter plates on the flow past a circular cylinder in the range $10^4 < R < 5\times10^4$. *Journal of Fluid Mechanics, 61*(01), 187-198.

Artana, G., Sosa, R., Moreau, E., and Touchard, G. (2003). Control of the near-wake flow around a circular cylinder with electrohydrodynamic actuators. *Experiments in Fluids, 35*(6), 580-588.

Assi, G. R. S., Bearman, P. W., and Kitney, N. (2009). Low drag solutions for suppressing vortex-induced vibration of circular cylinders. *Journal of Fluids and Structures, 25*(4), 666-675.

Bearman, P. (1965). Investigation of the flow behind a two-dimensional model with a blunt trailing edge and fitted with splitter plates. *Journal of Fluid Mechanics, 21*(02), 241-255.

Bearman, P., and Harvey, J. (1993). Control of circular cylinder flow by the use of dimples. *AIAA journal, 31*(10), 1753-1756.

Berger, E. (1967). Suppression of vortex shedding and turbulence behind oscillating cylinders. *The Physics of Fluids, 10*(9), S191-S193.

Bernitsas, M. M., and Raghavan, K. (2008). *Reduction/suppression of VIV of circular cylinders through roughness distribution at* $8\times10^3 < Re < 1.5\times10^5$. Paper presented at the ASME 2008 27th International Conference on Offshore Mechanics and Arctic Engineering.

Bernitsas, M. M., Raghavan, K., and Duchene, G. (2008). *Induced Separation and Vorticity Using Roughness in VIV of Circular Cylinders at* $8\times10^3 < Re < 2.0\times10^5$. Paper presented at the ASME 2008 27th International Conference on Offshore Mechanics and Arctic Engineering.

Bhattacharyya, S., Dhinakaran, S., and Khalili, A. (2006). Fluid motion around and through a porous cylinder. *Chemical Engineering Science, 61*(13), 4451-4461.

Bloor, M.S., (1964). The transition to turbulence in the wake of a circular cylinder. *Journal of Fluid Mechanics, 19*, 290-304.

Bridge piers, (2019). https://www.quora.com/How-do-they-build-bridges-in-sea

Bruneau, C. H., and Mortazavi, I. (2004). Passive control of the flow around a square cylinder using porous media. *International Journal for Numerical Methods in Fluids, 46*(4), 415-433.

Bruneau, C.H., and Mortazavi, I. (2006). Control of vortex shedding around a pipe section using a porous sheath. *International Journal of Offshore and Polar Engineering, 16*(02).

Bruneau, C.-H., Mortazavi, I., and Gilliéron, P. (2008). Passive control around the two-dimensional square back Ahmed body using porous devices. *Journal of Fluids Engineering, 130*(6), 061101.

Chang, C.-C., Ajith Kumar, R., and Bernitsas, M. M. (2011). VIV and galloping of single circular cylinder with surface roughness at $3.0\times10^4 \leq Re \leq 1.2\times10^5$. *Ocean Engineering, 38*(16), 1713-1732.

Chen, W.-L., Xin, D.-B., Xu, F., Li, H., Ou, J.-P., and Hu, H. (2013). Suppression of vortex-induced vibration of a circular cylinder using suction-based flow control. *Journal of Fluids and Structures, 42*, 25-39.

Chen, Z., and Aubry, N. (2005). Active control of cylinder wake. *Communications in Nonlinear Science and Numerical Simulation, 10*(2), 205-216.

Chimneys, (2019). http://en.uzmk-vnzm.ru/products/chimneys/chimneys/

Dantec Dynamics, (2019). https://www.dantecdynamics.com/measurement-principles-of-piv

Durhasan, T., Aksoy, M.M., Pinar, E., Ozkan, G.M., Akilli, H. and Sahin, B. (2016). Vortex street suppression of a circular cylinder using perforated semi-circular fairing in shallow water. *Experimental Thermal and Fluid Science, 79*, 101-110.

Durhasan, T., Pinar E., Ozkan, G. M., Akilli H. and Sahin B. (2019). The effect of shroud on vortex shedding mechanism of cylinder. *Applied Ocean Research, 84*, 51-61.

Durhasan, T., Pinar E., Ozkan, G. M., Aksoy, M.M., Akilli H. and Sahin B. (2018). PIV measurement downstream of perforated cylinder in deep water. *European Journal of Mechanics - B/Fluids, 72*, 225-234.

Enloe, C., McLaughlin, T. E., VanDyken, R. D., Kachner, K., Jumper, E. J., Corke, T. C., and Haddad, O. (2004). Mechanisms and responses of a single dielectric barrier plasma actuator: geometric effects. *AIAA journal, 42*(3), 595-604.

Feng, L.H., Wang, J.J., Pan, C., (2010). Effect of novel synthetic jet on wake vortex shedding modes of a circular cylinder. *Journal of Fluids and Structures, China, 26* (2010) 900–917.

Fujisawa, N., and Nakabayashi, T. (2002). Neural network control of vortex shedding from a circular cylinder using rotational feedback oscillations. *Journal of Fluids and Structures, 16*(1), 113-119.

Fujisawa, N., Kawaji, Y., and Ikemoto, K. (2001). Feedback control of vortex shedding from a circular cylinder by rotational oscillations. *Journal of Fluids and Structures, 15*(1), 23-37.

Gao, Y., Fu, S., Wang, J., Song, L., and Chen, Y. (2015). Experimental study of the effects of surface roughness on the vortex-induced vibration response of a flexible cylinder. *Ocean Engineering, 103*, 40-54.

Gerard, J.H., (1964). The mechanics of the formation region of vortices behind bluff bodies. *Journal of Fluid Mechanics, 25*, 401-413.

Gerrard, J. (1966). The mechanics of the formation region of vortices behind bluff bodies. *Journal of Fluid Mechanics, 25*(02), 401-413.

Gim, O.-S., Kim, S.-H., and Lee, G.-W. (2011). Flow control behind a circular cylinder by control rods in uniform stream. *Ocean Engineering, 38*(17-18), 2171-2184.

Glezer, A., and Amitay, M. (2002). Synthetic Jets. *Annual Review of Fluid Mechanics, 34*(1), 503-529

Gozmen, B., Akilli, H., and Sahin, B. (2013). Passive control of circular cylinder wake in shallow flow. *Measurement, 46*(3), 1125-1136.

Gozmen, B., Akilli, H., and Şahin, B. (2013). Vortex control of cylinder wake by permeable cylinder. *J. Faculty Eng. Arch, 28*, 77-85.

Ho, C.M., and Huerre, P., (1984). Perturbed free shear layers. *Annual Review of Fluid Mechanics, 16*, 365-424.

Hyun, K., and Chun, C. (2003). The wake flow control behind a circular cylinder using ion wind. *Experiments in Fluids, 35*(6), 541-552.

Igbalajobi, A., McClean, J. F., Sumner, D., and Bergstrom, D. J. (2013). The effect of a wake-mounted splitter plate on the flow around a surface-mounted finite-height circular cylinder. *Journal of Fluids and Structures, 37*, 185-200.

Kawamura, T., Takami, H., and Kuwahara, K. (1986). Computation of high Reynolds number flow around a circular cylinder with surface roughness. *Fluid Dynamics Research, 1*(2), 145-162.

Keane, R. D., and Adrian, R. J. (1990). Optimization of particle image velocimeters. I. Double pulsed systems. *Measurement science and technology, 1*(11), 1202.

Kiu, K. Y., Stappenbelt, B., abd Thiagarajan, K. P. (2011). Effects of uniform surface roughness on vortex-induced vibration of towed vertical cylinders. *Journal of Sound and Vibration, 330*(20), 4753-4763.

Knell, B.J., (1969). The drag of a circular cylinder fitted with shrouds. *Natl. Phys. Lab., UK*, Aero. Rep. no. 1297.

Kwon, K., and Choi, H. (1996). Control of laminar vortex shedding behind a circular cylinder using splitter plates. *Physics of Fluids, 8*(2), 479-486.

Landreth, C., & Adrian, R. (1988). *Measurement and refinement of velocity data using high image density analysis in particle image velocimetry.* Paper presented at the 4th International Symposium on Applications of Laser Anemometry to Fluid Mechanics.

Marine cable, (2019). https://www.orange.com/en/actus-courtes-tuiles/responsabilite/actions/Environnement/On-course-for-the-COP-episode-5

Meinhart and Soloff, (1999). Cleanvec‖ software, Turbulence Laboratory, University of Illinois at Urbana-Champaign

Meinhart, C. D., & Adrian, R. J. (1995). On the existence of uniform momentum zones in a turbulent boundary layer. *Physics of Fluids, 7*(4), 694-696.

Merrick, R., and Bitsuamlak, G. (2008). *Control of flow around a circular cylinder by the use of surface roughness: A computational and experimental approach.* Paper presented at the 4th International Conference Advances on Wind and Structures (A WAS08).

Mertz, B. E., and Corke, T. C. (2011). Single-dielectric barrier discharge plasma actuator modelling and validation. *Journal of Fluid Mechanics, 669*, 557-583.

Mimeau, C., Mortazavi, I., and Cottet, G.-H. (2014). Passive flow control around a semi-circular cylinder using porous coatings. *International Journal of Flow Control, 6*(1).

Mutschke, G., Shatrov, V., and Gerbeth, G. (1998). Cylinder wake control by magnetic fields in liquid metal flows. *Experimental Thermal and Fluid Science, 16*(1), 92-99.

Nakamura, Y. (1996). Vortex shedding from bluff bodies with splitter plates. *Journal of Fluids and Structures, 10*(2), 147-158

Offshore structures, (2019). https://www.popularmechanics.com/technology/infrastructure/g2926/7-of-the-biggest-offshore-structures/

Oruç, V., Akilli, H., and Sahin, B. (2016). PIV measurements on the passive control of flow past a circular cylinder. *Experimental Thermal and Fluid Science, 70*, 283-291.

Ozkan, G. M., Firat, E., and Akilli, H. (2017). Control of Vortex Shedding Using a Screen Attached on the Separation Point of a Circular Cylinder and Its Effect on Drag. *Journal of Fluids Engineering, 139*(7), 071107.

Ozkan, G. M., Firat, E., and Akilli, H. (2017). Passive flow control in the near wake of a circular cylinder using attached permeable and inclined short plates. *Ocean Engineering, 134*, 35-49.

Ozkan, G. M., Oruc, V., Akilli, H., and Sahin, B. (2012). Flow around a cylinder surrounded by a permeable cylinder in shallow water. *Experiments in Fluids, 53*(6), 1751-1763.

Ozono, S. (1999). Flow control of vortex shedding by a short splitter plate asymmetrically arranged downstream of a cylinder. *Physics of Fluids, 11*(10), 2928-2934.

Park, D., Ladd, D., and Hendricks, E. (1994). Feedback control of von Kármán vortex shedding behind a circular cylinder at low Reynolds numbers. *Physics of Fluids, 6*(7), 2390-2405.

Pinar, E., Ozkan, G. M., Durhasan, T., Aksoy, M. M., Akilli, H., and Sahin, B. (2015). Flow structure around perforated cylinders in shallow water. *Journal of Fluids and Structures, 55*, 52-63.

Rashidi, S., Hayatdavoodi, M., and Esfahani, J. A. (2016). Vortex shedding suppression and wake control: A review. *Ocean Engineering, 126*, 57-80.

Rodríguez, I., Lehmkuhl, O., Piomelli, U., Chiva, J., Borrell, R., and Oliva, A. (2016). Numerical simulation of roughness effects on the flow past a circular cylinder. *Journal of Physics: Conference Series, 745*(3), 032043.

Roshko, A. (1954). *On the drag and shedding frequency of two-dimensional bluff bodies. Tech*. Retrieved from

Roussopoulos, K., and Monkewitz, P. A. (1996). Nonlinear modelling of vortex shedding control in cylinder wakes. *Physica D: Nonlinear Phenomena, 97*(1), 264-273.

Ruck, B., Klausmann, K., and Wacker, T. (2012). *The flow around circular cylinders partially coated with porous media.* Paper presented at the AIP Conference Proceedings 4.

Said Turki (2008). Numerical Simulation of Passive Control on Vortex Shedding Behind Square Cylinder Using Splitter Plate. *Engineering Applications of Computational Fluid Mechanics, 2*(4), 514-524,

Sarioglu, M. (2017). Control of flow around a square cylinder at incidence by using a splitter plate. *Flow Measurement and Instrumentation, 53*, 221-229.

Seal, C., and Smith, C. (1999). The control of turbulent end-wall boundary layers using surface suction. *Experiments in Fluids, 27*(6), 484-496.

Sheng, J., Meng, H., & Fox, R. (2000). A large eddy PIV method for turbulence dissipation rate estimation. *Chemical Engineering Science, 55*(20), 4423-4434.

Shukla, S., Govardhan, R. N., and Arakeri, J. H. (2009). Flow over a cylinder with a hinged-splitter plate. *Journal of Fluids and Structures, 25*(4), 713-720.

Shukla, S., Govardhan, R. N., and Arakeri, J. H. (2013). Dynamics of a flexible splitter plate in the wake of a circular cylinder. *Journal of Fluids and Structures, 41*, 127-134.

Sintu Singha, K. P. S. (2011). Control of vortex shedding from a circular cylinder using imposed transverse magnetic field. *International Journal of Numerical Methods for Heat & Fluid Flow, 21*(1), 32-45.

Strouhal, V. (1878). Ueber eine besondere Art der Tonerregung. *Annual Review of Physical Chemistry (Wied. Ann. Phys.), 5*, 216-251.

Tao, J., Huang, X., and Chan, W. (1996). A flow visualization study on feedback control of vortex shedding from a circular cylinder. *Journal of Fluids and Structures, 10*(8), 965-970.

Tensi, J., Boué, I., Paillé, F., and Dury, G. (2002). Modification of the wake behind a circular cylinder by using synthetic jets. *Journal of Visualization, 5*(1), 37-44.

Thomas, F. O., Kozlov, A., and Corke, T. C. (2008). Plasma actuators for cylinder flow control and noise reduction. *AIAA journal, 46*(8), 1921.

Unal, M., and Rockwell, D. (1988). On vortex formation from a cylinder. Part 2. Control by splitter-plate interference. *Journal of Fluid Mechanics, 190*, 513-529

Underwater pipelines, (2019). http://octa-innovation.eu/polynesie-francaise-une-pratique-exemplaire-en-matiere-de-climatisation/underwater-pipeline-2/

Valipour, M. S., Rashidi, S., Bovand, M., and Masoodi, R. (2014). Numerical modeling of flow around and through a porous cylinder with diamond cross section. *European Journal of Mechanics - B/Fluids, 46*, 74-81.

Westerweel, J., Dabiri, D., and Gharib, M. (1997). The effect of a discrete window offset on the accuracy of cross-correlation analysis of digital PIV recordings. *Experiments in Fluids, 23*(1), 20-28.

Westerweel, J., Draad, A., Van der Hoeven, J. T., and Van Oord, J. (1996). Measurement of fully-developed turbulent pipe flow with digital particle image velocimetry. *Experiments in Fluids, 20*(3), 165-177.

Willert, C. E., and Gharib, M. (1991). Digital particle image velocimetry. *Experiments in Fluids, 10*(4), 181-193.

Williams, J. F., and Zhao, B. (1989). The active control of vortex shedding. *Journal of Fluids and Structures, 3*(2), 115-122.

Wind turbine towers, (2019). https://www.azocleantech.com/article.aspx?ArticleID=704

Wu, J., Sheridan, J., Hourigan, K., Welsh, M, C. and Thompson, M. (1994). Longitudinal vortex structures in a cylinder wake. *Physics of Fluids 6*(9), 2883-2885

Yu, M., and Monkewitz, P. A. (1990). The effect of nonuniform density on the absolute instability of two-dimensional inertial jets and wakes. *Physics of Fluids A: Fluid Dynamics, 2*(7), 1175–1181

Zdravkovich, M. (1981). Review and classification of various aerodynamic and hydrodynamic means for suppressing vortex shedding. *Journal of Wind Engineering and Industrial Aerodynamics, 7*(2), 145-189.

Zhang, H., Fan, B.-C. and Chen, Z.-H., (2009). Optimal control of cylinder wake flow by electro-magnetic force based on adjoint flow field. *European Journal of Mechanics B/Fluids, China, 29*(2010) 53–60.

Zhang, H., Fan, B.-C. and Chen, Z.-H., (2010). Computations of optimal cylinder flow control in weakly conductive fluids. *Computers and Fluids, China, 39* (2010) 1261–1266.

Zhao, M., and Cheng, L. (2010). Finite element analysis of flow control using porous media. *Ocean Engineering, 37*(14-15), 1357-1366.

Zhou, B., Wang, X., Gho, W. M., and Tan, S. K. (2015). Force and flow characteristics of a circular cylinder with uniform surface roughness at subcritical Reynolds numbers. *Applied Ocean Research, 49*, 20-26.

Zhou, L., Cheng, M., and Hung, K. (2005). Suppression of fluid force on a square cylinder by flow control. *Journal of Fluids and Structures,21*(2), 151-167.

CURRICULUM VITAE

Aykut ÇETİN was born in Adana in 1991. He graduated from Kuleli Military High school in Istanbul. Then he dropped out of Turkish Military Academy and he entered in Mechanical Engineering Department of Çukurova University. He graduated as a Mechanical Engineer from the university in June 2015 and completed his military service in December, 2016.